PREPARATION AND CHARACTERIZATION OF WATER-IN-OIL (W/O) NANO-EMULSIONS

Ph.D. THESIS

by

HEMANT KUMAR

**DEPARTMENT OF CHEMICAL ENGINEERING
INDIAN INSTITUTE OF TECHNOLOGY ROORKEE
ROORKEE-247667 (INDIA)
FEBRUARY, 2019**

PREPARATION AND CHARACTERIZATION OF WATER-IN-OIL (W/O) NANO-EMULSIONS

A THESIS

Submitted in partial fulfilment of the requirements for the award of the degree

of

DOCTOR OF PHILOSOPHY

in

CHEMICAL ENGINEERING

by

HEMANT KUMAR

**DEPARTMENT OF CHEMICAL ENGINEERING
INDIAN INSTITUTE OF TECHNOLOGY ROORKEE
ROORKEE-247667 (INDIA)
FEBRUARY, 2019**

INDIAN INSTITUTE OF TECHNOLOGY ROORKEE

<u>CANDIDATE'S DECLARATION</u>

I hereby certify that the work which is being presented in the thesis entitled **"PREPARATION AND CHARACTERIZATION OF WATER-IN-OIL (W/O) NANO-EMULSIONS** " in partial fulfilment of the requirements for the award of the Degree of Doctor of Philosophy and submitted in the Department of Chemical Engineering of the Indian Institute of Technology Roorkee is an authentic record of my own work carried out during a period from July, 2014 to February, 2019 under the supervision of Dr. Vimal Kumar, Associate Professor, Department of Chemical Engineering, Indian Institute of Technology Roorkee.

The matter presented in this thesis has not been submitted by me for the award of any other degree of this or any other Institution.

(HEMANT KUMAR)

This is to certify that the above statement made by the candidate is correct to the best of my knowledge.

(Vimal Kumar)
Supervisor

The Ph. D. Viva-voice Examination of Hemant Kumar, Research Scholar, has been held on……………….....

Chairperson, SRC   **Signature of External Examiner**

This is to certify that the student has made of the corrections in the thesis.

Signature of Supervisor   **Head of the Department**
Dated:

ABSTRACT

The growing concern on green technology to protect the environment has encouraged the use of alternative ecofriendly formulations for nano-emulsion fuels. Nowadays, diesel engine is the most powerful and widely used internal combustion engine; its exhaust, owing to incomplete combustion, releases particulate matters (unburnt hydrocarbons) and detrimental gases like NO_X, CO, and CO_2 to the environment. It has been reported that the addition of water to diesel fuel brings significant reductions in the emission of unburnt hydrocarbons and NO_X gases due to reduced temperature in combustion chamber. Improved combustion properties like brake specific fuel consumption and increased brake thermal efficiency has been achieved because of ignition delay and micro-explosion. In case of water-in-oil (w/o NE) nano-emulsion fuel, smaller size droplets increase surface area that helps in efficient combustion improving brake specific fuel consumption (BSFC) and reducing combustion chamber temperature consequently helping in further reduction in NO_x and PMs. Moreover, their smaller size negates gravity induced separation and they make the balance between Brownian motion and surface induced properties making them stable for longer storage time.

Present work therefore, motivates us for the development of transparent and stable w/o nano-emulsions. A detailed study regarding formation of water-in-diesel oil is required by applying low and high energy methods. In this regard a detailed ternary diagram is required to study the instability mechanism and rheological analysis for the system being developed. Moreover, a strategic modeling approach is required to optimize the process parameters for the formation of o/w NEs. The overall objectives of the proposed work were the formation and characterization of nano-emulsion fuel.

Formation of water-in-diesel oil (w/o NE) nano-emulsion has been achieved by low energy emulsification method by stabilizing a new combination of non-ionic sorbitan esters surfactants, i.e. PEG20-sorbitan mono-stearate and sorbitan mono-oleate in mixed proportions. Different combinations of surfactants (T6+S8) have been tested and best possible combination of mixed surfactants is found at a surfactants ratio of 35:65 (wt. /wt.) for T6:S8 at HLB = 8.01, which resulted into smaller droplet size of 44.87 nm. A phase diagram study is performed to identify the zones of formation of transparent, translucent and opaque emulsions (44 nm<droplet size<700nm) at 37 ^{o}C. Mechanism responsible for instability of emulsion is explained by Ostwald ripening with inference describing a decrease in particle size with Ostwald ripening rate. In case of nano-emulsion of droplet size 64.28 nm the Oswald ripening rate is found as 0.0874×10^{-27} $m^3 s^{-1}$. Comparison of Ostwald ripening rate with other set of surfactants obtained

by different authors showed the lowest rate among them indicative of enhanced stability. A rheological study of tested set of nano-emulsions depicted Newtonian behavior ($1.0371 \leq n \leq 1.0826$) over a wider range of shear rate (10 - 1000 s^{-1}) at different temperatures (25 - 40 ^{o}C).

An energy efficient and scalable method is designed to form stable and transparent water-in-oil (w/o) nano-emulsion. Application of high energy in addition to the low energy at the optimized conditions have been targeted to make the process energy efficient, since later part is applied to droplets formed at less energy. In the present work, formation of combined energy mixed surfactant nano-emulsion is achieved by combined approach of isothermal low energy followed by high energy method (ultrasonication). A mixture of two functional groups (ether and ester) non-ionic surfactants is used at optimized ratio of 0.71/0.29 (Span 80/Tx-100; w/w). Optimization of ultrasonicated parameters resulted in 25% amplitude, 0.5 pulse mode factor and 8.5 minutes of sonication time. A ternary diagram study has been performed to recognize the compositions accountable for the formation of transparent, translucent and opaque emulsions in the bounded range of water fraction 0.02 to 0.11 and surfactant fraction 0.10 to 0.20. Surfactant-to-water (β) ratio found applicable for the production of nano-sized droplets in the range of $2 \leq \beta \leq 3$. A minimum droplet size of 25±1 nm is attained in the present study. An increase in surfactant fraction decreased average droplet size, whereas, increase in water fraction increased average droplet size. Reduction in droplet size is prominently found in the range of energy density from 15.23 J.ml^{-1} to 40 J.ml^{-1} thereafter, it decelerated up to 160 J.ml^{-1}. Prediction of average droplet size modeled with energy density fitted well and could be used for scaling up and tuning the droplet size. Resultant nano-emulsion samples displayed kinetic stability whereas long term stability (45 days) assessed using Ostwald ripening model showed stability in the order of $\beta=2.0>\beta=2.5>\beta=3.0>\beta=4.0$.

Furthermore, statistical and mathematical approach has been implemented in finding out optimal values of process parameters that could formulate water emulsified diesel fuels with lower droplet size (D$_{z\text{-avg.}}$) of dispersed phase and at the same time possesses lower values of kinematic viscosity. In order to impart optimal properties in the diesel, an integral hybrid genetic algorithm (GA) has been implemented with back propagation artificial neural network (BPANN) and response surface methodology (RSM) based on rotatable central composite design (RCCD). Process parameters as input to the proposed models were water fraction (0.05-0.11, w/w), surfactant fraction (0.10-0.020, w/w), power density (21.25-46.75, W.cm^{-2}), and ultrasonication time (4-10, min.). Response variables like D$_{z\text{-avg.}}$ (nm) and kinematic viscosity (mm^2.s^{-1}) are employed as output variables. In the anticipated hybrid GA model, a multi objective optimization

is performed wherein, model equations obtained from RCCD-RSM are used as fitness function and output from RSM-BPANN are used as initial population. Hybrid GA model predicted optimum values of $D_{z\text{-avg.}}$ and kinematic viscosity as 53.54 nm and 1.459 $mm^2.s^{-1}$, respectively, with percent errors as 2.17% and 0.34 % respectively. However, optimized process parameters has been predicted as water fraction-0.052 (w/w), surfactant fraction-0.105 (w/w), power density-29.94 ($W.cm^{-2}$), and ultrasonication time-9.7 minutes. Hybrid GA model proposed in this study is found effective in predicting the optimized values of process variables in the formation of nano-emulsion diesel fuel with optimized values of avg. droplet size and kinematic viscosity.

ACKNOWLEDGEMENT

I also like to express a profound gratitude to my parents for their continuous support. Same gratitude goes to my sibling for all their help and encouragement. The unfailing supports from the above people have been very instrumental in the completion of my PhD journey.

My deepest gratitude goes also to my family for their indefatigable love and support throughout my life. To all of them I dedicate this thesis.

Above all, I thank 'Almighty' with whose beatitude, I could reach this far.

(HEMANT KUMAR)
FEBRUARY, 2019

CONTENTS

LIST OF TABLES

LIST OF FIGURES

ABBREVIATIONS

ANN	artificial neural network
BBD	Box-Behnken design
BSFC	brake specific fuel consumption
FFBP-ANN	feed forward back propagation-artificial neural network
BTE	brake thermal efficiency
CCD	central composite design
CEMSNE	combined energy mixed surfactant nano-emulsion
CMC	critical micelle concentration
CI	compression ignition engines
CTAB	cetyltrimethylammonium bromide
DCAT	dynamic contact angle meter and tensiometer
DLS	dynamic light scattering
FFBP	feed forward back propagation neural network
GA	genetic algorithm
GDP	gross domestic product
HEM	high energy method
HLB	hydrophilic-lipophilic Balance
IFT	interfacial tension
KV	kinematic viscosity
LEM	low energy emulsification methods
LOF	lack of fit
NE	Nano-emulsion
o/s	oil-to-surfactant ratio
o/w	oil-in-water ratio
PCS	photon correlation spectroscopy
PD	power density
PDI	polydispersity index
PIT	phase inversion temperature
PM	particulate matter
RCCD	rotatable central composite design

RPM	revolutions per minute
RSM	response surface methodology
S80	span 80
SDS	sodium dodecyl sulfate
T60	tween 60
TX-100	triton X-100
TS	mixed surfactant including Span 80 and Tween 60
UT	ultrasonication time
w/o	water-in- oil ratio
w/w	ratio of two quantities measured on weight basis

SYMBOLS

a	activity
ΔA	change in interfacial area, m^2
CO_x	oxides of carbon as atmospheric pollutants
Cp	center points in rotatable central composite design
d	translational diffusion coefficient ($m^2.s^{-1}$)
D_{max}	size of a largest eddy, m
$D_{z-avg.}$	Z-average droplet size of dispersed phase, nm
$D_{o,z-avg.}$	Z-average droplet diameter at zero time, nm
DOF_{LOF}	ratio of media of degree of freedom of lack of fit
DOF_{PE}	ratio of media of degree of freedom of pure error
$F_{LOF,PF}$	F-distribution using the ratio of media of square of lack of fit and of pure error
$g(\tau)$	correlation function of the scattered electric field
$G(\tau)$	photocount correlation function
ΔG	Gibbs free energy change, J
k	flow consistency index, $Pa.s^n$
MS_{LOF}	ratio of media of square of lack of fit
MS_{PE}	ratio of media of square of pure error
n	flow behavior index
p	Laplace pressure, pascal

P_v	power density, $W.cm^{-2}$; power density applied to unit volume of sample, $W.cm^{-2}.ml^{-1}$
r	average radius of droplet size, nm
r_c	critical size of bubble formed during cavitation effect in ultrasonication, m
R	gas constant, $J.mol^{-1}K^{-1}$
Re	Reynolds number
ΔS	change in entropy, $J.K^{-1}$
SS_{LOF}	ratio of sum of the square of lack of fit
SS_{PE}	ratio of sum of the square of pure error
t	time (s)
t_R	residence time, s
T (K)	absolute temperature, K
u	local flow velocity, $m.s^{-1}$
u'	root mean square velocity, $m.s^{-1}$
U	velocity gradient, s^{-1}
v	linear liquid velocity in conduit, $m.s^{-1}$
V_{mol}	molar volume of dispersed phase, $m^3.mol^{-1}$
w/d	water-in-diesel emulsion
W_b	Weber number
$W_{b,crit}$	critical Weber number
x_o	smallest size of eddy, m

GREEK SYMBOLS

α	distance from center of the design space to the star point, for RCCD $|\alpha| > 1$
β	surfactant-to-water ratio (w/w)
ε	statistical error
ε_v	energy density, $J.ml^{-1}$
ρ	density, $Kg.m^{-3}$
η	viscosity of a given sample, Pa.s
η_c	viscosity of continuous phase, Pa.s
η_d	viscosity of dispersed phase, Pa.s

τ	correlator time delay or time difference of the correlator
Γ	surface excess, moles.m^{-2}
μ_{ratio}	viscosity ratio of dispersed phase viscosity over continuous phase viscosity
γ	interfacial tension, N.m^{-1}
θ	scattering angle (degree)
Φ_w	weight fraction of water
Φ_s	weight fraction of surfactant
Φ_o	weight fraction of oil
π	decision vector containing parameters to be optimized
Π	set of optimized solution depending upon constraint functions
$\psi (D_{z\text{-avg.}})$	solubility surrounding the droplet diameter ($D_{z\text{-avg.}}$), mol.m^{-3}
$\psi (\infty)$	solubility at the bulk phase, mol.m^{-3}
ω	coalescence frequency per unit surface area, m^{-2}.s^{-1}
ω_q	q=2: constant surface rate, ω_2, controlled by permeation across the surfactant films, m^{-2}.s^{-1}; q=3: constant volume rate ω_3 controlled by molecular diffusion across the continuous phase (Ostwald ripening rate), m^{-2}.s^{-1}

CHAPTER 1
INTRODUCTION

1.1 GENERAL

An emulsion system is thermodynamically unstable liquid-in-liquid system consisting of two or more immiscible phases wherein one phase is dispersed in another phase. The inner encapsulated phase is dispersed or internal phase and the other outer phase is known as continuous phase or external phase. Since immiscible liquids cannot be blended due to high surface tension or interfacial tension, a surface active agent is then required to form the dispersion of one phase to another by reducing the interfacial tension (IFT) through reduction in Laplace pressure. Another role of surfactant is in stabilizing the system by avoiding coalescence between dispersed droplets by providing electrical double layer near the interfaces (Baskar and Kumar, 2017; Bidita et al., 2014).

Nano-emulsions are kinetically stable heterogeneous colloidal systems with average droplet size typically in the range of 20–200 nm (Ee et al., 2008; Gutiérrez et al., 2008; Solans et al., 2005), wherein droplets of one phase are dispersed in the immiscible continuous phase surrounded by a film of surfactant stabilizing the emulsion (Du et al., 2016; Homayoonfal et al., 2014). However, according to some studies, there is a variation in the range of particle size of nano-emulsions with the lower limit of 50 nm (Noor El-Din et al., 2017; Tadros et al., 2004; Yukuyama et al., 2016) and the upper limit of 500 nm (Bidita et al., 2016; Feng et al., 2016; Porras et al., 2004). Bounding the lower and upper limits of nano-droplet size is not a decisive issue because no qualitative differences have been reported in the literature (Gutiérrez et al., 2008).

Excellent properties like large surface area per unit volume, optical transparency, long-term stability, and tunable rheology make nano-emulsions unique for industrial applications (Feng et al., 2016; Noor El-Din et al., 2013a; Tadros et al., 2004). Nano-emulsions are applicable in providing bioavailability of hydrophobic drugs, increasing transport efficiency, drug targeting and diagnosis in the field of pharmaceuticals (Gupta et al., 2016; Kumar et al., 2008; Lovelyn and Attama, 2011; Shakeel et al., 2007). Nano-emulsions enable proteins and polysaccharides for encapsulating, protecting and delivering lipophilic compounds, oil soluble vitamins, colors and nutraceuticals (Matalanis et al., 2011). Large surface area per unit volume, transparent appearance and tunable rheology ascertains the unique properties of the nano-

emulsions for tuning up cosmetic and personal care products (Izquierdo et al., 2002; Ribier and Simonnet, 1980; Tadros et al., 2004).

Compression ignition engines are extensively used in transportation and heavy industries due to their capability to generate high torque at low speed with better fuel efficiency (Ithnin et al., 2014; Oldfield and Thompson, 2010; Vellaiyan and Amirthagadeswaran, 2016a). Due to the incomplete combustion, some constraints like particulate matters (PMs) and detrimental gases majorly in the form of NO_x, CO, and CO_2 emerging from the C.I. engine though poses a serious threat to the environment (Al-Sabagh et al., 2011; Bidita et al., 2016; Ghannam and Selim, 2014). Stringent government rules pertaining to emissions require either some change in engine design or improvement in the fuel properties, though later option is a more practical solution. Growing concern on green technology to protect the environment encourages the use of emulsified fuels that reduce the NO_x and PM by secondary atomization through reduced combustion chamber temperature and at the same time gives increased fuel efficiency (Ishiguro and Naito, 2010).

Major fuel additives blended with diesel are oxygenated fuels, such as alcohols, ethers, esters, etc. Furthermore, biodiesel is a renewable resource of energy consisting of mono-alkyl ester based oxygenated fuel derived from the natural renewable resources like vegetable oils and animal fats derived from transesterification reaction. Among commonly tested alcoholic groups, methanol (Soni and Gupta, 2017; Yao et al., 2008; Yilmaz, 2012) and ethanol (He et al., 2003; Kwanchareon et al., 2007; Satgé De Caro et al., 2001; Shi et al., 2006; Xing-Cai et al., 2004) are blended with diesel fuel because of their specific properties like high latent heat of vaporization and low boiling point. Moreover, biodiesel can dissolve in diesel completely. Its high cetane value, high oxygen content (10-12 wt. %), absence of sulfur and aromatic contents makes it blendable with diesel and hence reduce dependency on diesel fuels (Dwivedi et al., 2011; Khalife et al., 2017).

Oxygenated additives like alcohols and biodiesels reduce brake thermal efficiency (BTE) and brake specific fuel consumption (BSFC) of the engine because of their low calorific value. Alcohols induce ignition delay because of high latent heat of vaporization and low cetane number hence decrease power and torque. Higher NOx emissions in case of biodiesel and alcohols is problematic due to their high oxygen content, therefore antioxidants blending is required for the reduction of NOx emissions. There is a considerable reduction in emissions of PMs, and sulphur by blending alcohols and biodiesel with diesel oil. High oxygen content and lower aromatics may be the cause of this behavior. However, properties specifically of

biodiesel like high density and viscosity make them difficult for atomization in air. Water-in-diesel oil emulsions on the other hand have emerged as a new alternative. It has been now consistently reported that NOx and PM are specifically reduced by water emulsified fuels. NOx and PMs reductions up to 30% and 60%, respectively, have been reported by water emulsification up to 15% (water) in emulsions (Vellaiyan and Amirthagadeswaran, 2016b).

1.2 THEORY OF EMULSIONS

Emulsions are example of colloids in metastable state. Emulsion comprise of two immiscible liquid phases wherein one phase being dispersed in the other in the presence of surface active agent. They are formed by shearing two immiscible fluids that leads to the fragmentation of one phase dispersed into the other (Leal-Calderon et al., 2007).

Two types of emulsions are possible, two and three phase emulsions. Two phase emulsion depends on continuous and dispersed phase concentrations, surfactant properties and mixing type (Chen and Tao, 2005; Hasannuddin et al., 2016; Kundu et al., 2013; Stalidis et al., 1990). Classification of these emulsions is water-in-oil (w/o) and oil-in-water (o/w) (Chiaramonti et al. 2003). If the dispersed phase is water, emulsion is known as w/o emulsion whereas the reverse is known as o/w. Moreover, formation of w/o emulsion takes place when stabilizing agent or surfactant is solubilized in oil phase, however o/w emulsion forms when surfactant is solubilized in water phase. Three phase emulsions are classified based on the dispersed phase and continuous phase as w/o/w (water-in-oil-in-water) and o/w/o (oil-in-water-in-oil) emulsion. Application of water-in-oil-in-water emulsions lies in cosmetics, food and pharmaceutical products, whereas, oil-in-water-in-oil emulsion has application in engines as fuels (Lin and Wang, 2004a). Based on the droplet size of the dispersed phase, emulsions can be classified as macro-emulsion (0.1-5 μm) showing kinetic stability, nano-emulsions and micro-emulsions (5-50 nm) depicting thermal stability (Solans et al., 2005; Tadros, 2013).

HLB system determines the type of surfactant used for a particular emulsion system (4-8: w/o; 8-10: bi-continuous; 10-18: o/w). The important property a surfactant should possess is its burning without polluting the environment (Lif and Holmberg, 2006; Nadeem et al., 2006). Some of the studies reveal burning of non-ionic surfactants ecofriendly in the combustion chamber (Vellaiyan and Amirthagadeswaran, 2016b).

Nano-emulsions are non-equilibrium systems and hence cannot be formed spontaneously or the requirement of energy is indispensable to generate the droplets (Pey et al.,

2006; Porras et al., 2008; Tadros et al., 2004). Subsequently, the required energy input may be achieved either from mechanical devices or from the chemical potential of the components by implementing high (e.g., high shear stirrer, high-pressure homogenization, ultrasonics, and microfluidization) or low (e.g., phase inversion temperature or PIT) energy input methods (Al-Sabagh et al., 2011; Anton and Vandamme, 2011; Solans and Solé, 2012; Vellaiyan and Amirthagadeswaran, 2016b).

High-energy methods have the advantage of controlling droplets size, although the high energy requirement to overcome the interfacial tension of the two immiscible phases limits the use of these methods (Noor El-Din et al., 2013b; Peng et al., 2010; Yukuyama et al., 2016). Alternatively, low energy methods have gained recognition in the last decade as they employ the energy stored in the system by applying a comparatively lower amount of energy or by gentle mixing to create nanometer droplets of mono-dispersity (Feng et al., 2016; Yukuyama et al., 2016). Application of this method may be achieved by three different ways: (1) drop-wise addition of water in the premixed solution of oil and surfactant, (2) drop-wise addition of oil in the premixed solution of water and surfactant, and (3) simultaneous mixing of all components in required compositions.

1.2.1 Emulsification mechanism

Emulsification process being non-spontaneous shows tendency to separate the phases, therefore high energy is required for the preparation of emulsion oil. In this process expansion of interface takes place by the energy input of $\Delta A \gamma$ magnitude, where ΔA is the incremental interfacial area from A_1 of the bulk of the oil to the A_2 of new large number of droplets produced ($A_2 > A_1$), γ is interfacial tension of dispersed and continuous phase system. As γ has positive value, energy required to expand the surface is large and positive. Since the term $T\Delta S$ (entropy of dispersion) in Eqn. (1.1) is also positive and small, ΔG is positive, indicative of non-spontaneous emulsification process. Hence energy is required to form the droplets (Tadros et al., 2004).

$$\Delta G = \Delta A \gamma - T\Delta S$$

$$(1.1)$$

The formation of macro-emulsion consisting of large droplets of few micrometers, is therefore, comparatively easy and as a result high speed mixers are sufficient to form the emulsion. Instead formation of very small droplets of the order of nanoscale requires either high energy requirement or large amount of surfactant or both simultaneously.

1.2.2 High energy requirement

Formation of nano-emulsions by implementing high energy can be explained by Laplace pressure p, the difference in pressure between inside and outside the droplet (Tadros et al., 2004).

$$p = 2\gamma[\frac{1}{r_1} + \frac{1}{r_2}]$$ (1.2)

Where r_1 and r_2 refers to the principle radius of curvature of the drop are. Since, for a spherical drop, $r_1 = r_2 = r$, Eqn. (1.2) reduces to

$$p = 2\gamma\left[\frac{1}{r}\right]$$ (1.3)

Breaking of a droplet into smaller drops needs high shearing that increases the value of p. Deformation of spherical drop into the smaller prolate ellipsoidal drops needs more stress for deformation. This stress is transmitted by the surrounding liquid requiring violent agitation and hence more energy is required to form small droplets.

1.2.3 Role of surfactant

In the formation of emulsions, significant role is played by surfactants. Surface active agents lower the interfacial tension and hence reduce the value of p (Eqns. 1.2 and 1.3). Consequently, lower stress is required to deform the drops. Moreover, surfactants avoid coalescence of newly formed drops. Emulsification process is basically a dynamic process in which two competing process takes place, disruption of the bulk liquid in to smaller droplets and recombination of newly formed droplets.

1.2.4 Types of surfactants used in nano-emulsion formation

Surfactants are used in the formation of nano-emulsions because of their property to reduce surface tension whereas, a layer of surfactant on the nano droplet avoids colliding of the droplets with each other. Classification of surfactants is carried out considering type of hydrophilic group as:

(i) Anionic: hydrophilic head consists of a negative charge

(ii) Cationic: hydrophilic head consists of a positive charge

(iii) Nonionic: hydrophilic head retains no charge

(iv) Zweitterionic: hydrophilic head retains both negative and positive charges

Polyelectrolytes such as poly (methacrylic acid) can also be applied as emulsifiers. Mixtures of polymers and surfactants are ideal in achieving ease of emulsification and stabilization of the emulsion. Lamellar liquid crystalline phases that can be produced using surfactant mixtures are very effective in emulsion stabilization. Solid particles that can accumulate at the o/w interface can also be used for emulsion stabilization. These are referred as Pickering emulsions, whereby particles are made partially wetted by the oil phase and by the aqueous phase (Tadros, 2013). The selection of surfactants for a particular application is based on their HLB values (Table 1.1).

Table 1.1: Surfactants classification based on their HLB values

Types of surfactants	HLB range
Oil soluble	<10
Water soluble	>10
Anti-foming agent	4-8
Water-in-oil emulsifier	7-11
Oil-in-water emulsifier	12-18 or >18
Wetting agent	11-14
Detergent	12-15
Solubilizer	16-20

1.2.5 Methods of emulsion formation

It is critical to understand the physics of formation of nano-emulsion for controlling the droplet size of nano-emulsion. Since emulsion formation inherently obligates $\Delta G=+ve$, application of external energy to the system is mandatory for producing the nano-drops (Pey et al., 2006; Porras et al., 2008). In the process of producing nano-emulsions, energy input to the system may be applied either of two ways high or low energy method. Formation of nano-sized emulsion needs high energy compared to the micro-emulsion as nano-sized droplet needs high energy since large Laplace pressure ($p=2\gamma/r$) is required to deform a spherical droplet of radius, r. High shear/pressure homogenizer, ultrasonication and microfluidization (Solans et al., 2005) are examples of high energy method. Application of high energy though produces tunable nano sized droplets with control over emulsion characteristics (Ramisetty et al., 2015). Low energy input method employs change in chemical potential of the components through phase inversion

temperature where surfactant reduces the interfacial tension γ that sequentially reduces the Laplace pressure p.

According to Tadros (Tadros, 2013), techniques of emulsions formation can be classified based on energy input (Low, medium or high) to the system or on mode of operation (batch/continuous):

- Low energy: Simple pipe flow includes low agitation energy.
- Low to medium energy: Static mixers and magnetic stirrers or general stirrers.
- Medium energy: High-speed mixers. Ultrasonication.
- High energy: High shear or pressure homogenizers.

Further they can be classified based on batch or continuous operation or based on simultaneous batch/continuous method:

- Pipe flow & static mixers (Continuous operation)
- Stirrers & Ultraturrax (Batch/ Continuous operation)
- Colloid mill & homogenizers (Continuous operation)
- Ultrasonication (Batch/ Continuous operation)

1.2.6 Droplet breakup in laminar flow

First step involves low energy method where mechanism of splitting of droplets is achieved in viscous shear flow (Boxall et al., 2012; Hinze, 1955) applied through rotating flow. Droplets deform into prolate ellipsoidal shape (Hinze, 1955; Tadros et al., 2004). Stress exerted on a drop during laminar flow (η_c U), is balanced by Laplace pressure that can be represented as dimensionless Weber number (Walstra, 1993) as shown in Eqn. (1.4):

$$W_e = \eta_c U r / \gamma \tag{1.4}$$

where, η_c and η_d are the viscosities of continuous and disperse phase, respectively, U and r indicates the velocity gradient and droplet radius r, respectively. Droplet breakup takes place when Weber number exceeds critical Weber number (Eqns. 1.5 and 1.6), i.e.

$$W_e > W_{e,crit} \text{ : Droplet breaks} \tag{1.5}$$

$$W_{e,crit} = f\left(F\text{low type}, \eta_d / \eta_c\right) \tag{1.6}$$

7

1.2.7 Droplet breakup in turbulent flow

Second step involves the use of high energy method (ultrasonication), at optimized parameters. At high Reynolds number and smaller length scale, isotropic turbulence exists and flow is characterized by Kolmogorov theory. Range of eddy sizes is obtained in that case, where the lower eddy size contains higher velocity gradient till gradient is so high that eddy dissipate their kinetic energy into heat. The smallest size of eddy is known as Kolmogorov scale and below than that size possibility of droplet deformation is not possible. Fairly larger eddies are known as energy-breaking eddies accountable for droplet break up. Largest eddy that exists in turbulent flow regime is calculated by Eqn. (1.7) (Leong et al., 2009).

$$D_{max} = CP_v^{-2/5}\gamma^{3/5}\rho_c^{-1/5} \tag{1.7}$$

where C is a constant, P_v is power density and ρ_c is density of the continuous phase. Karbstein and Schubert though argued about uneven distribution of power density. Therefore, a concept of power density and residence time t_R was used in the above Eqn. (1.7) (Karbstein and Schubert, 1995; Leong et al., 2009). Formation of nano-emulsion requires intensive shear force produced by high power ultrasonication through acoustic cavitation that involves formation and rapid growth of microbubble produced by cyclic pressure variations (Gupta et al., 2016; Leal-Calderon et al., 2007; Peshkovsky et al., 2013). Cycle is repeated until a critical size (r_c) of bubble is obtained. The bubble eventually implodes and generates a localized hot spot comprising of high temperature (≈5000K) and pressure (≈1000 bar) (Leal-Calderon et al., 2007; Sivakumar et al., 2014). Capability of ultrasonication regarding generation of drops<100nm has been reported by many researchers (Carpenter and Saharan, 2017; Leong et al., 2009; Sivakumar et al., 2014) that provides longer stability due to smaller droplet size.

1.3 STABILITY OF NANO-EMULSIONS

Emulsion stability can be defined as the emulsion ability to resist the changes in the properties as time progresses. Hence the more stable the emulsion, more slowly its properties will be changing in terms of coalescence, breaking, creaming and flocculation.

The stability of emulsions can be understood by four major mechanisms viz. creaming or sedimentation, flocculation, coalescence, and Ostwald's ripening. First two mechanisms represent a reversible process wherein size of the droplets are retained. On the other hand, later two mechanisms represent an irreversible breakage of the droplets. Breakdown processes of

emulsions may take place during storage that depends on droplet size distribution and difference in densities of droplets and continuous phase. Flocculation is determined by the magnitude of the attractive vs. repulsive forces. Stability of emulsions is desired in case where they can be stored for a longer time like water-in-diesel emulsion, dispersion of essential oils in water, personal care products and food grade emulsions, etc. Whereas, in some cases like drug delivery system, oil recovery, etc. breaking of emulsion is accomplished by environmental conditions like temperature and pH and considered as a necessary step.

Based on difference in density between medium (continuous phase) and droplet (dispersed phase), various breakdown processes may take place when emulsion is stored for a longer period of time. Flocculation is determined by the extent of the attractive versus repulsive forces. Ostwald ripening is determined by dispersed phase droplets solubility and distribution of particle size. Coalescence is determined by film surrounding the droplet, i.e. kept suspended in the medium. The other process is phase inversion (Tadros, 2013). Creaming or sedimentation does not occur in nano-emulsions due to negligible gravitational force experienced on miniscule size. Moreover, Brownian motion is enhanced at excessively small droplet size of nano-emulsions. Furthermore, flocculation is also reduced at very small particle size. Probable mechanisms defining the increase in droplet size with respect to time in the case of nano-emulsions are coalescence and Ostwald ripening.

1.3.1 Flocculation

Association of particles to form large aggregates in the emulsion defines the Flocculation phenomena. However these aggregates can be easily re-dispersed upon shaking. It is considered as a precondition for the irreversible coalescence. Flocculation differs from coalescence mainly in a fact that individual droplets and interfacial film surrounding the droplets remain intact.

1.3.2 Creaming or sedimentation

The upward or downward movement of dispersed particles is known as creaming or sedimentation, respectively. In emulsions, creaming or sedimentation happens based on the densities of continuous and dispersed phases. Creaming or sedimentation is unfavorable as it may end up in coalescence. Rate of creaming is governed by Stoke's law. Factors affecting rate of creaming are droplet size (creaming is directly proportional to square of droplet radius), and

viscosity of continuous phase (creaming is inversely proportional to viscosity of continuous phase).

1.3.3 Coalescence

The process wherein the dispersed phase particles join to form larger particles is known as coalescence. Mechanical strength of electrical barrier between adjacent suspended particles avoids coalescence and considered as a major factor. Coalescence refers to the phenomena wherein, thinning and disruption of the film surrounding the droplets results in that merging of two or more droplets to form larger droplets. In the limiting case, coalescence leads to separation of the emulsion completely into two distinct phases of liquids. Surface or film fluctuations is the driving force for coalescence resulting in a close approach of the droplets wherein, the van-der-Waals forces appears strong preventing the separation (Tadros, 2013). If coalescence is the driving force for emulsion instability, changes in droplet size with time are described by Eqn. (1.8)

$$\frac{1}{r^2} = \frac{1}{r_o^2} - \frac{8\pi}{3\omega t} \qquad (1.8)$$

where r_o and r represents the avg. droplet radius at time zero and t, and ω is the frequency of rupture in a unit droplet surface area. The coalescence frequency (ω) strongly depends on the size of the droplets and increases with an increase in the size of coalescing drops (Wright and Ramkrishna, 1994). However, smaller droplets are less vulnerable to surface fluctuations and hence coalescence is reduced .

1.3.4 Ostwald's ripening

Instability mechanism based on different in solubility of different sized droplets is explained by Ostwald ripening. Larger droplet grows at the expense of smaller one caused by the molecular diffusion through the continuous phase. According to the Lifshitz -Slezov and Wagner (LSW) theory a relation for the Ostwald ripening rate, ω, is given by the relation Eqn. (1.9):

$$\omega = \frac{dr^3}{dt} = \frac{8}{9}\left[\frac{C_\infty \gamma V_m D}{dRT}\right] \qquad (1.9)$$

where t and C_∞ are the storage time and solubility of the dispersed phase in continuous phase, respectively, γ is the interfacial tension between the continuous and dispersed phases, V_m is the

dispersed phase molar volume, D is the diffusion coefficient of dispersed phase in the medium, d R, and T represents the density, gas constant and absolute temperature. A nano-emulsion with better stability should possess a smaller avg. droplet size and lower values of Ostwald ripening rate.

1.3.5 Phase Inversion

Internal phase becomes external phase. Diagram depicting instability of emulsions by different possible mechanisms explained in the previous sections regarding emulsion braking is shown in Fig. 1.1.
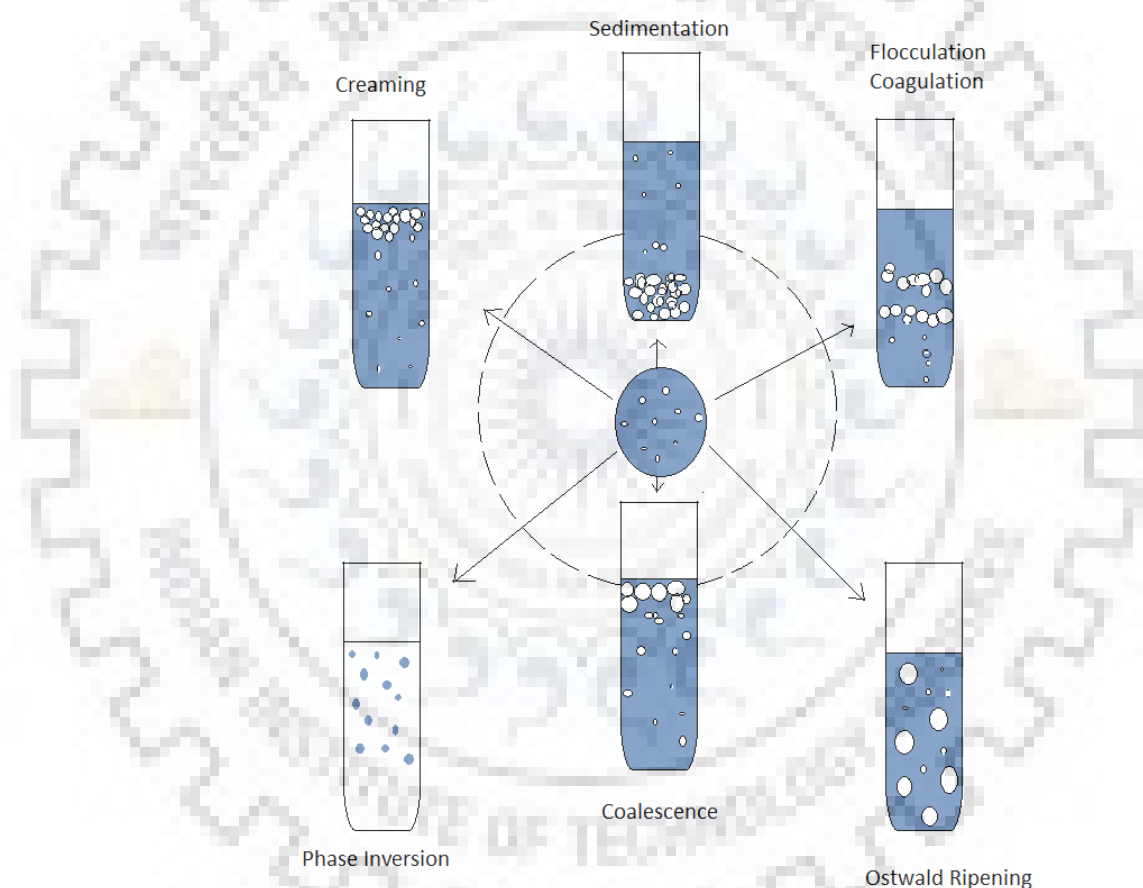
Fig. 1.1: Diagram depicting instability of emulsions by different possible mechanisms of emulsion braking.

1.4 MOTIVATION FOR THESIS AND RESEARCH BACKGROUND

World energy demand is increasing due to ever increasing economic growth that can be directly linked by global increase in gross domestic product (GDP). According to the report of

International Energy Outlook 2017 (IEO2017) global GDP in terms of purchasing power will increase 3% per year from year 2015 to 2040 (Fig. 1.2). Total energy consumption rise in year 2015 as 575 quadrillion Btu to 736 quadrillion Btu in 2040 as 28% rise. To cope up the present scenario though consumption of renewable resources will increase but still 77% fossil fuel will fulfil the demand in year 2040. To avoid the overuse of liquid fuels like diesel and kerosene new technologies are required that not only enhance combustion properties but also improve emission standards. More specifically diesel is used in heavy duty vehicles/ machines comprised of powerful compression ignition (CI) engines. CI engines though provide high torque at low speeds however at the same time limits the environmental issues like NO_x and particulate matter (PM) emissions. There are number of ways to solve the issue like blending of oxygenated fuels with diesel, biodiesel etc. with their own pros and cons like reduction in BTE, BSFC and higher NOx emissions due to high oxygen content.
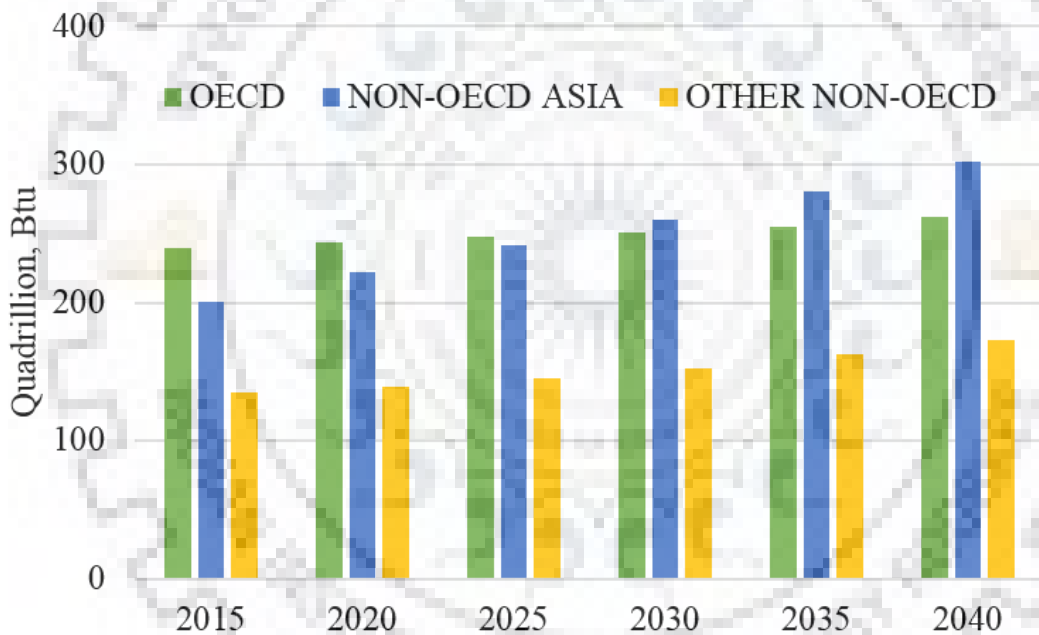
Fig. 1.2: World energy consumption (history and projection) quadrillion Btu. [Source: U.S. Energy Information Administration (May 2017)]

One of the recent research in this context is water emulsified fuel that not only works without any modifications in the engine but also enhance the combustion properties and emission standards due to its properties like high latent heat of vaporization and micro-explosion. Improvement in combustion properties like Brake specific fuel consumption and emission standard such as NOx and particulate matters are reduced. Use of water-in-diesel nano-emulsions have shown good potential towards further reduction in pollutant levels like

NOx and PMs. The growing concern on green technology to protect the environment has encouraged the use of alternative ecofriendly formulations for nano-emulsion fuels. It has been reported that the addition of water to diesel fuel works in following ways (Ghannam and Selim, 2014):

- Significant reduction in the emission of unburnt hydrocarbons and NO_X gases due to reduced temperature in combustion chamber.

- Improved combustion properties like brake specific fuel consumption and increased brake thermal efficiency because of ignition delay and micro-explosion (Ithnin et al., 2014).

- In case of w/o nano-emulsion fuel, smaller size droplets increases surface area that helps in efficient combustion improving BSFC and reducing combustion chamber temperature consequently helping in further reduction in NO_x and PMs. Moreover, their smaller size negates gravity induced separation and they make the balance between Brownian motion and surface induced properties making them stable for longer storage time (Bidita et al., 2014).

The above observations for w/o emulsified fuel, therefore, motivates the development of transparent and stable w/o nano-emulsions. During the storage of emulsions, several breakdown process may occur depending on particle size distribution and density difference among them. Among the four major available mechanisms that explains the stability of emulsion, creaming or sedimentation and flocculation represents reversible breakage under the influence of density difference among the dispersed particles. However, coalescence, and Ostwald's ripening represents an irreversible separation of dispersed phase that negates the influence of gravity on nano-sized suspended particles and explains instability mechanism of nano-emulsions.

Flow behavior and deformation of fluids is an important property that has been described by rheology. There may be the fluids that may show ideally viscous behavior or solids that shows ideally elastic behavior or in between them, viscoelastic fluids that shows both behavior. Emulsion, however, is a mixture of three major ingredients like water, surfactants and oil, therefore, their different mixing percentages may form a different flow behavior fluid. Therefore, it is necessary to assess the relation between shear stress and rate of shear of the formed nano-emulsion. Moreover, formed product, if, behaves as an ideal fluid or follows the Newtonian behavior, makes it easy to transport (or pumping of fluid) without disturbing it structure, even at high shears.

1.4.1 Approach for research and development

Formation of water-in-oil nano-emulsion was achieved by application of low and high energy methods. The approach used in this study was based on development of a ternary diagram that specified the zones of formation of transparent, translucent and opaque emulsions within the bounded range of surfactant (Φ_s), water (Φ_w) and oil (Φ_o) fraction on the weight basis, respectively. Resulted nano-emulsion was then characterized for their droplet size, stability and flow behavior properties (Rheology). Detailed methodology regarding the formation of water-in-oil nano-emulsions (w/o NEs) based on energy input (low/high) to the emulsification process is shown in Fig. 1.3. An isothermal dilution method was adopted in case of low energy input shown as [A] in the Fig. 1.3, however, combined approach of low and high (ultrasonic cavitation) energy input is shown by [B] in the Fig. 1.3. Nano-emulsions formed by application of combined approach was named CEMSNE (combined energy mixed surfactant nano-emulsion).

Development of new products was achieved by optimizing new combinations of non-ionic surfactants used in the formation of w/o nano-emulsions to improve droplet size (nm) and their stability:

1. Span 80 (HLB: 4.3) / Tween 60 (HLB: 14.9): Sorbitan monooleate/ PEG-20 Sorbitan monostearate.
2. Span 80 (HLB: 4.3) / Triton x-100 (HLB: 13.5): Sorbitan monooleate/ Ether and Ester group.

First combination of non-ionic surfactants (S80/T60) was applied in mixed proportions for the formation of w/o nano-emulsions via isothermal dilution method. Whereas, second combination of non-ionic surfactants was used in the formation of w/o nano-emulsions via CEMSNE method.
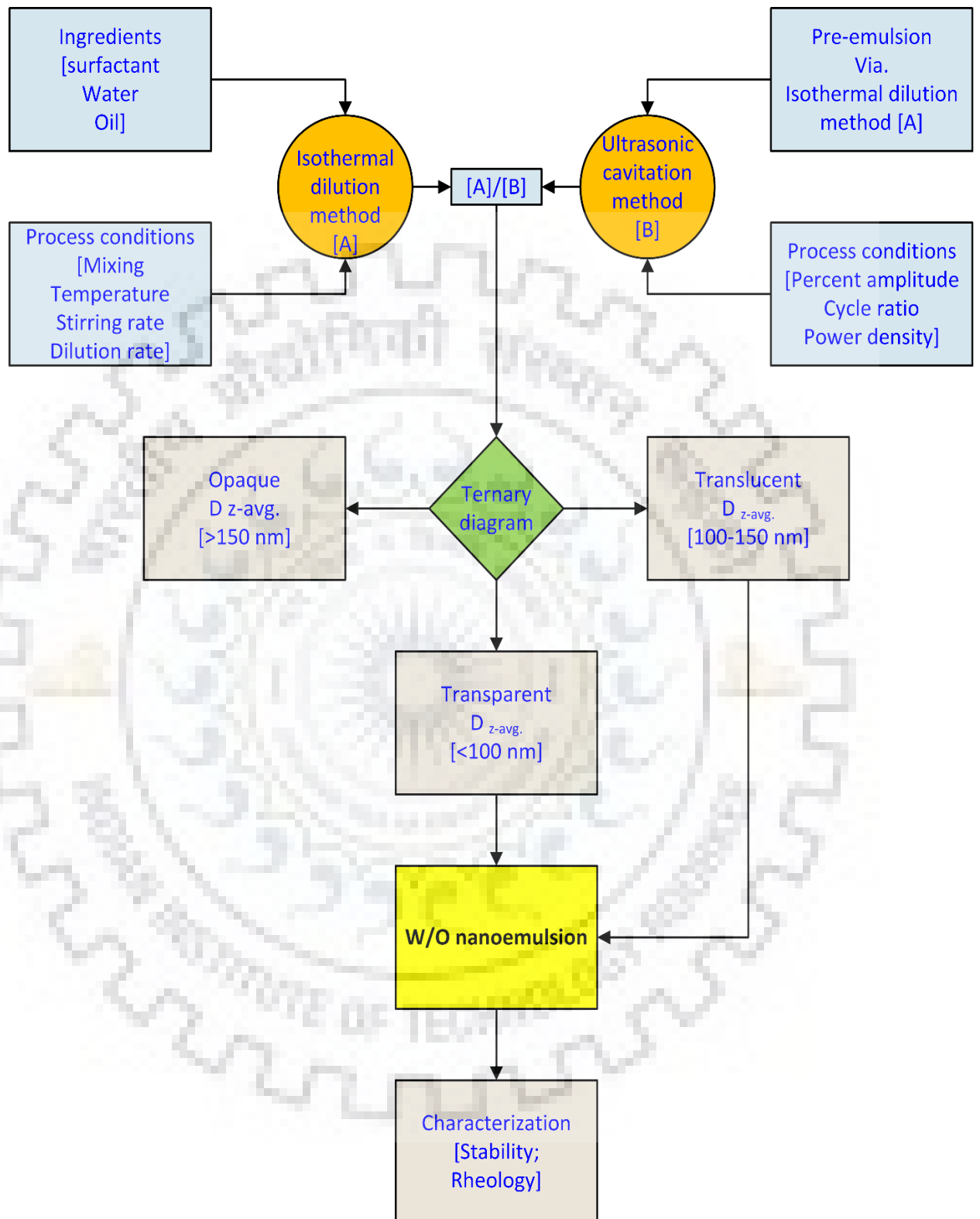
Fig. 1.3: Methodology for the formation of water-in-oil nano-emulsions based on type of input energy (low/high).

1.5 OBJECTIVES

The overall objective of the proposed work is the formation and characterization of water-in-oil (w/o) nano-emulsion fuel system for their longer stability and rheological behavior. The specific objectives of the proposed research work are as follows:

- To select an emulsifying agent for the preparation of water–in–oil (w/o) nano–emulsions.
- Preparation of water-in-oil (w/o) nano-emulsion by phase inversion and high energy methods.
- To develop ternary phase diagram and investigate the phase behavior of ternary systems consisting of diesel oil, non–ionic surfactant and water at different ratios, by application of phase inversion and high energy method.
- Find out scale up parameter for the formation of w/o nano-emulsions.
- To prepare w/o emulsion using high energy method and investigate the effect of process parameters on the droplet size and stability of the emulsions.
- To study the rheological behavior of w/o nano-emulsion.
- To optimize the effect of concentration of surfactants and water on the formation of w/o emulsions through various optimization techniques.

1.6 THESIS ORGANIZATION

Based on the objectives of the proposed work, thesis has been organized into the six sections in the form of chapters explained as follows:

Chapter 1 introduces the background and motivation of the thesis. Objectives are explained with the thesis organization.

Chapter 2 explains the critical review regarding the formation of nano-emulsions by application of low as well as high energy methods, stability and rheology of the water-in-oil nano-emulsions.

Chapter 3 explains the methodology of w/o nano-emulsion formation, and emulsion characterization techniques. Statistical modeling and optimization techniques for the formation of w/o nano-emulsion are also explained in this section.

Chapter 4 describes the preparation of w/o nano-emulsions by means of low (isothermal dilution method) and high (ultrasonication) energy methods. Optimization of HLB value for mixed non-ionic surfactant systems along with detailed discussion about ternary diagram is explained. Stability analysis of w/o nano-emulsions through different mechanisms is also included in the section. Furthermore, the rheological behavior of nano-emulsion samples formed by application of mixed surfactants and different preparation methods is also been studied. Different rheological models were fitted to explain flow behavior of nano-emulsions. Effect of temperature on rheological behavior is also described in this section.

Chapter 5 describes the different optimization techniques for finding the optimal process parameters responsible for the formation of w/o nano-emulsions. Response surface methodology, artificial network and hybrid genetic algorithm techniques were used in optimizing the variables.

Chapter 6 summarizes the overall conclusions inferred from the work and possible recommendations helpful in carrying out the research work in future.

CHAPTER 2
LITERATURE REVIEW

Nanotechnology has been evolved in past two decades specifically in the formation of nano-particles. Whereas, nano-emulsion formation has started in past decade and finds wide applications in the field of pharmacy, food, petroleum sector as means of enhanced fuel recovery and transportation sector as an emulsified fuels. In recent years, ample work has been carried out in the field of formation of nano-emulsions through various techniques based on energy supplied to the system. Mechanism of droplet deformation has been reviewed in different flow regimes that can be precisely helpful in process scale up and nano-emulsion formation. Studies on performance and characteristics of water/diesel nano-emulsion can be specifically helpful in finding the composition of all constituents and type of surfactant giving better emission standards and combustion properties. Nano-emulsion characterization techniques specifically in terms of their stability and rheological properties has been reviewed in this chapter.

2.1 FORMATION OF NANO-EMULSIONS

A detailed literature survey has been carried out on the preparation and characterization of nano–emulsions (NEs). It has been found that little attention has been made in the formation of nano-emulsions as compared to the emulsions at micro-level. Most of the work available in the literature is carried out during the last decade and it is continuously gaining attention (Table 2.1).

Principles of formation and stability of nano-emulsions (NEs) was explained and reviewed in detail by Tadros et al. in the year 2004. The concerned study emphasized on the benefits of nano-emulsion onto macro-emulsion for cosmetics and personal care products. Moreover, difficulties regarding lacuna in the development of nano-emulsions were explained in detail. In the subsequent section emulsification mechanism and size measurement of nano-drops via dynamic light scattering technique were explained in detail. Three different methods of preparation of nano-emulsions specifically low and high energy, and phase inversion temperature was explained. Role of thickness of adsorbed layer on dispersed phase and steric stabilization was defined thoroughly. Explanation about key instability mechanism like Ostwald ripening and their possible remedial methods of reduction was reported. Study included some practical examples of nano-emulsion prepared by phase inversion temperature

as well as high pressure homogenizer and both methods were compared with Ostwald ripening rate. An important study about changing the length of alkyl group and branching of oil by considering examples of decane, dodecane, tetradecane, hexadecane and iso-hexadecane revealed that the branched chain oil like iso-hexadecane consists higher Ostwald ripening rate compared with linear oil chain possessing same carbon number.

Porras et al. (2004) studied w/o NEs formation by condensation method using a mixture of non-ionic surfactants (Span 20, Span 80, Tween 20 and Tween 80) as an emulsifying agent. Optimization of the mixed surfactants with respect to HLB values showed better performance than pure surfactant. Regions of nano- and microemulsion were investigated by measuring droplet sizes using dynamic light scattering. Droplet size in the range of 30-120nm were obtained in the study and it was inferred that bigger droplets size were formed due to high water percentage in the sample. Stability of nano-emulsion samples showed evolution of droplet size with time. Ostwald ripening instability mechanism found applicable in case of low water concentration, whereas, coalescence breakdown mechanism attributed to high water concentration.

More details on the formation of nano-emulsions (20-200 nm) and their classification into mini-emulsion, ultrafine emulsion and submicron emulsions was summarized by Solans et al. in the year 2005. Properties and applications of nano-emulsions were reviewed by taking suitable examples. In this article more emphasis was given to low energy emulsification or condensation methods (based on phase transition methods) as compared to high energy methods to produce oil-in-water (o/w) or water-in-oil (w/o) nano-emulsions (NEs). A phase behavior study was performed and concluded that droplet size is controlled by phase structure of surfactant either lamellar or bicontinuous micro-emulsion at the inversion point induced by either temperature or composition. Explanation about stability of nano-particles was given owing to their small droplet size that stabilizes them against creaming or sedimentation depicting Ostwald's ripening as a key instability mechanism of nano-drops. An application of nano-emulsions was explained in reference of formation of complex polymeric materials along with hybrid inorganic/organic materials, such as magnetic polymeric nano-spheres. New applications like controlled drug delivery and targeting was also explained as an active development.

Emulsion inversion point method was used by Sole' et al. in the year 2006 in forming the nano-emulsions in the ionic system consisting of oleic acid–potassium oleate in the formation of o/w (hexadecane/water) emulsion by condensation (Solè et al., 2006). To obtain

nano-emulsions containing 80% water, potassium hydroxide solution was added to oleic acid–C12E10/hexadecane solutions at a constant temperature of 25 ºC with a stoichiometry ratio of oleic acid/KOH. In doing so, formation of the ionic surfactant (potassium oleate) took place alongside the emulsification path in an equilibrium phase diagram. Ostwald Ripening was found as most probable breakdown mechanism of the nano-emulsions.

Pey et al. in the year 2006, optimized preparation of nano-emulsions by low energy (LEM) emulsification methods at a constant temperature by using a factorial design. In this study composition and methods of preparation of o/w nano-emulsions were optimized by adding one of the components at a constant emulsification temperature. Process variables were optimized using central composite design that generates response surfaces describing nano-emulsion preparation method. This work concluded that droplet size and polydispersity index changes as a change in composition and preparation method is made. A linear relationship between o/s ratio and droplet size was obtained with the inference that high surfactant percent produces lower droplet size. Moreover a linear relationship between addition rate and droplet size was obtained as a result of CCD-RSM optimization.

A process of formation of oil-in-water nano-emulsions for pesticide formulations was described by Wang et al. (2007) using poly (oxyethylene) nonionic surfactant. Formation of nano-emulsion for the system water/methyl decanoate was described in two steps at 25 ºC. In the first step, all constituents were mixed at a certain composition to form a micro-emulsion concentrate, thereafter, a rapid large dilution of concentrate (micro-emulsion) in water formed nano-emulsion. Study revealed that bluish color transparent o/w nano-emulsions formed only in the bi-continuous micro-emulsion (BC) or o/w micro-emulsion (Wm) region. Optimum ratio of oil/surfactant in the region of BC or Wm phases specifies the phase behavior and concentrate composition as significant factors in the formation of nano-emulsions. The system developed in the study was employed in formulating a pesticide β-cypermethrin (water-insoluble) nano-emulsion. A comparison of pesticide, thus obtained, and commercially available β-cypermethrin micro-emulsion was done in terms of stability of formulation sprayed on substrate.

Gutiérrez et al. in the year 2008, reported that nano-emulsions as non-equilibrium system possessing properties and characteristics that not only depend on composition of constituents but also on the methods of their preparation. The researcher further explained that nano-emulsion formation was started about two decades back specifically in the formation of nanoparticles but in the recent years nano-emulsion formation found applicable specifically in

the field of pharmaceuticals and cosmetics targeting consumer products. Necessity of optimization techniques was explained for preparation of nano-emulsions considering recent applications.

Wooster et al. (2008) examined that transparent and stable nano-emulsions formation poses two challenges, like the formation of nano-emulsion consisting droplet size distribution < 80 nm and to stabilize the nano-emulsion against Ostwald ripening effect. It was further revealed that the formation of nano-emulsion and their stability specifically depends on the oil phase physical properties and surfactant layer nature. Study revealed that the higher the viscosity of oil phase in case of long chain triglycerides resulted in large droplet diameter measuring 120 nm, whereas, lower viscosity oil like hexadecane resulted in smaller diameter measuring 80 nm. Considerably small diameter nano-emulsions were formed when surfactant and ratio of dispersed and continuous phases viscosity (η_d/η_C) was optimized. Low viscosity samples like long chain triglycerides (LCT) showed outstanding stability not undergoing Ostwald ripening and nano-emulsions could stabilize up to 3 months. Prevention of Ostwald ripening was achieved by means of larger amount of long chain triglyceride oils that makes them water insoluble. Therefore, a kinetic barrier to Ostwald ripening was provided by LCT.

Optimization of the w/o NEs system using low energy method (LEM) was achieved by Peng et al. (2010). A system water/mixed surfactants viz. polyoxyethylene 2-lauryl ether ($C_{12}E_2$) and polyoxyethylene 4-lauryl ether ($C_{12}E_4$)/isohexadecane was studied by changing ratio of mixed surfactant, concentration of oil and mixed surfactant in the nano-emulsion. The system was characterized by HLB temperature and study of phase diagram. Coalescence and Ostwald ripening mechanisms were tested for instability of the formed nano-emulsion by measuring change in droplet size with respect to time. Study concluded that minimum droplet size with higher stability was obtained in case of mixed surfactant as compared to the single surfactant. Composition of nano-emulsion was optimized to give high storage capability of 200 days period. Optimum composition of formed w/o nano-emulsion was found as 70:6:4:20 for the system water/ mixed surfactant ($C_{12}E_2/C_{12}E_4$)/isohexadecane ratio on weight basis.

Water-in-diesel nano-emulsion formation and their properties related to surface activation was studied by Al-sabagh et al. (2011). Non-ionic surfactants were used to study the stability of the system viz. Tween 80 and Emarol 85 in mixed proportions. Three different water compositions of 5, 10 and 14% on volume basis were used in the study to observe the effect of water percent on nano-emulsion formation. Stabilization of nano-emulsion was performed using individual surfactant and their mixed proportions, respectively.

22

Thermodynamic properties and interfacial tension of individual and blended emulsifiers were studied. Critical micelle concentration and surface active properties of w/o nano-emulsions were assessed by the interfacial tension measurements at a constant temperature of 30 ºC. Droplet size in the range of 19-39 nm were obtained depending on water and mixed surfactant composition in the nano-emulsion. This study revealed that blended surfactant gave minimum surface tension of 10.85 mN/m as compared to individual surfactants like Emarol 85 and Span 80 as 12.77 and 17.13 mN/m, respectively. TEM images of formed emulsions supported the droplet sizes obtained by dynamic light scattering technique.

Difference between nano-emulsions and micro-emulsions, their terminology, differences in various aspects, and similarities were reviewed by McClements in the year 2012. Specific use of nano and micro-emulsion in food and pharmaceutical in the context of delivering lipophilic bio-active compounds, encapsulation and protection was explained. Study revealed that droplet sizes, r < 100 nm gave excellent properties like long term stability, transparent appearance and enhanced bioavailability. A study further explained that microemulsions are thermodynamically stable, whereas nano-emulsions does not show that behavior. Differences and similarities among nano and micro emulsions were reviewed in context of their method of formation, properties, stability and compositions.

Formation of nano-emulsion by micro-emulsion dilution was studied by Solè et al. (2012) to predict the effect of different dilution processes on the properties of o/w nano-emulsions attained by diluting of w/o and o/w micro-emulsions. A model system was chosen as water/SDS-co-surfactant/dodecane using co-surfactant either pentanol or hexanol. In the process of dilution, step-wise addition of micro-emulsion (or water) over water or addition in a single step over water (or micro-emulsion) was followed. In case of diluting o/w micro-emulsion with water, nano-emulsion obtained measured droplet size as 20 nm independent of the method of dilution and micro-emulsion composition. Conversely, w/o micro-emulsion dilution resulted in o/w nano-emulsion only when the conditions allowed in the micro-emulsion domain. Addition of hexanol as co-surfactant compared to pentanol gave lower droplet size, polydispersity and higher stability.

Noor El-Din et al. (2013a) worked on preparation and stability of water-in-diesel (w/d) fuel nano-emulsions prepared by high energy method (HEM). Mixed nonionic surfactants were used to prepare w/d fuel nano-emulsions with five emulsions consisting of different water contents ranging from 5 to 9% (w/w). Optimized HLB value was searched by making five different nano-emulsions consisting of different ratios of sorbitan monooleate and

polyoxyethylene (20) sorbitan monooleate resulting HLB values ranging from 9.6 to 10.4. Droplet size formation was studied by varying the concentration of water, mixed surfactant and HLB value of the prepared nano-emulsion samples. Droplet sizes ranging from 49.55 to 190.1nm were obtained during the study.

A study performed on non-ionic (Span 20/ Tween 20) and ionic surfactants (CTAB-cetyltrimethylammonium bromide /SDS-Sodium dodecyl sulfate) by Xin et al. (2013) explained the effect of surfactant concentration on stability of nano-emulsions through zeta-potential measurement. Formation of nano-emulsion was achieved by emulsion inversion phase method at 25 °C. Study was carried out as change in properties with amount of emulsifier agent and addition of ionic surfactants CTAB and SDS. It was revealed that increase in surfactant (Span 20/ Tween 20) concentration decreased droplet size and PDI (polydispersity index). Likewise droplet diameter decreased with an increase in CTAB and SDS concentration. Value of zeta potential without SDS and CTAB found negative whereas, more negative values of zeta potential found in case of SDS indicative of better electrostatic interaction between droplets and hence showing better stability. Conversely, increase in CTAB concentration showed less negative zeta potential showing weak electrostatic interactions between droplets hence showing lower stability. As a result, zeta potential was found as one of the key parameter responsible for nano-emulsion stability.

Table 2.1: Process parameters, surfactant used and method of formation of nano-emulsions.

S. No.	Ref.	Objectives	Surfactant used	Parameters	Methods	Remarks
1.	Tadros et al. (2004)	Reviewed the formation and stability of nano-emuslions (NEs). Comparative study of two methods was done by taking hexadecane and iso-hexadecane as the oil phase/non-ionic emulsifier/ water system. (O/W nano-emulsion)	Non-ionic surfactant -Brij 30 ($C_{12}EO_4$)	25-80 nm globule size at 3-8% surfactant concentration	PIT and high energy homogenizer	1. Droplet size and PDI decreased with increase in surfactant conc. in both iso-hexadecane and linear hexadecane 2. The branched oil iso-hexadcecane showed higher Ostwald ripening rate when compared to linear chain oil.
2.	Porras et al. (2004)	Preparation of w/o NEs in water /mixed non-ionic surfactant /oil system 2. The appropriate ratio between two surfactants was studied. (W/O Nano-emulsions)	Mix. of S20, S80, T20 and T80	30 and 120 nm globule size. (Ternary diagram was studied at different W /Surfactant /O percentage)	Condensation method	Higher the water conc. (W %), higher the globule size. NE breakdown corresponded to Ostwald ripening and coalescence for low and high W%, respectively.
3.	Solans et al. (2005)	Preparation, properties and applications of NEs in polymeric nano-particles by using a monomer as the disperse phase	Surfactants containing a polymerizable group used in NE polymerization	20-200 nm droplet size (same in both preparation method)	HEM and LEM emulsification System :	For LEM, the size of the droplets controlled by the surfactant phase structure (Bicontinuous micro-emulsion or lamellar) at the phase inversion point.

4.	Solè et al. (2006)	Nano-emulsions preparation by low energy methods for system, water/oleic acid–potassium oleate–C12E10/hexadecane.	Potassium oleate (Ionic surfactant)	17 nm at R= 30/70 (hexadecane / [oleic acid–C12E10(3/7)]). Transparent. O/W (80%W) at 25ºC.	Low energy method (Emulsion inversion point method)	Formation of NE for the present system was achieved only when equilibrium was achieved in a cubic liquid crystal phase.
5.	Pey et al. (2006)	Optim. of composition and preparation method of NEs O/W by addition of one of the components at a constant temperature. System: (water–Tween 20/Span 20–liquid paraffin)	Tween 20, Span 20	80.6 - 164 nm to 70% Water (w/w) at different O/S ratio.	Low-energy emulsification .	1. Lower droplet sizes attained by applying higher surfactant %. 2. The best NE droplet size attained at lowest addition rate of dispersed phase.
6.	Wang et al. (2007)	Oil-in-water nano-emulsions for pesticide formulations. System (water/poly(oxyethylene) nonionic surfactant/methyl decanoate) at 25 ºC	Poly (oxyethyl-ene) lauryl ether, with 7 moles of ethylene oxide per surfactant molecule.	28 nm (bluish, transparent) with 50% water, At constant o/s ratio (ROS=1)	Low-energy emulsification	Micro-emulsion was formed first, thereafter, its large dil. in water formed bluish NE, based on equilibrium phase diagram.
7.	Gutiérrez et al. (2008)	New applications of nano-emulsion and optimization of their preparation.	The incorporation of retinol to a self-nanoemulsifying formulation was studied.	20-200 nm regardless of preparation method.	Low-energy emulsification	High oil/surfactant ratio, produced greater droplet sizes, however, NE formation was based on optim. HLB and mixed surfactant ratio.

8.	Wooster et al. (2008)	Impact of oil type on NE formation and stability. High (long chain triglycerides (LCT) and low (hexadecane (D)) viscous oils were compared for droplet sizes formed during nano-emulsification process.	SDS (0.5-5.6 wt. %) and PEG (0-18.9 wt. %)	<40 nm to 120 nm	Microfluidics M-110Y Micro-fluidizer TM	High viscous oil produced larger droplets (120 nm), however low viscous oils formed 80 nm. Optimization of surfactant and η_D/η_C, (viscosity ratio), formed smaller size NEs
9.	Porras et al. (2008)	Properties of w/o NEs formed by LEM was described. A system water/mixed non-ionic surfactant/decane was used in NE formation.	S20, S80, T20 and T80	30 nm to 120 nm.	low-energy emulsification	Optim. w/o micro-emulsion formed in 8–12, HLB range. NE formation achieved by varying Span/Tween ratio, and W% at a const. surfactant/oil ratio.
10.	(Peng et al., 2010)	Optimization of w/o NEs by mixed surfactants. System: isohexadecane/mixed nonionic surfactant/water	$C_{12}E_2$ and $C_{12}E_4$	21nm	low-energy emulsification	Optimized ratio for w/o NEs for isohexade-cane/$C_{12}E_2$/$C_{12}E_4$/water found as 70:6:4:20 (w/w). Optimized w/o NEs formed at 7.48 HLB value and mixing ratio of 6:4 $C_{12}E_2$ to $C_{12}E_4$
11.	Al-Sabagh et al. (2011)	Formations of water-in-diesel oil NEs using water/ mixed non-ionic surfactant /diesel oil system.	Span 80 and Emarol 85	19.3 and 39 nm	HEM ultraturrax homogenizer	Stability of emulsions increased with increase in total emulsifier conc. at low water content.

		Three emulsions with water composition as 5%, 10% and 14% (v/v)) using different water contents were studied.				Surfactants Span 80 and Emarol 85 in mixed form provided nano-sized droplets
12.	Solè et al. (2012)	Effect of different dil. methods on the properties of o/w NEs achieved by dil. of o/w and w/o micro-emulsions. System considered: water /SDS /co-surfactant / dodecane	SDS with co-surfactant hexanol or pentanol	20 nm	LEM	Alcohol as co-surfactant played a key role on the properties of the NEs. Hexanol used a co-surfactant produced NEs with smaller size, lower in PDI, and high stability compared to pentanol.
13.	Noor El-Din et al. (2013b)	W/D fuel NEs were prepared with mixed non-ionic surfactants. Emulsions with different water compositions (w/w) viz. 5, 6, 7, 8, and 9% prepared.	poly-oxyethylene (20) sorbitan monooleate & sorbitan monooleate	49.55 and 190.1 nm	high-energy method (turbine homogenizer	Ostwald ripening described the stability mechanism. Reduced ripening rate observed with increase in surfactant conc. Stability increased with increased surfactant in the range 6 to 10%.

Note: C12E2: polyoxyethylene 2-lauryl ether; C12E4: polyoxyethylene 4-lauryl ether; HEM: high energy method; LEM: low energy method; NE: nano-emulsion; S20: Span 20; S80: Span 80; T20: Tween 20; T80: Tween 80; W/D (or w/d): water-in-diesel.

Water-in-diesel (w/d) nano-emulsions were prepared by Mehta et al. in the year 2014 with blending of nano-aluminum particles in water phase to enhance the combustion properties. Stabilization of nano-emulsions thus formed was assessed based on different surface active agents like S80 (Span 80), TX-100 (Triton X-100), CTAB (cetyltrimethylammonium bromide) and dicationic surfactants. Properties of the surfactants used in the work by assessing their interfacial tensions and critical micelle concentration. Among the tested surfactants Triton X-100 resulted in better stability of nano-emulsion for more than 8 hours. Thermodynamic stability of w/d nano-emulsions was shown by 1% water (vol. %) and blending of 0.1% nano-Al along with 1% water in w/d nano-emulsions.

2.2 STABILITY OF NANO-EMULSIONS

Stability of the emulsion is a measure of resisting the change in properties with time. The more stable is the emulsion, lesser is the change in its properties in terms of creaming, flocculation, coalescence and Ostwald ripening. Creaming or sedimentation is observed due to the density difference of the two immiscible phases. Dispersed phase either rises to the surface or moves downward. In case of w/o emulsion dispersed phase accumulates at the bottom and form a creamy layer. Flocculation takes place when droplets associate together due to the colloidal forces and forms large aggregates while individual drops remain separated by a thin film of continuous phase. Thin film reduces in thickness attributable to the van-der-Waals forces and forms large flocks promoting coalescence process. Therefore, flocculation could be understood as a precondition to coalescence. Flocculation process may be reversible or irreversible depending on the nature of interactions of the drops to be weak or strong. Coalescence is the process of merging two or more droplets in a single larger unit of reduced surface area compared to the individual droplets. Droplets now are no longer separated by a thin continuous film and the areas where the films are weak have tendency to fuse together eventually due to the attractive forces or hydrodynamic instabilities (Velev et al. 1997). The physical factors that increases the coalescence mechanism are principally droplet size and fraction of the dispersed phase. However, physical factors that avoids coalescence are low interfacial tension, high surface and bulk viscosity, large electric double layer, small volume of the dispersed phase and lower droplet size. Ostwald ripening differs from coalescence in the fact that the film surrounding the droplets does not involve rupture of the thin film. Instead mechanism involves difference in solubility of different size of droplets as they possess different Laplace pressure. Larger the difference between the droplet sizes, the greater will

be the Ostwald ripening rate. Physical factors increasing the Ostwald ripening rate are bulk phase solubility, interfacial tension, molar volume and diffusion coefficient of the disperse phase. However, the factors responsible for lower rates of the Ostwald ripening are density of the dispersed phase and temperature of the system.

Effect of surfactant percent (wt. %) on stability of nano-emulsion was studied and the detailed stability was reviewed by Tadros et al. (2004). Surfactant C12E4 was used for polyoxyethylene 4-lauryl ether. Steric stabilization and the role of the adsorbed layer thickness was explained in detail. By considering Ostwald ripening as a key instability process, instability of nano-emulsions was described by him taking real examples of NE formation. Moreover, methods that can be applied to reduce Ostwald ripening were also discussed. This intricate addition of a second less soluble oil phase like as squalene and/ or addition of a strongly adsorbed and water insoluble polymeric surfactant. Further discussed a few examples of NEs prepared by the phase inversion temperature (PIT) method as well as high pressure homogenizer. They compared the two methods (PIT and high pressure homogenizer) for the preparation of NEs and the rate of Ostwald ripening for both cases. The effect of changing the alkyl chain length and branching of the oil was examined using decane, dodecane, tertadecane, iso-hexadecane and hexadecane. The branched oil iso-hexadcecane showed higher Ostwald ripening rate when compared with a linear chain oil with the same carbon number. For system, water/C12EO4/hexadecane as the surfactant percent increased from 4 to 8%, Ostwald ripening rate increased from 2×10^{-27} to 39.7×10^{-27} $m^3.s^{-1}$ whereas, system water/$C_{12}EO_4$/hexadecane, as the surfactant percent increase from 3 to 6%, rate increased from 4.1×10^{-27}-50.7×10^{-27} $m^3.s^{-1}$ respectively. Parameter related to the stability of nano-emulsions can be summarized by Porras et al., (2004). The effect of water concentration on w/o nano-emulsion stability was studied. A conclusion based on study infers that in the system water/C12E4/isohexadecane when squalene amount increased from 0-20%, Ostwald ripening rate started decreasing.

Solans et al., (2005), suggested that addition of small amount of second oil in the o/w system further lowers the Ostwald ripening rate. According to Chen and Tao (2005), surfactant concentration is important for stability of emulsion and an optimal dose is suitable for a particular system (Chen and Tao 2005). In the formation of nano-emulsions, factors like oil to water ratio (stability increases with decrease in o/w ratio), stirring intensity (high), mixing temperature (optimum) and mixing time (high). Nadeem et al. (2006) reported that the factors responsible for

emulsion stability depends on water content, surfactant percent, temperature, viscosity and specific gravity. Ee et al. (2008), studied the stability of the system n-decane/ polyoxyethylene lauryl ether/water nano-emulsions, prepared by phase inversion temperature. Peng et al. (2010), increased water percent on nano-emulsion stability and studied coalescence and Ostwald ripening rate. Watanabe et al. (2010) emphasized on selection of the surfactant, appropriate agitation frequency and emulsification period. Al-Sabagh et al. (2011) studied the effect of increase of water and surfactant percent on nano-emulsion (water/ emarol 85: Span 80/diesel) stability. Xin et al. (2013), woked on oil-in-water (o/w) nano-emulsions with paraffin as an oil phase and tested the stability of the nano-emulsion. Destabilizing the emulsion during engine operation may bring failure of engine and it may damage the engine parts (Ithnin et al. 2014). Going away from the optimal dosage or high concentration, emulsion stability decreases due to rapid coalescence, whereas, at low concentration destabilization occurs due to agglomeration of the oil drops. For the application of NEs as an emulsified fuel for CI engines stability criteria is an important factor of emulsified fuels considered for proper running in the engines as it influences the fuel injection system (Vellaiyan and Amirthagadeswaran, 2016a). Work related to the stability of the nano-emulsion by different researchers is summarized in Table 2.2.

2.3 RHEOLOGICAL BEHAVIOR OF NANO-EMULSIONS

The rheological behavior of w/d (water-in-diesel) fuel NEs stabilized by mixed non-ionic surfactants was assessed by Noor El-Din in the year 2013. The mean droplet size of the formed water-mixed surfactant-diesel NEs was found in the range of 49–140 nm. The effect of increase of water percent (5, 6, 7, 8 and 9 wt. %) on rheology was evaluated at temperatures 10, 20, 30, 40 and 50 °C for different time lengths of 0, 1 and 2 weeks, respectively. Results revealed that the formed w/d NEs demonstrated low viscosity Newtonian fluids at all tested water ranges (5–9 wt. %) and temperatures ranges (10–50 °C). The viscosity of nano-emulsion systems was found more than that of either water or diesel at the same tested conditions. Arrhenius equation described viscosity-temperature relationship with high coefficients of correlation. Moreover, it was found that the higher the volume fraction of the dispersed water phase, the larger was the water droplet size along with higher viscosity of the NE system. It was concluded that the influence of time on the rheology of the NEs effected due to growth of water droplet size described by Ostwald ripening instability mechanism.

31

Table 2.2: Summary of nano-emulsions stability

Reference	Study parameters	Remarks
Tadros et al. (2004)	Effect of surfactant percent (wt. %) on stability of nano-emulsion prepared. Surfactant $C_{12}EO_4$ was used for polyoxyethylene 4-lauryl ether.	For system, water/ $C_{12}EO_4$/hexadecane as the surfactant percent increased from 4-8%, Ostwald ripening rate increased from $2x10^{-27}$ to $39.7x10^{-27}$ m^3/s whereas, system water/$^*C_{12}EO_4$/hexadecane, as the surfactant percent increase from 3-6%, rate increased from $4.1x10^{-27}$-$50.7x10^{-27}$ m^3/s.
Solans et al. (2005b)	Suggested that addition of small amount of second oil in the o/w system further lowers the Ostwald ripening rate.	In the system water/$C_{12}E_4$/isohexadecane when squalene amount increased from 0-20%, Ostwald ripening rate started decreasing.
Porras et al. (2004)	Effect of water concentration on w/o nano-emulsion stability was explained.	For low water conc., NEs breakdown attributed to Ostwald ripening and for high water conc., NE breakdown attributed to coalescence.
Ee et al. (2008)	Stability of n-decane/ polyoxyethylene lauryl ether/water nano-emulsions, prepared by phase inversion temperature.	The system depart from the optimum temperature, an increase in droplet size observed that lead to the instability of nano-emulsion.
Porras et al. (2008)	Stability of the water/mixed non-ionic surfactant/ oil performed by variations in water conc.	Stability study showed that NE breakdown attributed to Ostwald ripening and coalescence instability mechanism, depending on the water conc.
Peng et al. (2010)	Increase of water percent on nano-emulsion stability was studied considering coalescence and Ostwald ripening.	Addition of a second surfactant in mixed proportions provided more stable NEs with the minimum size, compared to individual surfactant. Increase in water percent increased Ostwald ripening rate. Optimization of parameters for the NEs formation gave higher stability over a period of 200 day.
Al-Sabagh et al. (2011)	Effect of increase of water and surfactant percent on nano-emulsion (water/ Emarol 85: Tween 80/diesel) stability was studied.	Increase in surfactant percent from 5-8% for water conc. of 5 and 14% in two different studies decreased Ostwald ripening rate for both water concentrations. Whereas, increase in water conc. (5-14%) at constant surfactant conc. (5-8 %) in two different study increased the Ostwald ripening.

Xin et al. (2013)	Stability of o/w NEs with paraffin as an oil phase	Stability of the NEs enhanced by adding SDS. CTAB and SDS induced a decreased droplet size with opposite stability trends.
Patil et al. (2015)	Effect of increase of surfactant and water percent on the stability of water/ Span 80: Tween 80/diesel nano-emulsion was studied.	Variations in surfactant conc. effected emulsion stability. Stabilization time for w/d emulsion increased with an increase in the surfactant conc. An increase in water conc. in the W/D emulsion decreased the emulsion stability. The w/d emulsion achieved good stability for 5 and 10% water conc. Stability lowered drastically beyond 25% water conc. and thereafter no change noticed.
Feng et al. (2016)	Effect of addition sequence of organic phases and initial location of emulsifiers on the stability of pesticide nano-emulsions.	NE (A) prepared by adding aqueous phase into organic phase displayed highest stability. Stability of NE (C) (prepared by addition of organic phase into the aqueous phase) comes second. However, NE (B) (prepared by addition of organic phase into the aqueous phase with emulsifiers) and D (prepared by addition of aqueous phase with emulsifiers into the organic phase), depicted creaming with larger droplets that increased for a period of time.

Note: CTAB: cetyltrimethyammonium bromide; SDS: sodium dodecyl sulfate

Rheological properties of stable NEs is essential to understand the flow characteristics. Three samples w/d emulsions with varied water compositions (vol. %) 10%, 20%, and 30% along with pure diesel were examined by Ghannam and Selim in the year 2014. Diesel fuel exhibited Newtonian profile, however w/d emulsions displayed non-Newtonian (pseudoplastic) behavior. Viscosity of the w/d emulsions decreased with water loading at increased shear rates. Power law showed best fit in case of pure diesel, whereas, Casson model described the flow behavior of all three w/d emulsions.

Three types of oil viz. Crodamol GTCC, Crodamol PC, and oleic acid were analyzed for the rheological properties of nano-emulsions tested by Jaworska et al., in the year 2015. Emulsions were stabilized by Polysorbate 80. Geranic acid was selected as a model active substance. Rheological study of nano-emulsion samples showed a pseudoplastic non-Newtonian behavior. Herschel-Bulkley model fitted well for the formed NEs.

Rheological study on w/o emulsions by Pajouhandeh et al. (2017) explained that the various factors likes as droplet size distribution, fractions of dispersed phase and surfactants plays a key role in characterizing their flow properties. However, emulsion stabilization by nanoparticles (solids) improved the stability and rheological properties and therefore, increased the oil recovery in the proposed work. Fumed silica particles (Aerosil R972) were used in the experiments. It was observed that the effect of nano-particles on the viscosity of w/o NEs influenced by the different factors viz. number of nanoparticles, water/oil ratio, shear rate and angular frequency. A decrese in water droplet size with increased stability, viscosity and elasticity was observed by adding nano-particles. Nanoparticle decreased water droplet diameter and increased stability, elasticity and viscosity of the emulsion. In addition, for a better understanding of the effect of these parameters on the viscosity of the w/o emulsions, apparent viscosity models were used. Based on the experimental data, a new equation was developed to estimate the relative viscosity of solid-free and solid-stabilized emulsions. The obtained results demonstrated that the proposed model has increased accuracy than previously published correlations.

A rheological study on diesel fuel nano-emulsions (NEs) by perfoming tests on different frame of time (0, 1, 2 and 3 months) was performed by Noor El-Din et al. (2017). Effect of variations of water and surfactants in the range of 5 to 10% and to 4 to 10% (w/w) was studied for testing the flow behavior. Prepared samples showed non-Newtonian behavior in the shear rate

range of 132 to 191 s^{-1}. Whereas 6 wt. % water content tested on time frame of 2 months showed Newtonian behavior.

Nano-emulsion (< 500 nm) possessing kinetically stable property with unique structural and physico-chemical properties was investigated by Kumar and Mandal (2018). NEs were prepared by using HEM (high energy method) for as system n-heptane/Tween 80 in the droplet size range of 91.05 to 40.16 nm, respectively. Effect of silica nanoparticles (NPs) addition in Tween 80 resulted in stabile NE with droplet sized ranging from 36.15 to 21.37 nm. The prepared NEs showed pseudo-plastic behavior in viscosity range of 9 to 12.5 mPa-s, which further improvement effected by the presence of NPs.

Study related to rheological behavior of nano-emulsions by different researchers is summarized in this section and findings related to the work is depicted in Table 2.3.

2.4 PERFORMANCE OF WATER-IN-DIESEL FUEL EMULSIONS

Performance of water-in-diesel (W/D) emulsions in terms of engine performance and emissions is explained in the following sections and the work performed on water emulsified systems by different researchers is summarized in Table 2.4. Performance and emission characteristics of water-in-diesel fuels in internal combustion engine is shown with and/or without additives. Nano-emulsions used in the study includes combustion properties like brake thermal efficiency and brake specific fuel consumption along with emission gases like NO_x and particulate matters (PMs). Some of the studies added some of the additives like cerium based additive, diglyme, Alumina NP, glycerin, CeO_2 etc. to enhance the combustion characteristics and improved emissions for emulsified fuels.

2.5 OVERVIEW OF LITERATURE REVIEW

Literature review illustrates the studies pertaining to the formation of nano-emulsion and its performance in the I.C. engines through various ionic and nonionic surfactants and based on energy input to the system. Studies regarded formation have made some of the common conclusion, like achieving minimum droplet size by using mixed surfactants, increase of surfactant gave decrement in size and increment of surfactant gave increased droplet size, etc. Stability mechanism of w/o nano-emulsions was explained in detail with respect to the various instability

models like Oswald ripening and coalescence model. Rheology was assessed by considering variations in water, surfactant and temperature. Most of the study concluded Newtonian behavior of nano-emulsion samples.

In the advent of increased energy demand emerged due to the increased world GDP growth, serious efforts are required to avoid overuse of non-renewable energy resources specifically liquid fuels like diesel and kerosene. More precisely, diesel, since, it is used in heavy duty vehicles/ machines comprised of powerful compression ignition (CI) engines. CI engines though provide high torque at low speeds, however at the same time limits the environmental issues like NOx and particulate matters (PMs) emissions. New technologies are therefore, required that not only improve combustion properties but also advances emission standards of liquid fuels. One of the recent research in this context is water emulsified fuel that not only works without any modifications in the engine but also enhances the combustion properties and emission standards due to its properties like high latent heat of vaporization and micro-explosion.

In this context a detailed literature review was performed in view of formation of w/o nano-emulsions. A chronological literature review reports on four vital study zones viz., formation, stability, rheology and performance of w/o nanoemulsions in I.C. engines in view of improved properties like lower droplet size, longer stability with respect to time, improved flow properties or rheological properties and emission standards.

Section 2.1: A chronological study on the formation of nanoemulsions reports on various formation techniques (isothermal dilution, phase inversion temperature and composition, and high energy methods) and effect of different parameters (water %, surfactant% and oil %) on nanoemulsion formation. Plenty of the nanoemulsions reported in literature describes the formation of nanoemulsion by taking examples of different dispersed and continuous phases (w/o or o/w) based on their end uses like as pesticides, pharmaceuticals, polymerization etc. Few studies on the formation of the nanoemulsion diesel fuels are reported with size controlled and scalable technology**.** This lacuna therefore motivated us for the formation of nanoemulsion by adopting different energy routes, separately, or in combination by optimizing process variables statistically and mathematically. In this regard, a noble way of finding co-ordinates of formation of NEs by triangular diagram was devised that may be applied for other systems as well.

Section 2.2: This section focuses on the stability of the nanoemulsions that reports various techniques adopted by different researchers in view of stabilizing the systems with different dispersed phases for longer time by testing the different mechanism like Ostwald's ripening and coalescence phenomenon. However, very few studies like Al-Sabagh et al. (2011) and Noor el-din et al (2013b) have worked on stability of water-in-diesel nanoemulsions. New techniques like optimization of different functional group surfactants in mixed proportions may help in finding stable nanoemulsion. In this regard, motivated study is much needed in carrying out the research work by identifying two different combinations of surfactants of different functional groups. Moreover, β ratio (S/W) was identified as a key factor responsible for longer time stability of the water-in-oil nano-emulsions.

Section 2.3: This section laid emphasis on rheological properties of the nanoemulsion systems formed under different set of conditions by different researches and suggested ways of improving flow behavior. The flow behavior of nano-emulsions by different researchers found Non-Newtonian (viscoelastic) for different systems, however, for diesel nanoemulsion both types viz. Newtonian and Non-Newtonian behavior are reported in literature. Therefore, an obvious reason prompted us in finding out the flow behavior of the developed nano-emulsion system. Present work, however, found noble as all nano-emulsion samples showed Newtonian behavior that advances the mobility characteristics of the formed systems without disturbing its structure.

Section 2.4: Highlights the performance and emission characteristics of the different water-in-diesel NEs helpful in finding industrial applications by understanding the engine performance and emission standard at different composition of constituents. The literature review however explores a new study, a future work for various researchers.

Table 2.3: Rheological study of nano-emulsions

Reference	Parameters Studied	Remarks
Noor El-Din et al. (2013)	Influence of time on the rheology of the nano-emulsions.	Evolution of water droplet size due to Ostwald ripening phenomenon and a slight decrease of viscosity indicated the change of rheological character of the NE system into time-dependent non-Newtonian character as a result of the interfacial relaxation stress by time.
Ghannam and Selim (2014)	Pure diesel fuel and three samples of w/d emulsions (10%, 20%, and 30% by volume water) were examined.	Pure diesel fuel exhibits a Newtonian profile since its viscosity remains constant with the shear rate. All w/d emulsions displayed higher viscosity than diesel fuel with non-Newtonian flow behavior of yield pseudo-plastic response. The viscosity of the w/d emulsions decreased with the shear rate and water addition. The Casson model very sufficiently fits the flow behavior of different w/d emulsions.
Jaworska et al. (2015)	NEs based on three types of oil phases, namely, Crodamol GTCC, Crodamol PC, and oleic acid, were analyzed and determined using Polysorbate 80.	The studied NEs were pseudoplastic non-Newtonian fluids. The Herschel-Bulkley model accurately describes the rheological properties of the developed systems. The phase inversion point for the Crodamol GTCC/Polysorbate 80/water system was observed at 50 wt. % dispersed-phase concentration. The rheological results served as the basis for calculation of a theoretical diffusion coefficient of the active ingredient in the studied NEs.
Angkuratipakorn et al. (2017)	Cellulose nanocrystals (CNC) with a non-ionic surfactant ($PG_{1.5}SFR_{0.05}$) and gum arabic were used to stabilize the bran o/w pickering emulsion.	The rheological data provided evidence of gel-like behavior in all emulsions. Rheological analysis showed high viscosity in the presence of gum arabic, due to flocculation of the structure of the emulsion

Pajouhandeh et al. (2017)	The effects of different parameters, including water volume fraction, nanoparticle concentration, shear rate, and angular frequency were investigated on the rheological behavior of w/o emulsion.	The obtained results from experimental measurements showed that the three models including Power Law, Bingham and Casson models can be used for prediction of rheological behavior of the crude oil, solid-free and solid-stabilized emulsions. The shear viscosity, complex viscosity, elasticity and time constant of water-in-oil emulsions are influenced by a number of nanoparticles, volume of water fraction, shear rate and angular frequency. Also, droplet size of emulsions decreases with the addition of nanoparticles. Rheological parameters were obtained through experiments and equations indicated the presence of elastic network structure.
Noor El-Din et al. (2017)	Twenty nano-emulsions were prepared at conditions of water and surfactant (Tween 85+Tween 80) ranging from 5-10 to 4-10 w/w, respectively at ambient temperature. The prepared W/D nano-emulsions were evaluated for the rheological behaviors at interval time as 0, 1, 2 and 3 months	The prepared nano-emulsions were evaluated for the rheological behaviors at interval time as 0, 1, 2 and 3 months. The results indicated that the rheological properties of the prepared emulsions behave as non-Newtonian flow in the range of shear rate from 132 to 191 s^{-1} with a yield value (τ) ranged from 2.14 to 5.11 D/cm^2 at 6 wt. % water content, 30 °C and 2 months' time laps followed by Newtonian regime.
Nash and Erk (2017)	Investigated the rheological behavior of o/w droplet interfaces stabilized by food-grade emulsifiers (soy lecithinor Tween 20) under controlled aqueous conditions.	This investigation indicates that the formation of surfactant-laden interfacial layer with high viscoelasticity may provide additional benefits in food based O/W nano-emulsion delivery systems.

Kumar and Mandal (2018)	Nano-emulsions prepared by high energy method using Tween 80 and n-heptane with droplet size in the range 91.05 to 40.16 nm was tested without (T80: 0.25-2 wt.%) or with addition of silica nanoparticles (0-2 wt.% np) for its rheological properties.	A pseudo-plastic nature or non-Newtonian behavior was shown by the prepared nano-emulsions with increase of shear rate. The apparent viscosity curves with increasing shear rate at different Tween 80 surfactant concentrations and temperatures (303 K, 323 K and 343 K). The reduction of viscosity with increase in shear rate may be attributed to disentanglement of emulsion droplets and there arrangement along a flow streamline.

Table 2.4: Performance and emission characteristics of water-in-diesel fuels in I.C. engine with/without additives.

Ref.	Test fuel	Composition (vol. %)	Type of engine	Objectives	Fuel property improvement
Lin and Wang, (2004b)	Diesel-water-surfactant + additive (diglyme)	W (10), S (2)	4-stroke, water-cooled, DI mode	Performance and emissions of three phase emulsion (O/W/O) using additive as combustion improver	Additive in O/W/O emulsion increased NO_x and combustion efficiency. Lowered fuel consumption rate and BSFC. PM and CO decreased whereas CO_2 increased.
Abu-Zaid, (2004)	Diesel-water-surfactant (*)	W (5-20), S (2)	1-cylinder diesel engine (1200–3300 rpm)	Performance and gases exhaust temperature	Torque, power and BTE increased (for 20 % W, 3.5 % increase over diesel) with water percentage whereas BSFC and gases exhaust temperature decreased with water %.
Armas et al., (2005)	Diesel-water-surfactant (polyethylene-glycole monoleate and sorbitole sesquioleate)	W (10), S (†)	Turbocharger, intercooler, IDI mode	Performance and emissions	Improved brake efficiency and significantly reduced thermal NO, soot, hydrocarbons and PM.

Farfaletti et al., (2005)	Diesel-water-additive (cerium based additive)	HD emulsion: D (88), W (12), S(†) LD emulsion: D (94), W (6), S(†) HD/LD emulsion + Additive (0.35) to the blend	EURO-3 LD diesel vehicles	Emissions of experimental LD emulsion, HD emulsion and combustion improver additive	The emulsion fuel reduces the PM emissions with -32% for LD vehicles and -59% for the HD engine. NO_x emissions remained unchanged, +26% hydrocarbons (HC), +18% CO and +25% PM increased for LD vehicles In contrast, CO (-32%), and NO_x (-6%) were reduced by the emulsion for the HD engine and only hydrocarbons were slightly increased (+16%). Additive was insufficient to reduce the emissions in HD engine but improved all emissions in LD engine.
Nadeem et al., (2006)	Diesel-water-surfactant (sorbitan mono-oleate / Gemimi)	W (5-15), S (†)	4-cylinder, 4-stroke, DI mode	Performance and emissions	PM, NO_x, CO and SO_x decreased using W (15) with surfactant but no change in engine's efficiency
Lin and Chen, (2006)	Diesel- water-surfactant (*)	W (15), S (2)	4-cylinder, 4-stroke, DI mode	Performance and emissions of 2-phase and 3-phase emulsion	In comparison to two phase (w/o), three phase emulsion (o/w/o) found decreased NO_x and smoke. Increased CO and CO_2. BSFC and BTE increased.

Ghojel et al., (2006)	Diesel- water-surfactant (*) -additive (2-EHN)	W (13), S (2), A (0.2) Emulsion	4-stroke, 4-cylinder, DI mode	Performance and emissions	Improved NO_x and HC. Retarded fuel injection, smaller ignition delay. Lower cylinder pressure and temperature.
Selim and Ghannam, (2010)	Diesel-water-surfactant (Triton X-100)	D (65-100), W (0-30), S (0-5)	1-cylinder, 4- stroke, IDI mode	Stability and performance of the emulsion.	Emulsion with specification: 10% W, 0.2% S at 15000 rpm found stable. Maximum pressure rise rate increased with increasing the amount of water and reduction in engine speed. At water > 20%, higher compression ratio (>22) required to run engine smoothly. Water addition reduced brake power output to drop slightly and BSFC to increase slightly, reduced power but improved NO_x emissions.
Alahmer et al., (2010)	Diesel-water-surfactant (Tween 20)	W (5-30), S (2)	4-stroke, 4-cylinder, DI mode (1000-3000 rpm)	Performance and emissions	Increased water content (5 to 30) resulted in high thermal efficiency, improved NO_x and BSFC, and decreased NO. Although CO_2 emission was higher than that of pure diesel.
Basha and Anand, (2011)	Diesel-water-surfactant (Tween 80+Tween 80) -Additives (Alumina NP)	W (15), S (2), A (25 ppm)	1-cylinder, 4- stroke, DI mode (1500 rpm)	Performance and emissions	Low cylinder peak pressure and heat release rate (short ignition delay). BTE improved by 28.9%; NO_x emission reduced (at full load is 891 ppm)

43

Yang et al., (2013)	Diesel-water-surfactant (*) - additive (nano-organic additive (glycerin)	W (10 and 15), S (†)	4-cylinder engine with common rail fuel injection system	Performance and emissions	For 10% emulsion fuel: BTE was significantly improved by 14.2% compared to pure diesel, and there was reduction NO_x emissions by 30.6% and considerable reduction in CO emissions.
Liang et al., (2013)	Diesel-water	W (20), D (80)	4-cylinder, 4-stroke, turbocharged engine (2000 rpm) at full load	Performance and emissions of oxygen enriched combustion (OEC)	Lower BSFC, higher cylinder pressure and shorter ignition delay using OEC alone. Opposite trends found using WDE. PM and NO_x reduced simultaneously by applying OEC combined with WDE.
Fahd et al., (2013)	Diesel-water – surfactant (*)	W (10), S (10)	4-cylinder, DI mode (800 to 3600 rpm) at 25 to 100% load	Performance and emissions of emulsion ED [10] (10% w) at different engine loads	In-cylinder pressure and heat release rate gave similar values like base diesel fuel alone. Reduced engine power output with higher. Lower exhaust gas temperature and NO at all loads and engine speeds. High CO emissions at low load and low engine speeds.
Bidita et al., (2014)	Diesel-water-surfactant (Triton X-100) - additive (CeO_2)	W (0.7-1), S (0.25-0.4), A (80 ppm)	Compact air cooled diesel engine (Model YANMAR L48N)	Performance and emissions with or without fuel additive.	Reduced BSFC and exhaust mass flow rate, increased BTE using emulsion with additive compared to neat diesel. There was reduction in CO_2, NH_3 and NO_x emissions with additive.

Syu et al., (2014)	Diesel-water-surfactant (Span 83 and Tween 80)	W (0-15), S (5) in wt. %. Surfactants	1-cylinder, 4- stroke DI mode	Thermal efficiency and emissions	Thermal efficiency increased up to 19.9%. Significant reduction in NO. PM emissions decreased at high loads. However, CO and HC significantly increased.
Sahin et al., (2014)	Diesel- water + air	W (2-10)	4-cylinder, 4- stroke, turbocharged, common-rail injection, 1.461 L, CR: 18.25:1	Water injection (WI) into intake air on the performance and exhaust emissions	Smoke index, K and NO_x emissions decreased as water ratio (WR) increased. Maximum decrease in NO_x emission (12.5%) for 9.4% WR at full load (149 N m) and 2500 rpm. At a particular load and 2000-3000 rpm there was no change or slight increase in BSFC. BSFC decreased by 4% water at a particular load and 3500 rpm. Showed no change in-cylinder pressure and indicated power.
Seifi et al., (2016)	Diesel-water-surfactant (*)	[W (2-10), D (90-98)] + S (2)	6-cylinder, DI mode	Evaluate engine power, torque and noise without.	Higher water addition showed decreased engine power, torque and no effect on noise. For 2% water addition showed improved engine power, torque and noise emission.
Baskar and Kumar, 2017)	Diesel-water-surfactant (*)	D + 21 % air; [D (90), W (10)] + S; D + 27% air.	1-cylinder, 4- stroke engine	Engine discharge and performance by two methods diesel with different percent of O_2 in air and with water.	BTE enhanced, improved combustion characteristics and reduction in HC emissions.

CHAPTER 3

MATERIALS AND METHODS

In this chapter, experimental details including chemicals, methods of preparation of water-in-oil nano-emulsions (w/o NEs) have been explained. A detailed discussion about low and high energy methods including set up details is described in section 3.1. Different techniques of characterization of nano-emulsions like droplet size measurement, surface tension, HLB value, ternary diagram analysis, rheological measurement and stability analysis of nano-emulsions are explained in detail in section 3.2.

3.1 EXPERIMENTAL DETAILS

3.1.1 Chemicals

Non-Ionic surfactants, PEG-20 Sorbitan monostearate (Tween 60 (T6); HLB=14.9) and polyethylene glycol p-(1,1,3,3-tetramethylbutyl)-phenyl ether (Triton X-100 (TX-100); HLB=13.5) were purchased from Sigma Aldrich, USA and Molychem, Mumbai, India. Sorbitan monooleate (Span 80 (S8); HLB=4.3) were purchased from Sigma Aldrich, USA. Diesel oil used in the present work was obtained from local market retail pump outlet Roorkee, India. All products used in the study were not additionally purified. Water used in the study was double distilled. Hydrophilic nature of Tween 60 is shown by high HLB value (14.9) whereas low critical micelle concentration (CMC) value (0.22×10^{-4}) indicated requirement of low amount of surfactant to saturate water-oil interface for micelle formation. Low HLB value (4.3) of Span 80 implies the lipophilic nature of surfactant while high value of CMC (1.82×10^{-4}) indicated requirement of high amount of surfactant for micelle formation. Chemical structures of Span 80, Tween 60 and Triton X-100 are shown in Fig. 3.1.

3.1.2 Nano-emulsion (W/O) preparation methods

Two different approaches based on application of energy to the system were adopted for the preparation of w/o nano-emulsions. First approach adopted was the isothermal dilution method based on low to medium shear application (isothermal dilution method) whereas the second approach used was the medium to high shear method (ultrasonic cavitation). In both methods different combination of mixed surfactants were used as stabilizing agents.

Table 3.1: Physical properties of surfactants.

Name	Formula	Avg. M.W. (g.mol⁻¹)	Solubility	HLB	Density g.ml⁻¹ (at 20 ºC)	SFT (mN.m⁻¹) at 25 ºC	IFT (mN.m⁻¹) at 25 ºC	CMC value (mM)
Triton X-100	$H_{22}O(C_2H_4O)_x$; x=9-10; avg. value of x = 9.5	625.0	Water soluble	13.5	1.01	29.9	3.3	*0.20
Tween 60	$C_{64}H_{126}O_{26}$	1311.70	Yellow paste	14.9	1.044 (at 25ºC)	38.16	2.8	0.22
Span 80	$C_{24}H_{44}O_6$	428.6	Oil soluble	4.3	0.99	22.0	3.2	1.82

Note: Physical properties of surfactants are referred from the Safety Data Sheet (SDS) Sigma-Aldrich SDS. * SFT and (Kothekar et al., 2007; Mehta et al., 2015) and IFT (Patist et al., 2000) in case of Tween 60 is measured at 1 wt. % concentration (Kothekar et al., 2007).
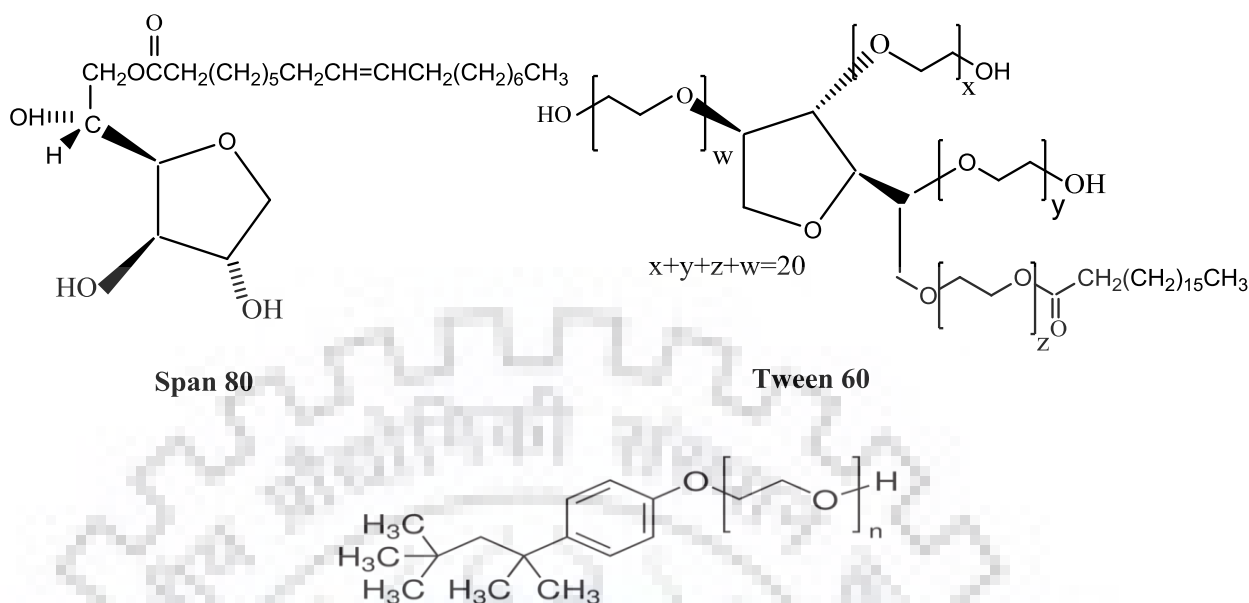
Fig. 3.1: Chemical structures of non-ionic surfactants Span 80, Tween 60 and Triton X-100

3.1.2.1 Isothermal dilution method

Low energy emulsification method was used for the preparation of water/mixed surfactant (T6:S8)/diesel oil nano-emulsion. Preparation method used in this work follows drop wise addition of water in pre-mixed oil and surfactant. At first Tween 60 and Span 80 were mixed with the help of a magnetic stirrer (Tarsons SPINIT - Digital Magnetic Stirrer, India) at a fixed ratio (wt. %) to obtain the required HLB of the mixed surfactant. Mixing of surfactants was continued at a constant temperature of 40 °C till the transparent homogenous mixer of surfactants was obtained. After the preparation of mixture of surfactants (Tween 60 and Span 80), a known amount (2-10%) of it was added to the known amount of diesel oil (78-86%) and kept on stirring until a homogenous solution was obtained.

Distilled water was then added drop wise to the known amount of mixture of oil and surfactants at a constant rate of 0.5 ml.min^{-1} (Miclins Peristaltic pump PP10, India) till desired quantity of water was mixed. The stirring rate was kept constant at 600 rpm and temperature was maintained at 37 °C on a magnetic stirrer. The resulting emulsion was kept at room temperature for further analysis (Fig. 3.2).
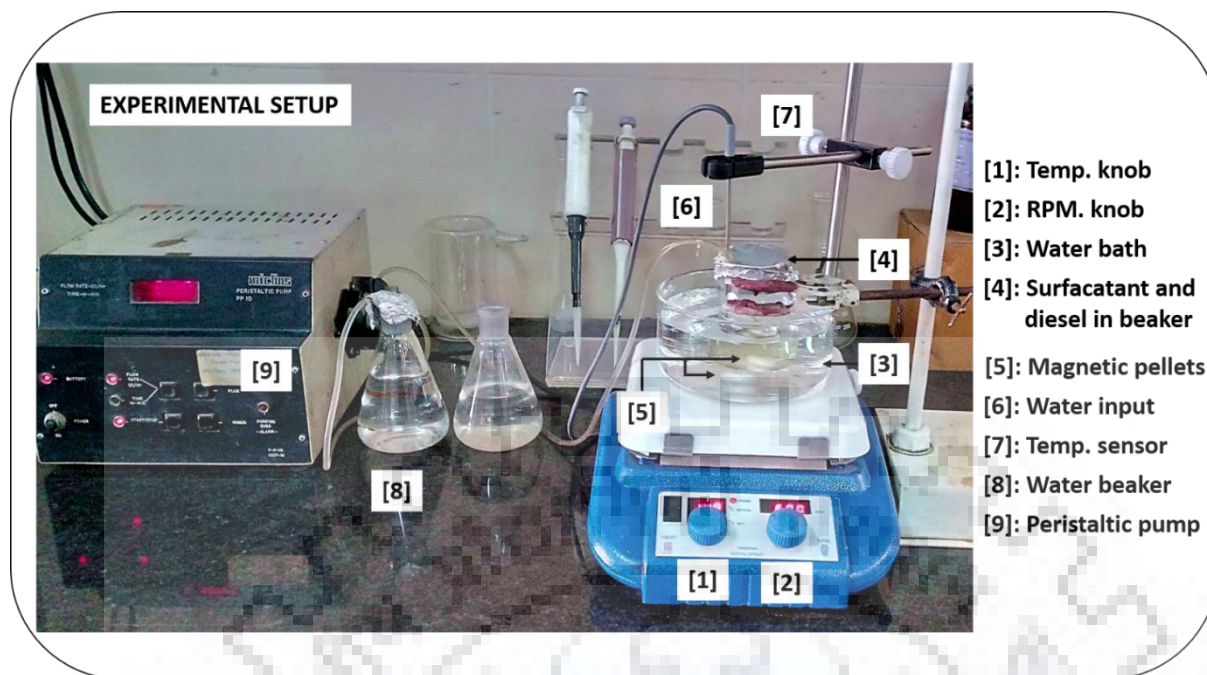
Fig. 3.2: Experimental set for preparation of w/o nano-emulsion through isothermal dilution method.

3.1.2.2 High energy method

Ultrasonicator of make Hielscher, GmbH, UP 400S with maximum acoustic power density of 85 W.cm^{-2} was used in the present study, as shown in Fig. 3.3 (b). For ultrasonification (Method B), pre-emulsified (Method A) sample was placed inside the glass beaker with fixed quantity of 50 gm to maintain the cavity intensity for all samples. To prevent the overheating of the sample a cold water bath was used that transfer the heat generated during the process. Sonication probe made up of titanium alloy was dipped in the sample up to 17 mm and kept constant for all the samples. Ultrasonic processor of 400W useful power used in the present study generates longitudinal mechanical vibrations by means of electric excitation, i.e. a reversed piezoelectric effect with a 24 kHz frequency. Amplification of vibrations was achieved through sonotrode (formed as a $\lambda/2$ vibrator) and transferred to the liquid to be sonically irradiated via its end face. The power output of the sonicator can be adjusted between 20% to 100% amplitude.

Formation of combined energy mixed surfactant nano-emulsion (CEMSNE) was achieved in two steps based on combination of low and high energy methods at optimized conditions. Non-ionic surfactants of two dissimilar functional groups viz. long chain of ether combined with hydrocarbon (TritonX-100: R-O-R') and ester (Span 80: RCOOR') groups, were used in mixed proportions to give the synergistic effect. High HLB value (13.5) of Triton X-100 indicates the hydrophilic nature whereas low CMC value (0.2 mM) represents a lesser amount

50

of surfactant required to saturate the water-oil interface for micelle formation. In contrast, low HLB value (4.3) of Span 80 is representative of lipophilic nature with high CMC value (1.82 mM) that implies a higher amount of surfactant required for micelle formation (Table 3.1).

Preparation of w/o CEMSNE was attained by combination of two methods, i.e. methods A and B, as shown in Fig. 3.3 (a) and (b). In method A, low energy method, i.e. dilution method at constant temperature, was applied for the formation of w/o emulsion. The best combination (S/W/O; w/w) responsible for the formation of transparent pre-emulsion was searched by plotting the appearance of nano-emulsion formed at their respective composition and droplet diameter ($D_{z\text{-avg}}$, nm) on ternary diagram. Emulsions obtained after Method A were further treated by Method B wherein, high energy method was used at optimized sonicated parameters. CEMSNE obtained by this method showed transparent (nanometer sized) emulsions with long time stability.
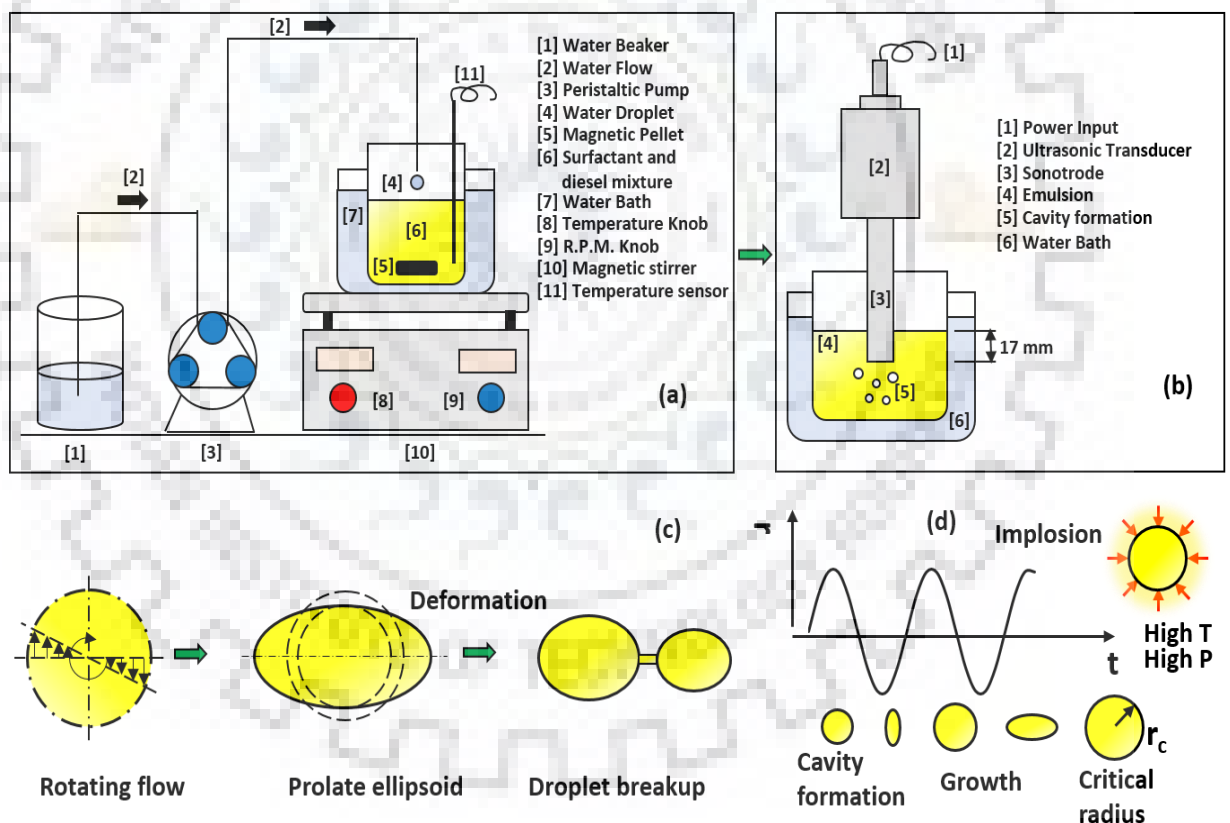
Fig. 3.3: Schematic diagram depicting two step method for preparing w/o nano-emulsion (a) Method A followed by (b) Method B. Mechanism of drop formation is depicted in (c) Method A and (d) method B.

3.2 EMULSION CHARACTERIZATION TECHNIQUES

Techniques used to characterize the nano-emulsions prepared by low and high energy methods can be summarized as follows:

3.2.1 Droplet size measurement

Particle size distribution of the dispersed phase was assessed by using the Zetasizer of the make Malvern Nano-Zs that is based on DLS (Dynamic Light Scattering) Technique (Barradas et al., 2015; Bazylin´ska et al., 2014). Mean droplet size of the dispersion was measured with argon laser at λ= 488 nm with scattering angle of 90° and all measurements of hydrodynamic diameter were performed at a constant temperature of 25 °C. Particle size of sample under test was reported as an average of its three consecutive measurements.

This method is also known as photon correlation spectroscopy (PCS) or Quazi-Elastic Light Scattering used for the calculation of the submicron particle or nanoparticle sizes in suspension. The basic concept in measurement of particle size lies in illuminating the suspension particles by a laser beam and measuring the fluctuation intensity caused by Brownian motion of nanoparticles. In the process, scattering is caused by the interaction of the photons with the electric field of the particles that induces the oscillating dipole movement and as the dipole moment changes it reradiates the light in all directions. The Brownian motion of the suspended nanoparticles changes with the particle size, the larger the particle the slower the motion. PCS technique measures the rate at which intensity of scattered light fluctuates due to Brownian motion of the particles. The fluctuation in the intensity will be rapid in case of small particles as compared to the larger ones and this fluctuation is measured by a correlator that constructs the correlation function $G(\tau)$ of the scattered light as shown in Eqn. (3.1) (Tadros et al., 2004).

$$G(\tau) = <I(t).I(t+\tau)> \qquad (3.1)$$

where t is time (s), τ is correlator time delay or time difference of the correlator (s) and I is the intensity. The correlation function $G(\tau)$, for polydispersed particles, can be modeled as exponential function of the corrector time delay τ and is represented by Eqn. (3.2).

$$G(\tau) = A(1 + B[g(\tau)]^2) \qquad (3.2)$$

where A is baseline of the correlation function at infinite time, B is intercept or amplitude of the correlation function and $g(\tau)$ is correlation function of the scattered electric field. In case of monodispersed particles, correlation function can be expressed with eqns. (3.3) and (3.4) as

$$G(\tau) = A(1 + B\exp(-2\Gamma\tau)) \tag{3.3}$$

$$\Gamma = dp^2 \tag{3.4}$$

where d is known as translational diffusion coefficient (this property defines the velocity of the Brownian motion) and p is the scattering vector (PCS theory) (Eqn. 3.5).

$$p = \frac{4\pi n}{\lambda_o}\sin(\theta/2) \tag{3.5}$$

where n is the refractive index of dispersant, λ_o is the wavelength of the incident light and θ is the scattering angle. Particle size (D) was measured in terms of hydrodynamic diameter by using Stokes-Einstein equation (Eqn. 3.6).

$$D = \frac{kT}{3\pi\eta d} \tag{3.6}$$

where k is Boltzmann's constant, T is the absolute temperature and η is the viscosity of the medium.

3.2.2 Surface tension and interfacial measurement

Surface tension of Tween 60 (T6), Span 80 (S8) and mixed surfactant (TS) was calculated by dissolving a fixed percentage (wt. %) of individual and mixed surfactants in diesel. Measurement of surface tension was performed by Du-Noüy ring (RG 11) method by using DCAT (Dynamic Contact Angle Meter and Tensiometer) of make Data Physics Instruments GmbH, Filderstadt, Germany. The values of surface tension ($mN.m^{-1}$) reported are averaged from the four set of individual readings of respective samples.

Fig. (3.4) shows the variation of surface tension with individual and mixed surfactants as well as variation of surface tension with increased percentage of surfactants in the sample. It is inferred from Fig. (3.4) that at a fixed percent (1% and 8%) of surfactant, surface tension of Tween 60 has a lowest value, Span 80 has a maximum value whereas mixed surfactants has value in between the maxima and minima. Moreover, as the surfactant concentration is increased from 1% to 8%, slight reduction in surface tension of individual surfactants was observed. Surface tension values of mixed surfactants (TS) lying in the middle of individual surfactants Tween 60 and Span 80 may be credited to the synergic effect of adsorption of individual surfactants on the

oil surface. Whereas interfacial tension in case of system Span 80 and Triton X-100 is summarized in Table 3.1.
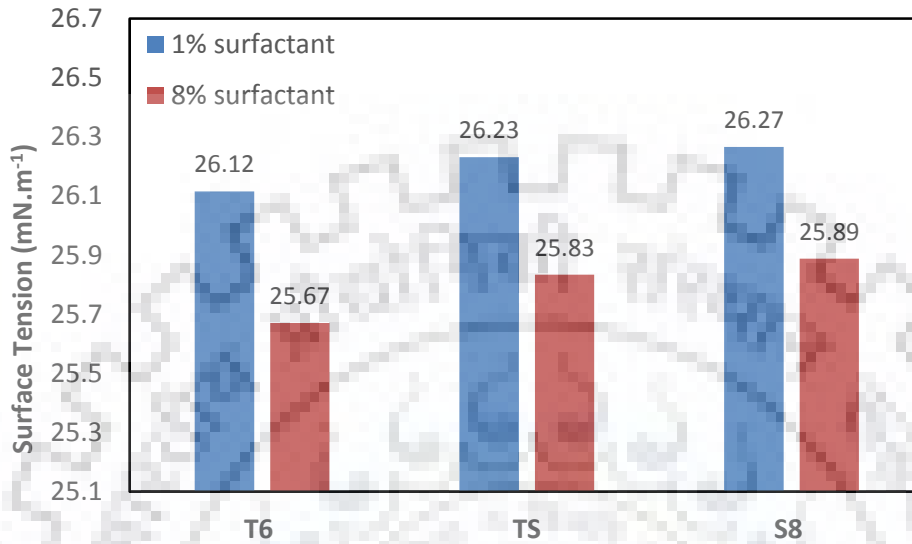
Fig. 3.4: Surface tension for Tween 60 (T6), Span 80 (S8) and mixed surfactant (TS) for different concentration in diesel (wt. %).

3.2.3 HLB value and ternary diagram study

An emulsifier stabilizes the dispersed particles once they are formed and it is characterized by its Hydrophile-Lipophile-Balance (HLB) value. It represents the relative degree of hydrophilicity or hydrophobicity of the individual component groups of the surfactants. Higher value of HLB indicates solubility of the surfactant in polar solvents like water whereas lower values indicate the solubility in the non-polar systems like oil. The HLB value of mixed surfactants was calculated by weighted average of its individual surfactants using the Eqn. (3.7) (Liu et al., 2011; Maali and Mosavian, 2013; Noor El-Din et al., 2014).

$$HLB_{T6S8} = HLB_{T6}(\%T6) + HLB_{S8}(\%S8) \qquad (3.7)$$

The mixing ratio of emulsifiers (T6+S8) for the system under consideration (water in diesel oil emulsion) was found by optimizing the HLB value, which gave the smallest possible droplet size in a given set of constant conditions, like mixing temperature, rotation speed, rate of addition of dispersed phase, and compositions of water, diesel and surfactant (wt.%). To achieve the best possible smaller particle size of high stability in a given set of parameters, different HLB values were generated ranging from 6.42 to 9.6, by varying the weight percent of Tween 60 from

20 to 50 percent in a mixture of Tween 60 and Span 80. A plot of average droplet size ($D_{z\text{-Avg.}}$) along with polydispersity index (PDI) against individual HLB values was prepared to find out the HLB value that could minimize the droplet size (dispersed phase) giving stable w/o nano-emulsion.

In the preparation of w/o nano-emulsion through high energy method, HLB optimization was performed on pre-emulsion (method A) by application of ultrasonic cavitation method at constant compositions (w/w) of surfactant, water and oil. At first mixing ratio (w/w) of surfactants was assessed based on the optimum HLB value at which minimum droplet size was obtained. HLB values at different weight fractions of TX-100 were calculated using Eqn. (3.8) (Alzorqi et al., 2016; Liu et al., 2011) keeping sonication time, amplitude percent and cycle ratio constant:

$$HLB_{T100S8} = 13.5x + 4.3(1-x) \tag{3.8}$$

where x is the weight fraction of TX-100 in the mixture of TX-100 and S80. W/O emulsions formed by Method A at different HLB values (5 to 8) were reported as average droplet size. Parameters surfactant fraction (Φ_s=0.075), water fraction (Φ_w=0.050) and emulsion temperature (37°C) were kept constant during the formation of emulsions. Weighed amounts of individual surfactants were first mixed at optimized HLB value (=7) with diesel oil thoroughly at 37°C thereafter, water was added to it at a constant rate of 0.5 ml.minute^{-1} by a peristaltic pump (Miclins Peristaltic pump PP10, Chennai, Tamil Nadu, India) (Fig. 3.3 (a)). Total weight of all constituents of emulsion was kept constant at 50g for all samples made during experiments. Constant stirring rate of 600 RPM was maintained by magnetic stirrer (Tarsons Spintop - Digital Magnetic Stirrer, Kolkata, West Bengal, India) whereas, constant temperature of 37°C was maintained by application of water bath and temperature sensor assembly. The pre-emulsions thus obtained were kept at room temperature for further analysis.

In case of isothermal dilution method, ternary diagram for water-mixed surfactants-diesel system was studied to predict the zones of formation of w/o nano-emulsions. Different compositions of all three constituents were studied within the fixed limits of water and mixed surfactant (T6+S8) as 4-20% and 2-10%, respectively, at an optimum HLB value of 8.01, as shown in Fig. 3.5. Compositions of different proportions of water, T6:S8 and diesel under the experimented limits were varied at a constant temperature of 37 ^{o}C according to ternary phase diagram coordinates.
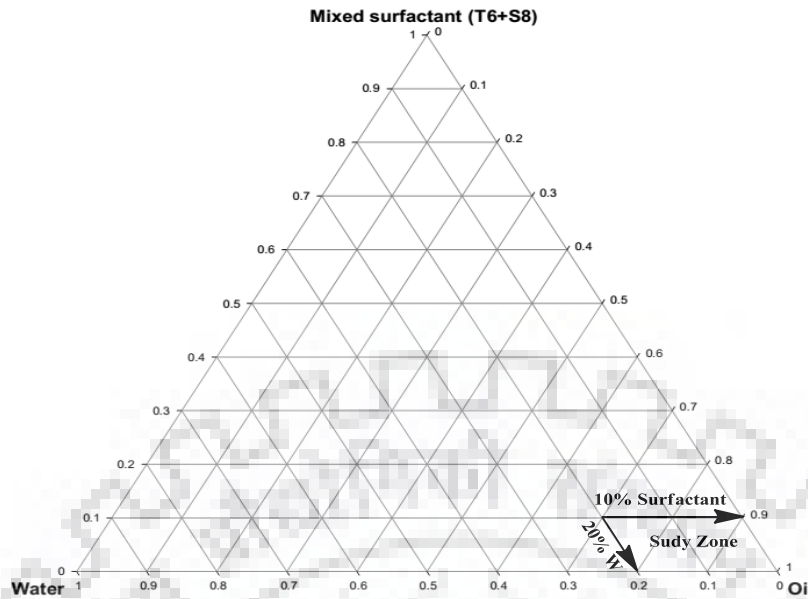
Fig. 3.5: Phase diagram showing the zone of study within the limits of 2-10% (w/w) mixed surfactants (T6+S8) and 4-20% (w/w) water (LEM).

In case of ultrasonication, for determination of the composition at which stable and transparent nano-emulsions formation take place, a ternary diagram study was performed by varying weight fraction of water (Φw) and mixed surfactant (Φs) from 0.02 to 0.11 and 0.05 to 0.20, respectively. Mixed surfactant ratio of S8/T100 (0.71/0.29) w/w, at a constant temperature (37°C), was maintained during experiments. This study also helped in finding the surfactant-water ratio (β) at which w/o nano-emulsions formation took place.

3.2.4 Rheological measurement

Rheological properties of emulsions is essential in understanding the flow behavior of fluids and their inter-particle interactions. An emulsion with high viscosity is always troublesome in transportation and pumping. An increase in the concentration of dispersed phase in the emulsion increases its viscosity which is responsible for the closed packing of dispersed phase in the emulsion. Moreover, deformation and flow behavior of fluids is described by rheology, therefore, rheometry of newly formed nano-emulsion is an obligatory step. For finding the steady state flow behavior and effect of temperature on the rheology of the formed NEs, a controlled stress rheometer of make Pysica MCR 702 Twin drive™, Antor Paar Germany, with an advanced feature of two torque transducers and drive units at once was implemented to shear the testing fluids at opposite directions (twin drive) was used. A cone and plate sensor (CP-50) was used to test the shear stress and shear strain analysis with cone angle of 0.998°, cone diameter of 49.95

mm and plate diameter of 60 mm. Details of Rheometer viscosity measurement system are summarized in Table 3.2.

In the study of low energy method, three samples of w/o nano-emulsions (8% S8+T6; 5:2 W/S; 8% S8+T6; 2:1 W/S; 10% S8+T6; 2:1 W/S) consisting of different compositions of water, surfactant, and diesel were tested in the temperature range of 25-40°C and the shear rate range of 10-1000 s^{-1}. CEMSNE samples tested for rheological behavior, were prepared at constant value of surfactant-to-water ratio ($\beta=2$). Moreover, in the case of CEMSNE samples, a detailed rheological analysis was performed at three different water fractions viz. 0.05, 0.08 and 0.11, respectively, at the shear rate and temperature range of 10-100 s^{-1} and 25-50 °C, respectively. In rheological analysis, every sample was tested at a particular constant temperature and the average of two measurements was reported. A steady shear rate behavior and power-law model fitting of w/o NEs was assessed to study the flow behavior of tested samples.

Table 3.2: Details of rheometer viscosity measurement system.

Measuring geometry	Specifications
Measuring system (ISO 3219)	CP-50-1/Ti (Cone and Plate)
Temperature controller	Peltier
Plate diameter	60.00 nm
cone diameter	49.95 nm
Cone angle	0.998°
Cone truncation	51.00 μm
Cone concentricity	±5.00 μm
Cone parallelity	±4.00 μm

3.2.5 Kinematic viscosity measurement

Kinematic viscosity measurement of all samples was performed in order to characterize the sample with their flow properties at 25 °C. Absolute viscosity (Pa.s) of a finally prepared sample was assessed in a rheometer (Anton Paar MCR 702, Germany) by plotting relation between shear stress (Pa) and shear rate (s^{-1}). Density measurement of all sample was performed in a 25 ml density bottle at 25°C ($kg.m^{-3}$). Kinematic viscosity ($m^2.s^{-1}$) of all samples was calculated by the estimating the ratio of absolute viscosity ($kg.m^{-1}.s^{-1}$) and density at 25 °C. Effect

of change of dispersed phase composition on the kinematic viscosity of formed NE was been assessed in detail in the chapter 5.

3.2.6 Error estimation

For analyzing the error associated between the model predicted and experimental values of experimental runs by adopting the response surface methodology (ANOVA test) and ANN (artificial neural network) data, a non-linear regression analysis was performed to assess the effect of different variables on NE formation. The regression models were assessed based on the following parameters shown in Eqns. (3.9) and (3.10) (Jacob and Banerjee, 2016).

$$MSE = \frac{1}{n}\sum_{i=1}^{n}(Y_{i,Exp} - Y_{i,ANN})^2 \tag{3.9}$$

$$R^2 = 1 - \frac{\sum_{i=1}^{n}(Y_{i,Exp} - Y_{i,Model})^2}{\sum_{i=1}^{n}(Y_{i,Exp} - \overline{Y}_{i,Exp})^2} \tag{3.10}$$

where, n is the number of data points or experimental runs, $Y_{i,Exp}$ is the ith experimental value, $\overline{Y}_{m,Exp}$ is the average of n experimental values, $Y_{i,Model}$ is the ith predicted value by model.

3.2.7 Emulsion stability

3.2.7.1 Analysis of kinetic stability

Kinetic stability of CEMSNE samples was tested to observe the possible breakdown due to creaming and coalescence phenomenon. The test was carried out in the centrifuge of make, Heraeus Biofuge Stratos Centrifuge (230V; 50/60H), Osterode, Germany at the room temperature using 5000 rpm rotation for 15 minutes by measuring the droplet size before and after the centrifugation under the centrifugal force of 4620 g.

3.2.7.2 Long term stability

Long term stability of the low energy and CEMSNE samples was studied by measuring droplet size as a function of time. Samples were stored at room temperature and their respective droplet sizes were measured at different time intervals for duration of 30 days in case of low energy method and 45 days in case of high energy method. Change in droplet size with respect to time was assessed. Instability models like Ostwald's stability and coalescence was fitted to know the instability rates of the tested samples.

3.3. EXPERIMENTAL DESIGN AND OPTIMIZATION ALGORITHM

The most recurrent aim for optimization is to exploit the benefits of nano-emulsions compared with the conventional macro-emulsions with respect to their smaller size and low polydispersity index. Parameters of heuristic and metaheuristic algorithms have been tuned by using different approaches by several researchers. In a metaheuristic approach, researchers have evaluated guidelines to select parameters for particle swamp optimization and validated them by using experimental design (Shi and Eberhart, 1998).Whereas in other studies parameters of Tabu search algorithm were tuned by factorial design (Taillard, 1991). Several studied have used experimental design (RSM) for getting the optimized combination of parameters that would help in fine tuning the artificial neural network (ANN). Likewise, many studies involved the use of different optimization techniques like Taguchi method, Evolutionary Algorithms, etc. for improvements in the performance of ANN (Ding et al., 2013; Khaw et al., 1995; Peterson et al., 1995). The lack of knowledge and information of these tools in analyzing the results poses the difficulty in working in this area (Bashiri and Farshbaf Geranmayeh, 2011). Present work therefore uses the heuristic approach wherein, algorithm includes first the parametric optimization through response surface methodology, thereafter ANN is applied on the RSM generated design points. Furthermore, genetic algorithm finally tunes the results by making use of hybrid GA technique wherein, RSM generated fitness function and ANN generated data points are used to initialize the algorithm. Therefore this work applies both of the models viz. CCD-RSM and ANN-GA for finding the efficient results regarding the formation of w/o NEs that comprises of minimum droplet with lower kinematic viscosity simultaneously.

3.3.1 Experimental design

RSM is a mathematical and statistical analytical tool based on developing model that inspect effect of multiple independent variables and their interaction with response variables. RSM was first developed in 50s by Box and collaborators (Bezerra et al., 2008). Box-Behnken (BBD) and central composite (CCD) designs are mostly used response surface designs applicable for optimizing the emulsification process. Both designs can accommodate second order terms, however, BBD is less expensive in experimentation than CCD since it includes less data points. CCD on the other hand is ideal for sequential experimentation and accommodates first and second order data points more efficiently because of inclusion of central and axial points to the existing factorial design. Therefore, CCD can model response points with a curvature. One additional advantage of selecting CCD is that it incorporates five levels in a single factor,

whereas, BBD is restricted to only three levels per factor. Optimization of w/o NEs was performed using CCD with 30 experiments designed by considering five level, four parameters such as water fraction (Φ_w), surfactant fraction (Φ_s), power density (W.cm^{-2}) and ultrasonication time (minute) as shown in Table 3.3.

Table 3.3. Analytical factors and levels for droplet size and kinematic viscosity in RSM-CCD model.

Variables	Factors	Coded Levels					Std. Dev.
		-2(-α)	-1(Low)	0(Mean)	+1(High)	+2(+α)	
Water (wt. fraction), Φ_w	A	0.02	0.05	0.08	0.11	0.14	0.027
Surfactant (wt. fraction), Φ_s	B	0.05	0.10	0.15	0.20	0.25	0.045
Power density (W.cm^{-2})	C	21.25	29.75	38.25	46.75	55.25	7.730
Ultrasonication time (minute)	D	1	4	7	10	13	2.730

Since, the number of variables operated for this work are less than 6 (Alzorqi et al., 2016), a full uniformly rotatable CCD (RCCD) was used in the study that consists of factorial points (2^k), star points (2k) and central points (C_p). In RCCD, if a distance of ±1 unit is maintained between the center of the design space to a factorial point, the distance of |α| >1 would obtained from center of the design space to the star point. However, star or axial point estimates the curvature of rotatable design. Estimation of total number of experimental points in the RCCD was calculated from the following Eqn. (3.11) (Bezerra et al., 2008):

$$N_T = 2^k + 2k + C_p$$

(3.11)

where, k is the number of variable, and C_p is the replicate number of central points. In case of k=4, value of C_p was six and varies according to the number of variables. In consistent with Eqn. (3.11), total 30 number of experimental points were considered in RCCD. α value in case of rotatable design was calculated from $\alpha=(2^k)^{1/4}$, that corresponds to 2 in the present study (Table

3.3). To determine the optimal conditions of RCCD generated data, multiple regression was performed on a quadratic polynomial Eqn. (3.12):

$$Y = \lambda_o + \sum_{i=1}^{k} \lambda_i X_i + \sum_{i=1}^{k} \lambda_{ii} X_{ii}^2 + \sum_{i<j}^{k} \sum_{j}^{k} \lambda_{ij} X_i X_j + \varepsilon$$

(3.12)

where λ_o is the constant term or offset, λ_i is the regression coefficients for linear effect or slope of input variable X_i, λ_{ii} is the quadratic effect ,λ_{ij} is the cross product term and ε is the statistical error (Montgomery, 2001; Myers et al., 2016). RCCD coded independent variables were calculated according to Eqn. (3.13).

$$z = [z_o - z_c] / \Delta z$$

(3.13)

where z, z_o, z_c and Δz are the coded level, actual value, central point value and step change, respectively. The individual values coded for all four independent variable viz. Φ_w, Φ_s, PD (power density), and UT (ultrasonication time) are summarized in Eqns. (3.14)-(3.17) as follows

$$A = [\Phi_w - 0.08] / 0.03$$

(3.14)

$$B = [\Phi_s - 0.15] / 0.05$$

(3.15)

$$C = [PD - 38.25] / 8.5$$

(3.16)

$$D = [UT - 7] / 3$$

(3.17)

Coded values of factors A, B, C and D are shown in Table 3.3. Design expert (Version 11, State-Ease Inc. Minneapolis, MN USA) was used to design total number of experiments, data analysis and model prediction.

3.3.2 Artificial Neural Network (ANN)

For finding the critical parameters for the formation of w/o NEs that involve the combination of isothermal dilution method and ultrasonic cavitation, no study have been performed with artificial neural network approach. Therefore present work explores the ANN in combination with RSM in tuning the process variables. ANN is a computational method comprising of collection of artificial neurons that imitates neurons in a biological brain (Bezerra et al., 2008; Kundu et al., 2015). ANN processes nonlinear signals through interconnected processing device known as neuron. As shown in Fig. 3.6 (a), these neurons are arranged in a

series of different layers consisting of an input layer of independent variables (water and surfactant fractions, power density and ultrasonication time), output layer (average droplet size and kinematic viscosity) and single hidden layer with n number of neurons that has to be decided by hit and trial methods. Each input neuron is connected to the n number of neurons in a hidden layer (as shown in Fig. 3.6 (a)), however, several hidden layers may be connected in ANN. Network training is executed by bringing out modifications in strength of the network connection with the target to minimize the changes between existing and desired outputs. In each hidden layer, interconnections among the neurons is established by weights and biases (Jacob and Banerjee, 2016). In training process, j number of neurons receives the input signals (x_i), aggregates and weights (w_{ij}) associated with them were summated according to Eqn. (3.18). Signals are then transformed with a suitable transfer function to get the required output (y_i) as shown in Eqn. (3.19) and schematically represented in Fig. 3.6 (b) and (c).
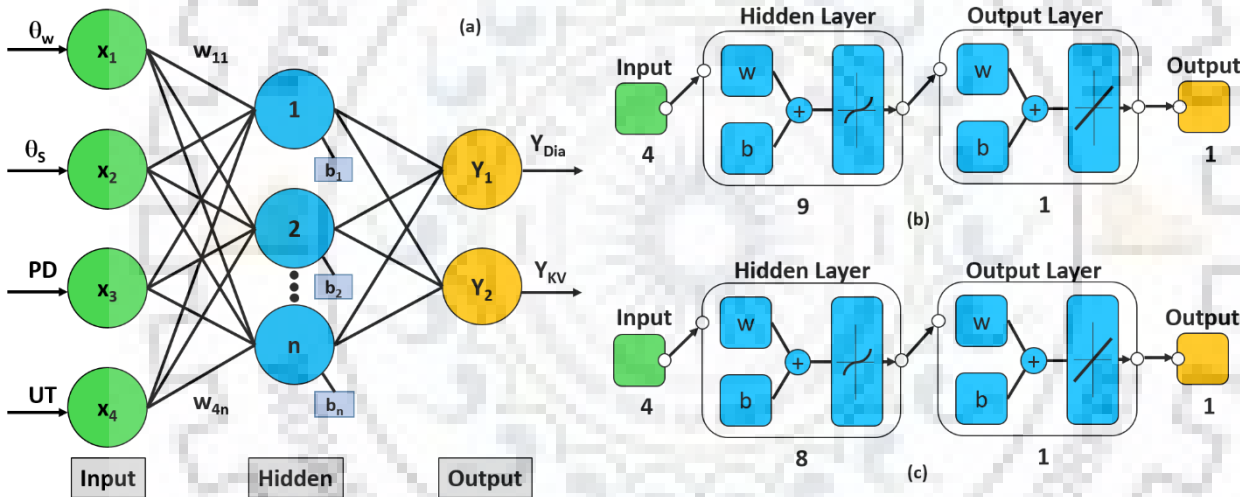
Fig. 3.6 (a) Structure of ANN (4-n-2) with four inputs (water fraction, surfactant fraction, power density and ultrasonication time), a hidden layer ('n' neurons) and two outputs viz. avg. diameter (Y_{Dia}) and kinematic viscosity (Y_{KV}); Optimized architecture of FFBP-ANN with topology input, hidden (TANSIG) and output (PURELIN) layer is depicted for predicting the responses **(b)** Y_{Dia} (4-9-1) and **(c)** Y_{KV} (4-8-1).

$$a_j = \left[\sum_j w_{ij} x_i \right] + b_j$$

(3.18)

$$y_i = f \left(\sum_j^n w_{ij} x_i + b_j \right)$$

(3.19)

where a_j is the output of jth neuron and b_j is the bias associated with the neuron j.
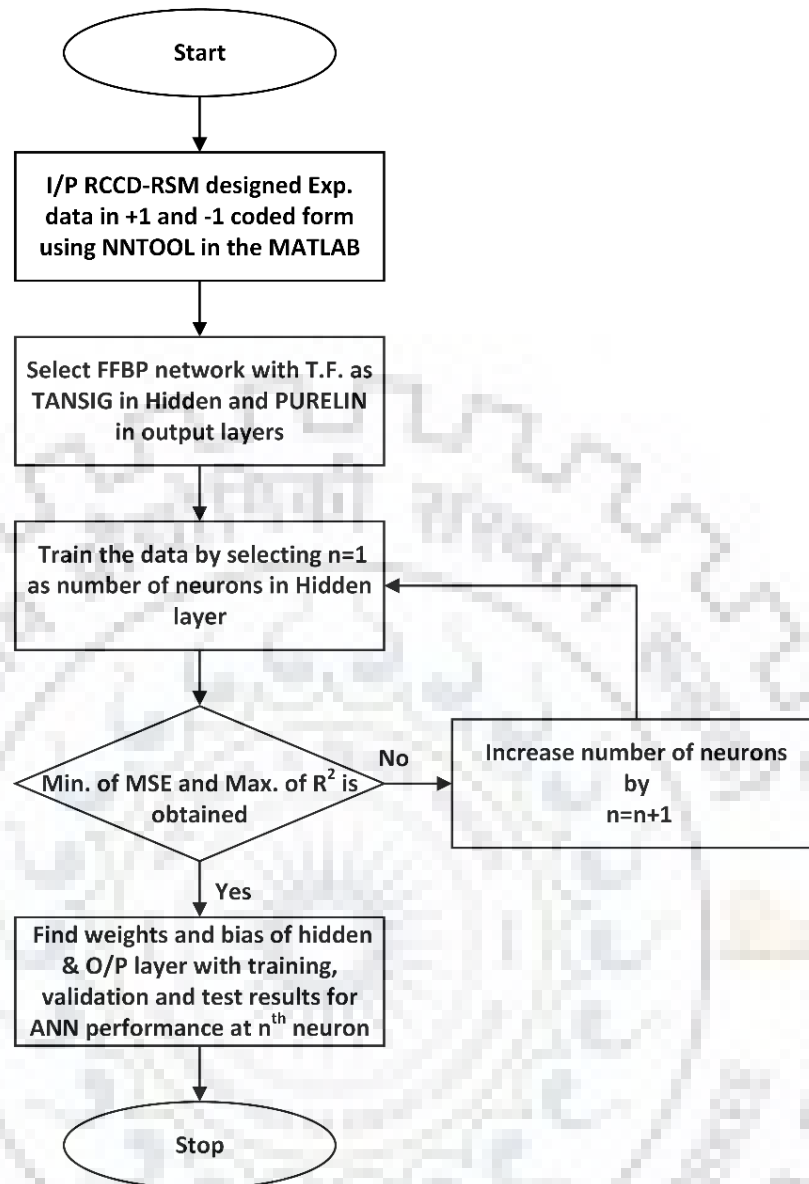
Fig. 3.7: ANN modeling scheme considered in training the process parameters of experimental data sets.

3.3.2.1 ANN modeling scheme

An effective approximation of response can be interpreted by selecting a single hidden layer with sufficiently large number of neurons in a input-output ANN structure as suggested by universal approximation theory (Kundu et al., 2016; Pareek et al., 2002). Consequently, a single hidden layer with n number of neurons was considered in the development of ANN structure. The ANN modeling scheme followed in the present work is as follows (shown in Fig. 3.7):

Step 1: Input and output data set to be used in the input layer was normalized prior to the training in order to make the ANN training more accurate and convergent. Highest value in a data subset

was assigned to +1 and the lowest to -1 according to Eqn. (3.20) (Suryawanshi and Mohanty, 2018).

$$Z_{norm} = \frac{(Z_{max} - Z_{min}) \cdot (X_{act} - X_{min})}{(X_{max} - X_{min})} + Z_{min}$$

(3.20)

where, Z_{norm} represents the normalized value of actual data point (X_{act}) to be normalized. Values, Z_{max} and Z_{min} represent the +1 and -1 values respectively, X_{max} and X_{min} values are maximum and minimum values, respectively, in a data subset to be normalized in the range of +1 and -1.

Step 2: Four input variables used in training the network were same as used in the RCCD-RSM design, whereas, output variables or responses corresponding to average diameter (nm.) and kinematic viscosity (mm^2.s^{-1}) were taken from the experimental results.

Step 3: BP-ANN (feed forward with back propagation) algorithm was applied for developing the ANN using Matlab R2015b (Mathworks Inc. Natick, USA). Weight matrix generated during training of the data was readjusted by minimizing the back propagation error.

Step 4: In order to find out number of neurons in a single hidden layer that could develop a suitable network structure, a hit and trial methodology was used. Number of neurons starting from 1 to 15 were varied and the neuron that could produce minimum MSE (mean square error) along with high correlation index (R^2) was considered as an optimum number of hidden neuron since single criteria can lead to over fitting of the data sets.

Step 5: Among all the available choices of transfer functions (linear, radial, hyperbolic tangent sigmoid function and logarithmic sigmoidal function), hidden and output layers were selected with the help of "nntool" module available in MATLAB.

Step 6: Optimization of neurons in a hidden layer for two responses (Y_{Dia}, Y_{KV}) was performed considering hit and trial method. Adequacy of developed model was verified by calculating MSE and correlation coefficient $R^{2,}$ as shown in Eqns. (3.9) and (3.10). Neurons with minimum MSE and maximum correlation coefficient R^2 were selected in the hidden layer of ANN structure.

3.3.2.2 Network training for function approximation

Steps for network training aimed for function optimization used in the present work are summarized as follows:

Step 1: For training the network, four input variables data viz. water fraction (Φ_w), surfactant fraction (Φ_S), power density (PD) and ultrasonication time (UT) were obtained from the RSM-RCCD design, whereas, two output data like average droplet size ($D_{z\text{-avg.}}$) and kinematic viscosity (KV) were obtained from the experimentation. Input and response data were trained using "nntool" graphical user interface in MATLAB (R 2015 b).

Step 2: After normalization of input and response data sets, weights and biases associated with a single hidden layer were generated automatically by the network. As per the structure shown in Fig. 3.6 (a), weights and biases associated with the hidden layer can be represented by the linear relationship (Eqn. 3.21).

$$a_{j,n} = \sum_{i=1}^{j}(w_{i,W}\cdot(\Phi_W)_n + w_{i,S}\cdot(\Phi_S)_n + w_{i,PD}\cdot(PD)_n + w_{i,UT}\cdot(UT)_n) + b_j \quad (3.21)$$

where j is number of neurons in a hidden layer and n is the number of experiments. Subscripts in $w_{i,w}$, $w_{i,S}$, $w_{i,PD}$ and $w_{i,UT}$ represent the weights for i^{th} neurons connected to input variables as water fraction (Φ_w), surfactant fraction (Φ_S), power density (PD) and ultrasonication time (UT), respectively. Symbols $(\Phi_w)_n$, $(\Phi_S)_n$, $(PD)_n$ and $(UT)_n$ represent the normalized values of input variables for n^{th} run or experiment.

Step 3: Activation or transfer function for hidden layer used in the study was hyperbolic tangent sigmoidal function that transforms input variables to the output response of a neuron. TANSIG transfer function usually takes input from any number within $+\infty$ to $-\infty$ and returns output between +1 and -1. Function for TANSIG can be represented by the Eqn. (3.22) that can be used specifically for the single hidden layer (Fig. 3.6 (b) and (c)).

$$TANSIG(a_{j,n}) = b_{j,n} = \left(\frac{2}{1+\exp(-2a_{j,n})}\right) - 1$$

$$(3.22)$$

Step 4: As shown in Fig. 3.6 (b) and (c), transfer function for the output layer was selected as PURELIN. Again weights and biases in this layer were network generated and allocated to the previous value $b_{j,n}$ as shown in Eqn. (3.22). Linear function for predicting the final output is then represented by Eqn. (3.23).

$$A_o = \sum_{i=1}^{j}(b_{i,n}\cdot w_i) + B_o$$

$$(3.23)$$

where w_i is the weight of the each neuron of output layer and $b_{i,n}$ represents the output values of TRANSIG function (Eqn. (3.22)). Term $b_{i,n}$ indicates the ith neuron out of total j neurons and the matrix (j x n) is extended up to n number of experimental data. B_o refers to the bias of output layer and A_o denotes the final normalized output values.

Step 5: In order to obtain a true value, final results obtained from Eqn. (3.23) needed to de-normalize. Eqn. (3.20) was used to get the actual results of the RSM-ANN scheme.

3.3.3 Genetic Algorithm (GA)

GAs are essentially a heuristic solution (optimization) technique, based on evolutionary approach (genetic selection) for evolving solution to a given problem (Kundu et al., 2015; Mccall, 2005). GA has potential to find out the global optima in problems of complexity by performing a global search in potential areas of state space. The sequence for solving the genetic algorithm involves steps like initialization, selection (fitness evaluation) followed by genetic operators like reproduction, crossover and mutation. The hybrid GA technique shows improvement in back propagation ANN training schemes (Karimi and Yousefi, 2012). In this hybrid GA scheme, initialization was performed by providing weights input from the BP-ANN and a global search was performed. Subsequently, search based on the initial weight input was refined to get the better estimate near to the global optimum value. A fitness function was used to evaluate the fitness of individual chromosome (known as response or dependent variable). A population of chromosomes was then generated randomly of size N. To assess the closeness of optimality of solution, fitness value was assigned to each solution or individual chromosome. A Tournament selection operator was then applied for keeping multiple copies of good solutions in population and eliminating the bad solutions from the population. The selected chromosomes thus obtained will undergo genetic transformations by genetic operators such as crossover and mutation. In the reproduction phase, crossover mechanism involves combination of two parent chromosomes producing two new chromosomes of same length. Crossover is applied to the randomly chosen pairs of parent chromosomes only. Each of the offspring thus produced inherits some gene information from their individual parent. Mutation mechanism randomly (with very low probability) changes genes of each child after crossover.

Data obtained from BP-ANN network were employed as an initial population (initialization). Dependent variables like average diameter of dispersed phase (water nanodrops) and kinematic viscosity of nano-emulsion diesel were fixed as chromosomes. Each chromosome consists of four genes (independent variables), viz. water fraction, surfactant fraction, power

density and ultrasonication time. A fitness function obtained from the RCCD-RSM was used to evaluate set of randomly generated chromosomes. An optimal solution in the form of minimum water droplet size and kinematic viscosity of nano-emulsion fuel resulted by repeated modified successive generations using genetic algorithm tool box of Matlab R2015b (Mathworks Inc. Natrick, USA).

3.3.4 Integrated Modeling (BP-ANN coupled with GA)

An integrated modeling approach was adopted for optimizing input variables more effectively in finding best possible multiple responses in the formation of water dispersed nano-emulsion diesel fuel. RSM was combined with BP-ANN and GA optimization tool in achieving the minimum droplet size and kinematic viscosity of w/o NEs sysyem. Algorithm for integrated modeling approach is shown in Fig. 3.8.

Rotatable CCD design was adopted so that equal variances of the predicted values of the response are obtained with additional star points covering the curvature of the design. These statistically arranged and normalized data points were used in training the back propagation ANN technique. Data obtained from BP-ANN scheme were finally used as initial population and a second order model equation generated by the RCCD-RSM method was adopted as fitness function in the hybrid GA. A multi-objective GA was performed including selection, crossover and mutation steps until the optimized results were obtained. Optimized input variables like Φ_w, Φ_s, power density and ultrasonication time obtained in RCCD-RSM and hybrid GA were finally tested as confirmatory experiments in tuning the response variables.
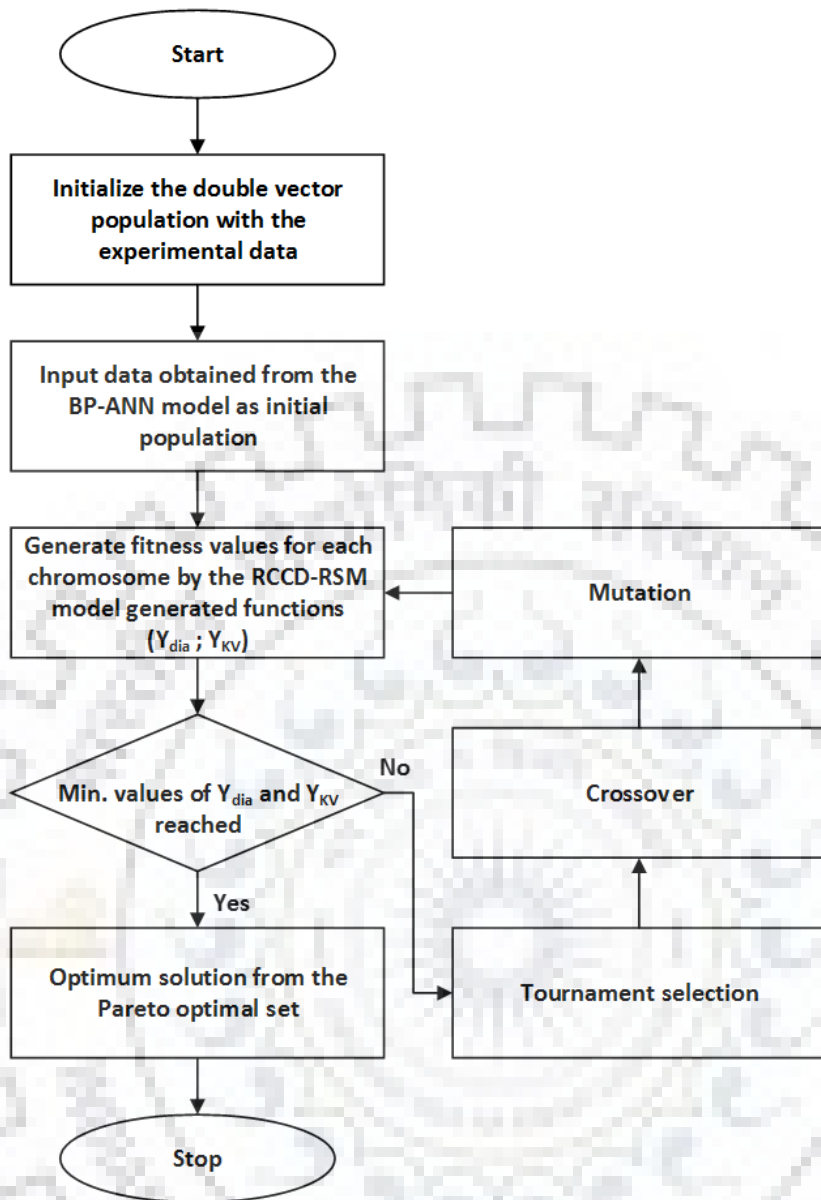
Fig. 3.8: Hybrid GA algorithm (BP-ANN coupled with GA) for solving multi-objective optimization.

CHAPTER 4

PREPARATION AND CHARACTERIZATION OF WATER-IN-OIL NANO-EMULSIONS

In this chapter, preparation, stability and rheology of water-in-oil nano-emulsions (w/o NEs) was studied. Formation of w/o nano-emulsion by both the methods (low and high energy) started with HLB optimization of individual surfactants in mixed proportions. An optimum mixing ratio (w/w) of two individual non-ionic surfactants at which minimum droplet size of dispersed phase was attained, fixed for rest of the study. Preparation of NEs was performed at a constant mixing temperature. Ternary diagram at fixed temperature, hydrophilic-lipophilic balance (HLB) and surfactant mixing ratio was studied where zones of transparent nano-emulsion was identified by changing water, surfactant and oil ratio at specified co-ordinates.

In sections 4.1.4 and 4.2.6 stability analysis was explained by modeling different instability mechanisms. This chapter includes the flow properties behavior of water-in-oil (w/o NEs) nano-emulsions by rheological analysis. Two different sets of mixed surfactants used for the preparation of w/o nano-emulsions by low and high energy methods were tested for their steady shear rate behavior at four different temperatures explained in sections 4.1.5 and 4.2.7, respectively.

4.1 LOW ENERGY METHOD

4.1.1 HLB optimization

It can be inferred from the Fig. 4.1 that as the HLB value increased from 6.42 to 8.01, at first the average droplet size and PDI decreased from 125.7 nm to 44.87 nm and 0.535 to 0.21, respectively. On further increasing the HLB values from 9.1 to 9.6, droplet size and PDI increased from 76.79 nm to 145 nm and 0.282 to 0.585, respectively. The smallest particle size of 44.87 nm was obtained at HLB value of 8.01 at constant emulsion composition (9% surfactant, 18% water and 73% oil) and temperature of 37±1 ºC and at a mixed surfactants ratio of 35:65 (wt. %) for Tween 60 and Span 80.

4.1.2 Ternary diagram analysis

Phase diagram for water in the diesel oil nano-emulsion was studied to find out the effect of change of composition of the constituents on emulsions to predict the formation zones of transparent emulsion. The phase diagram was constructed at a fixed weight ratio of Tween 60

and Span 80 (35:65). All samples marked in the phase diagram were measured at a constant temperature, stirring rate and dilution rate of 37°C, 700 rpm, 0.5 ml.min^{-1}, respectively, since variation in parameters may cause change in properties of the mixed surfactants. Variation in water was kept limited in the range of 4 to 20 wt. %, whereas mixed surfactants varied in the range of 2-10 wt. %.
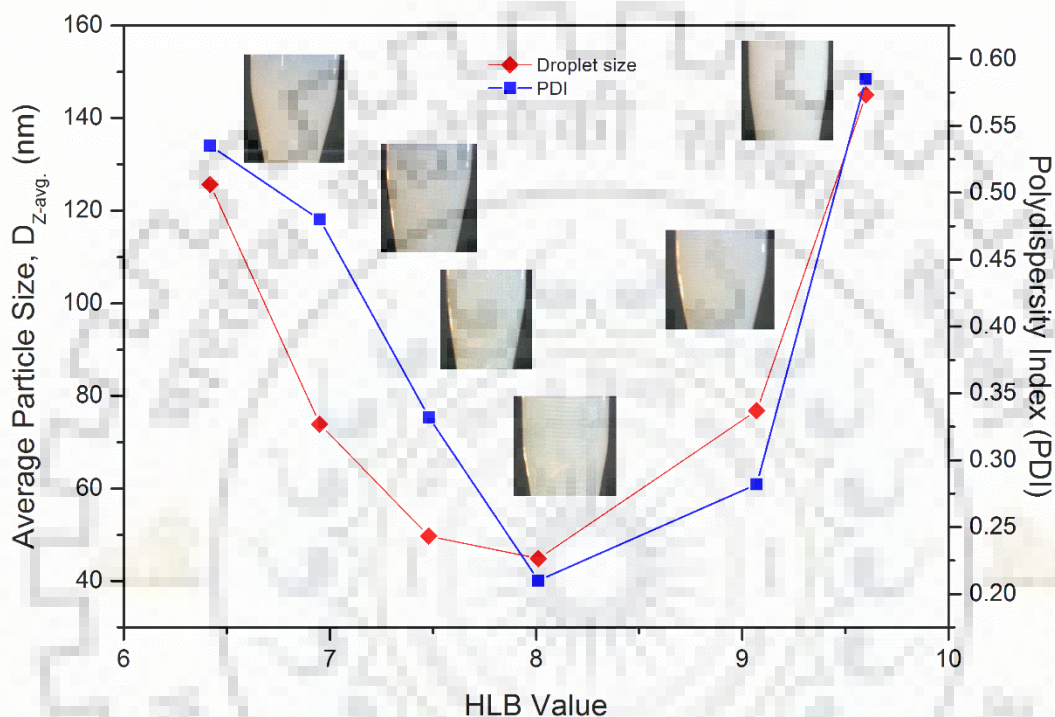
Fig. 4.1: Average particle size (D$_{z\text{-avg.}}$) as a function of HLB value and polydispersity index (PDI) for the mixed surfactant system T6:S8, water and diesel at 37 $^{\circ}$C.

Based on compositions, different sizes of emulsions were formed. Transparent emulsions were formed at the D$_{z\text{-avg.}}$ particle size of 45 to 69 nm, as shown in Fig. 4.2, by square blocks. In transparent zone four sets of equilibrium data points were formed at particle sizes of less than 63 nm and lowest droplet size of 45 nm at 8% surfactant and 20% water. One point of transparent nano-emulsion was found at 2% surfactant and 12% water with droplet size of 66.37 nm. The reason behind nano-emulsion appears transparent is due to the much smaller particle size of dispersed phase as compared to the wavelength of visible spectrum that causes very little scattering of light (Mason et al., 2006).
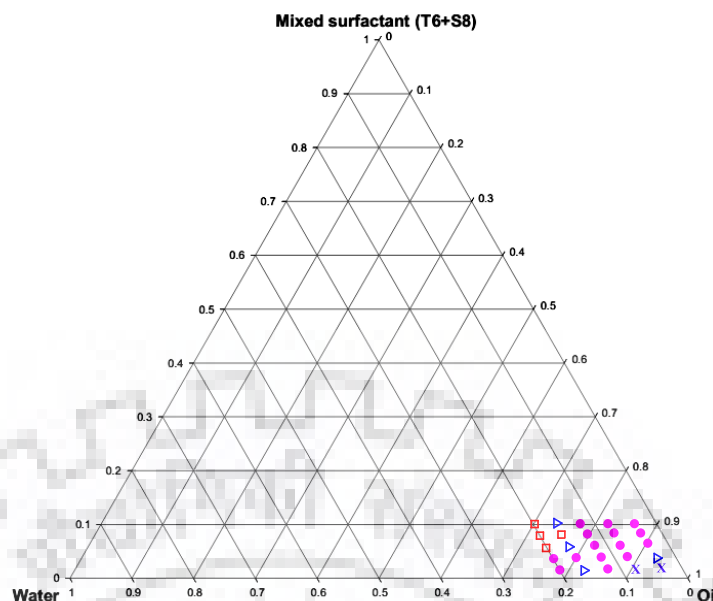
Fig. 4.2: Phase diagram of water/mixed surfactants/diesel oil with surfactants ratio of (T6: S8) 35:65 at 37°C. Tested compositions in the phase diagram are marked with different symbols as transparent [□]; translucent [▷]; opaque [●] and unstable [✕] emulsion. Formulations were tested for droplet size and found in the size range of 45 nm ≤ particle size ≤ 700nm.

Translucent emulsions are shown in Fig. 4.2 by triangular points with droplet sizes ranged from of 70 to 100 nm. As the droplet size increases, and approach near to 100 nm, nano-emulsion starts becoming hazier hence giving translucent appearance. The particle size greater than 100 nm appears white due to multiple scattering of light and opaque region or milky white emulsion was observed between 100 nm to 700 nm particle size (shown in phase diagram by circles). Compositions marked with cross sign in phase diagram are unstable emulsions separating into their original constituents.

4.1.3 Effect of surfactant concentration on particle size and stability

Fig. 4.3 (a) shows the effect of increase of oil to surfactant ratio on particle size at a constant concentration of water (12 wt. %) at 37 °C. It was observed that at lower o/s ratio, lower droplet size was obtained and with an increase in the o/s ratio, droplet size increased almost linearly.

Surfactant plays an important role in the formation and stability of emulsions. In the formation of w/o nano-emulsion, mixed surfactant consisting of Tween 60 and Span 80 was used at optimized composition of 35:65 and their variation as a function of particle size was studied by keeping the water concentration constant at 20 wt.%. Surfactant concentration was varied

from 2 to 10 wt. % and it was observed (Fig. 4.3(b)) that with an increase in surfactant concentration, droplet size decreased from 226 nm to 52 nm (Nejadmansouri et al., 2016; Nesterenko et al., 2014). It may be due to an increase in surfactant concentration in the emulsion causing an increase in the ratio of surface film thickness to the droplet size diameter, which in turn causes the reduction in the droplet size (Liu et al., 2006; Peng et al., 2010). The droplets with increased film of thickness of surfactant showed steric stabilization and hence are more resistant to flocculation.
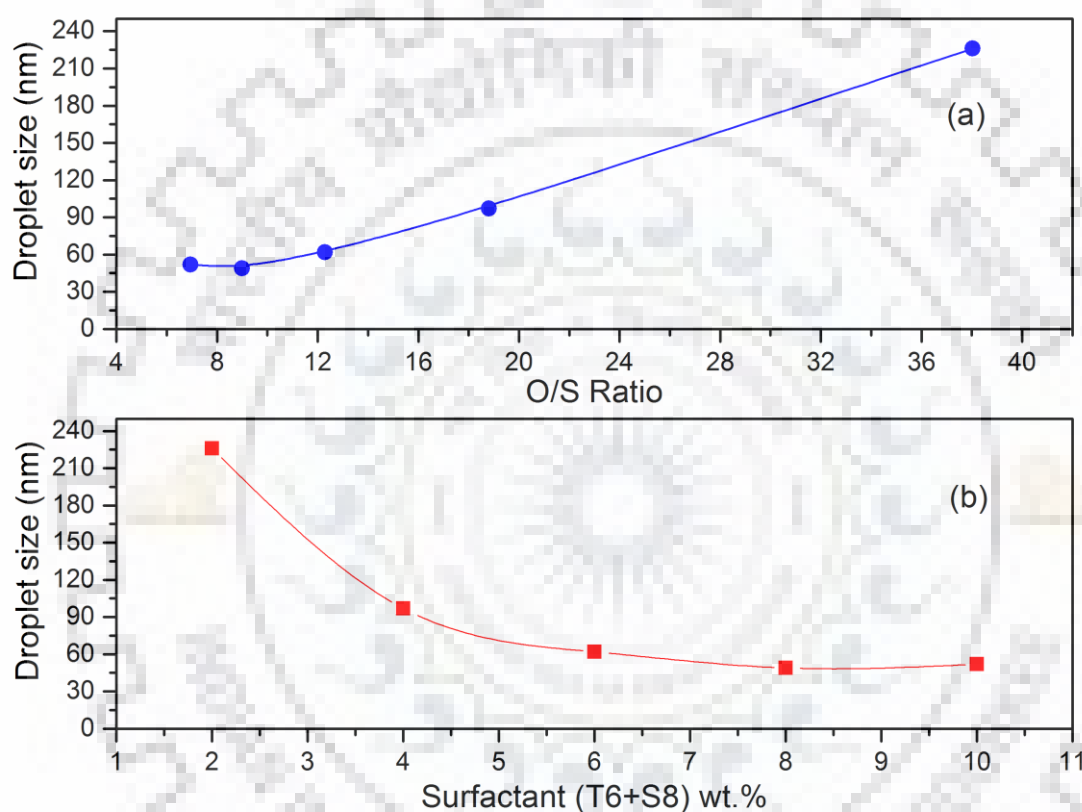
Fig. 4.3: (a) Droplet size (nm) as a function of oil to surfactant (T6+S8) ratio at fixed water concentration (20 wt. %) and **(b)** effect of mixed surfactant concentration on droplet size (nm).

Further, reason behind significant reduction in droplet size at higher concentration of surfactant of (10%) lays in the fact that adsorption of enhanced amount of surfactant takes place on the water/diesel oil interface. As a result reduction in interfacial tension in the system supports easier emulsification and increased stability of droplets against coalescence (Al-Sabagh et al., 2011).

4.1.4 Stability of emulsion

Stability of w/o NEs was studied for 30 days by using mixed surfactant comprising of Tween 60 and Span 80 at a room temperature, i.e. 25 °C. Variation of droplet size with respect to time was studied to know the rate of increase of particle size and probable breakdown mechanism (Rebolleda et al., 2015). Three different compositions of transparent nano-emulsions of different particle sizes were studied, as shown in Fig. 4.4 and tabulated in Table 4.1.

Table 4.1: Coalescence and Ostwald ripening rates of water droplets of different sizes in w/o NEs at 25°C.

Nano-emulsion	Composition (wt. %)	Droplet Size (nm)	PDI	Coalescence		Ostwald Ripening	
				ω (m^{-2}.s^{-1}). 10^7	R^2	ω_3 (m^3.s^{-1}). 10^{27}	R^2
sample 1	8% S8+T6; 5:2 W/S	111.95	0.538	0.723	0.925	0.570	0.983
sample 2	8% S8+T6; 2:1 W/S	73.19	0.476	2.804	0.937	0.167	0.917
sample 3	10% S8+T6; 2:1 W/S	64.28	0.438	3.333	0.717	0.087	0.914
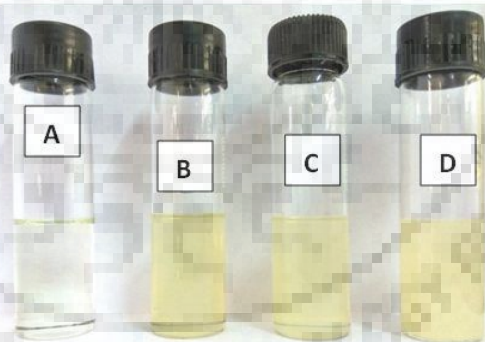
Fig. 4.4: Images of transparent w/o NEs with mixed surfactants (T6:S8) at 3.5: 6.5 weight ratio. sample marked with A is pure diesel oil, whereas B (10% T6+S8; 2:1 W/S), C (8% S8+T6; 2:1 W/S) and D (8% S8+T6; 5:2 W/S) are samples under stability analysis shown in Table 4.1.

All tested samples showed good stability with negligible phase separation and very less increase in droplet size within the stipulated time of 30 days. Nano-emulsion with 8% mixed surfactant and 5:2 W/S ratio, increased its particle size from 111.95 nm at time zero to 142 nm in 4 days whereas in rest of 26 days increase in particle size was merely 7 nm or almost constant as shown in Fig. 4.5. Likewise for w/o NEs of composition 8% S8+T6 and 2:1 W/S ratios, droplet

size increased from 73.19 nm to 93.22 nm in 30 days. Droplet size for 10% S8+T6 and 2:1 W/S increased from 64.28 nm to 79.21 nm in 30 days.

Nano-emulsions are not thermodynamically stable as compared to microemulsions, since w/o NEs form non-equilibrium systems that tend to increase the particle size with respect to time. Further interfacial area and Gibbs free energy tends to decrease with time (Helgeson, 2016; Kundu et al., 2013). Stability of emulsions can be understood by major mechanisms like creaming or sedimentation, flocculation, coalescence and Ostwald's ripening. Creaming or sedimentation does not take place in nano-emulsions because gravitational force reduces and Brownian motion enhances at excessively small particle size. Furthermore, flocculation is also reduced at very small particle size. Probable mechanisms defining the increase in droplet size with respect to time in case of nano-emulsions are coalescence and Ostwald ripening.
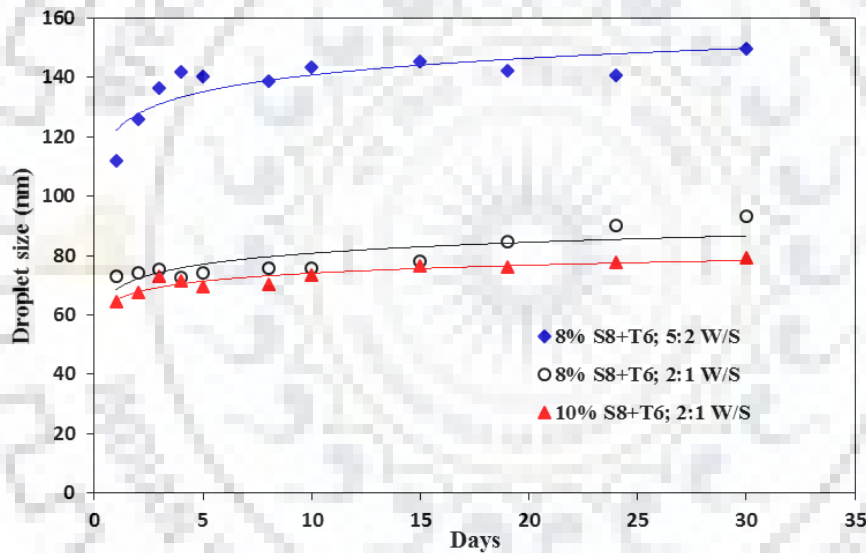
Fig. 4.5: Water droplet size as a function of time for different samples of w/o NEs kept at a constant temperature of 25 ºC. All samples were prepared by keeping constant HLB value (8.01) for the system water, S8:T6 (65:35), and diesel.

4.1.4.1 Instability mechanism by coalescence model

In coalescence two or more droplets merge together into a single larger unit causing reduction in total surface area (Schramm, 2005). Brownian motion of the droplets may cause the rupture and disruption of the film thickness resulting finally rupture of the film. The areas where the surface films are weak have the tendency to fuse together eventually. If the mechanism of instability of the nano-emulsion is coalescence, then rate of change of droplet diameter with respect to time is represented by the Eqn. (4.1) as follows (Usón et al., 2004):

$$\frac{1}{D_{z-avg.}{}^2} = \frac{1}{D_{o,z-avg.}^2} - \frac{2\pi}{3}\omega t \qquad\qquad (4.1)$$

where $D_{z-avg.}$ is the average droplet diameter (nm) at a particular time interval t (s), $D_{o,z-avg.}$ is droplet diameter at zero time; ω is known as coalescence frequency per unit surface area and assumed constant with respect to change in droplet diameter.
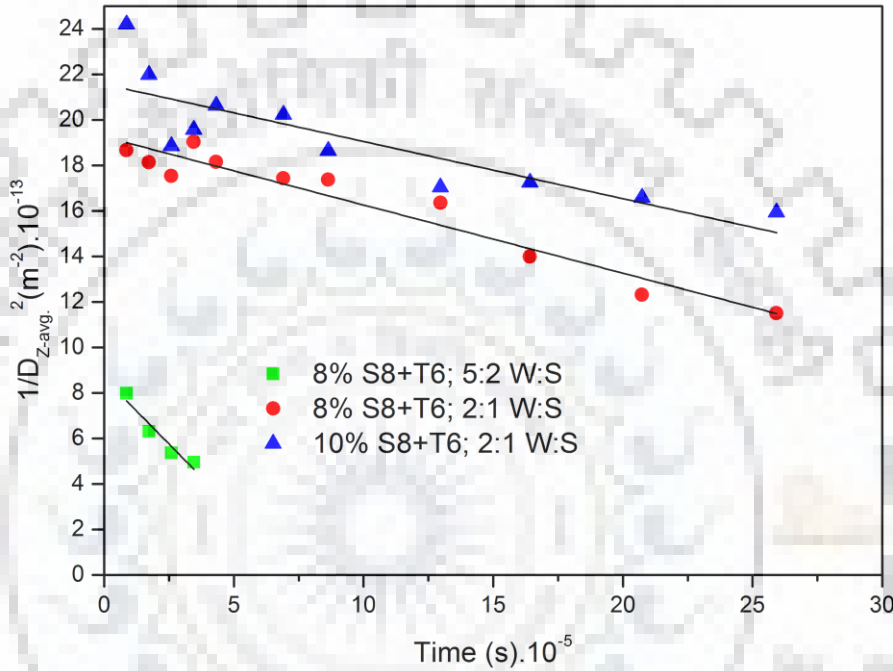
Fig. 4.6: Instability mechanism of w/o NEs shown by plotting 1/ $D_{z-avg.}{}^2$ as a function of time t for three different samples constituting of different compositions of surfactant, water and diesel oil at 25°C.

All three samples of different droplet sizes and compositions were modeled by plotting $1/D_{z-avg.}$ with respect to time t, as shown in Fig. 4.6. Sample 2 containing $D_{z-avg.}$ droplet size of 73.19 nm with composition 8% S8+T6 and 2:1 W/S ratio fit well (with $R^2 = 0.937$) as compared to Ostwald ripening ($R^2 = 0.917$). The reason behind coalescence model fit better for sample 2 lies in the fact that it contains lesser amount of surfactant (8%) resulting in thinner film droplets. Although surfactant concentration is same for samples 1 and 2, however sample 2 have less droplet size of 73.19 nm that makes it more susceptive to Brownian motion as compared to sample 1 resulting in coalescence of droplets with coalescence frequency per unit surface area of 2.804 $m^{-2}.s^{-1}$. Samples 1 and 3 do not fit coalescence model as it is clear from their respective correlation coefficients (Table 4.2).

75

4.1.4.2 Instability mechanism by Ostwald ripening

Ostwald ripening does not involve rupture of film surrounding the droplets like in case of coalescence; instead mechanism is driven by the difference in solubility of different droplet sizes. Droplet of smaller size diameter has higher Laplace pressure and higher solubility as compared to the one having larger diameter. Lord Kelvin first proposed the difference in chemical potential between different sized droplets (Anderson et al., 2014):

$$\Psi(D_{z-avg.}) = \Psi(\infty)\exp\left[\frac{4\gamma V_{mol}}{D_{z-avg.}RT}\right]$$

(4.2)

where, ψ ($D_{z-avg.}$) and ψ (∞) are the solubility (mol.m^{-3}) surrounding the droplet diameter ($D_{z-avg.}$) and the bulk solubility, respectively, γ (N.m^{-2}) is the interfacial tension between the polar and non-polar surfaces, V_{mol} (m^3.mol^{-1}) is the molar volume of dispersed phase, R (J.mol^{-1}K^{-1}) is the gas constant and T (K) is the absolute temperature. Solubility of two different size droplets of diameter $D_{1,z-avg.}$ and $D_{2,z-avg.}$ ($D_{1,z-avg.} < D_{2,z-avg.}$) were correlated by Eqn. (4.3).

$$\frac{RT}{V_{mol}}\ln\left[\frac{\psi(D_{1,z-avg.})}{\psi(D_{2,z-avg.})}\right] = 4\gamma\left[\frac{1}{D_{1,z-avg.}} - \frac{1}{D_{2,z-avg.}}\right]$$

(4.3)

This equation signifies that greater the difference between the diameters of two droplets, the higher is the Ostwald ripening rate. The mechanism of growth of droplet size in case of Ostwald ripening takes place by transferring the disperse phase from smaller droplets to the larger ones. Ostwald ripening is characterized by the two different rates depending on origin of transfer mechanism (Leal-Calderon et al., 2007).

$$\frac{dD_{z-avg.}^q}{dt} = \omega_q$$

(4.4)

1. A constant volume rate ω_3 controlled by molecular diffusion across the continuous phase ($q = 3$).

2. A constant surface rate ω_2 controlled by permeation across the surfactant films ($q = 2$).

where $D_{z-avg.}$ is average diameter of the droplets. Ripening controlled by molecular diffusion is found in submicron regions of diluted emulsions and can be stabilized by using ionic and/or anionic surfactants. Permeation controlled ripening is proposed in case of coarsening of concentrated air foams. The expression for Ostwald ripening rate is derived by using Lifshitz-

76

Slezov and Wagner (LSW) theory showing the change of cube of the droplet diameter linearly with time (Anderson et al., 2014; Li and Chiang, 2012).

$$\omega_3 = \frac{64}{9} \left[\frac{\psi(\infty)\gamma V_{mol} d}{\rho RT} \right]$$ (4.5)

where d is the molecular diffusion coefficient of dispersed phase in continuous phase and ρ is the density of water. Ostwald ripening rate was predicted for three samples of nano-emulsions consisting of different composition of surfactant, water and W/S ratios as 8% S8+T6, 5:2 W/S; 8% S8+T6, 2:1 W/S and 10% S8+T6, and 2:1 W/S. Fig. 4.7 depicts a plot of cube of average droplet diameter with time showing linear relationship among them and slope of these lines give the Ostwald ripening rate ω_3. Equation (4.5) was modeled for all samples and results are shown in Table 4.1 with their respective correlation coefficient. Following observations were made from Fig. 4.7:

1. Instability mechanism is governed by Ostwald ripening effect ($R^2 > 0.91$), as samples 1 and 3 showed better correlation coefficients, as compared to the coalescence.

2. As the average particle size decreased from sample 1 to sample 3 from 111.95 nm to 64.28 nm, respectively, the Ostwald ripening rate decreased from 0.5707×10^{-27} m^3/s to 0.0874×10^{-27} m^3/s and hence making the nano-emulsion more stable (Liu et al., 2011).

3. Decrease in oil to surfactant ratio from 78:8 to 70:10 (sample 1 to sample 3), also decreases the particle size. Availability of surfactant on the droplets increases as the o/s ratio decreases, resulted into the decrease in interfacial tension and more stable smaller droplet size as less gravitational force is experienced. Therefore, lower values of Ostwald ripening rates (ω_3) were experienced.

A comparative study of stability analysis shown in Table 4.2 represents the different Ostwald ripening rates obtained for 70 ± 7 nm droplet sizes by using different combination of mixed surfactants reported in the literature for 15 days stability analysis. Very low value of Ostwald ripening rate (ω_3) was observed in the present work for 30 days by using combination of Tween 60 and Span 80 surfactants. Stability analysis indicate the enhanced stability of the newly formed transparent nano-emulsion system.
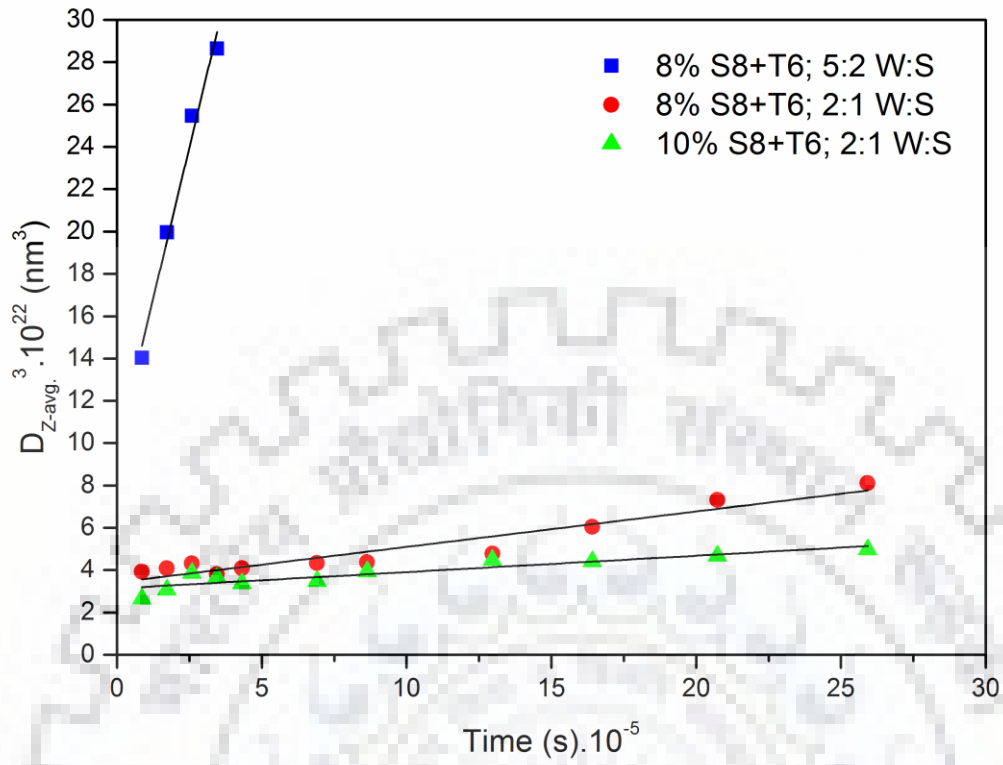
Fig. 4.7: Droplet diameter $D_{z\text{-avg.}}^{3}$ as a function of time for three samples of w/o NEs consisting of different compositions of surfactant, water and diesel oil at a HLB value of 8.01 and 25°C temperature.

Table 4.2: Comparative study of Stability analysis showing Ostwald ripening rate using high energy methods

System	Emulsification method	Surfactant	Droplet size (nm)	$\omega_3 . 10^{28}$ $(m^3.s^{-1})$	Stability analysis	Reference
Water/ Diesel oil	**Low energy**	**Tween 60/Span 80**	**64.28**	**0.874**	**30 days**	**Present work**
Water/ Decane	Low energy	Tween 20/Span 80	64.90	8	15 days	(Porras et al., 2008)
Water/ Diesel oil	High energy	Tween 80/Span 80	66.80	30	15 days	(Noor El-Din et al., 2013)
Water/ Diesel oil	Low energy	Tween 85/Span 80	77.05	80	15 days	(Noor El-Din et al., 2017)
Water/ Diesel oil	High energy	*Emarol 85/Span 80	39.00	39×10^7	15 days	(Al-Sabagh et al., 2012a)

*In case of Emarol 85/Span 80 the best possible data for droplet size near 70 ± 7 nm was 39 nm.

4.1.5 Rheological modeling of nano-emulsions formed using Span 80/ Tween 60

Rheological properties of emulsions is essential in understanding the flow behavior of fluids and their inter-particle interactions. An emulsion with high viscosity is always troublesome in transportation and pumping. An increase in the concentration of dispersed phase in the emulsion increases its viscosity which is responsible for the closed packing of dispersed phase in the emulsion.

In this work different sets of nano-emulsions were tested by using a controlled-stress rheometer (Physica MCR 702, Anton Paar, Germany). EC motor equipped with the rheometer provided the controlled stress and strain modes. A cone and plate sensor was used to test the shear stress and shear strain analysis with cone angle of 0.998^o, cone diameter of 49.95 mm and plate diameter of 60 mm.

4.1.5.1 Steady shear rate behavior

Three samples of w/o nano-emulsions consisting of different compositions of water, surfactant and diesel (Table 4.3) were tested for the temperature and shear range of 25 to 40 ^{o}C, and 10 to 1000 s^{-1}, respectively. Each sample was tested at a particular constant temperature and average of two measurements was reported.

Fig. 4.8 shows rheograms of different sets of w/o NEs at four different temperatures viz. 25 ^{o}C, 30 ^{o}C, 35 ^{o}C and 40 ^{o}C. Variation in shear stress with low to high shear rate range is depicted in plots for nano-emulsion samples, water and diesel. All four plots shown in Fig. 4.8 showed the Newtonian behavior of nano-emulsion samples, water and diesel at all temperatures. Sample 3 (20% water; 10% surfactant) and Sample 1 (20% water; 8% surfactant) showed higher shear stress at any value of shear rate between 10 to 1000 s^{-1} as compared to sample 2 (16 % water; 8% surfactant) with the diesel and water at the bottom (i.e. at 25 ^{o}C and 108 s^{-1} shear rate, shear stress for Sample 3, Sample 1, Sample 2, diesel and water were 0.689, 0.640, 0.566, 0.372 and 0.088 Pa, respectively).
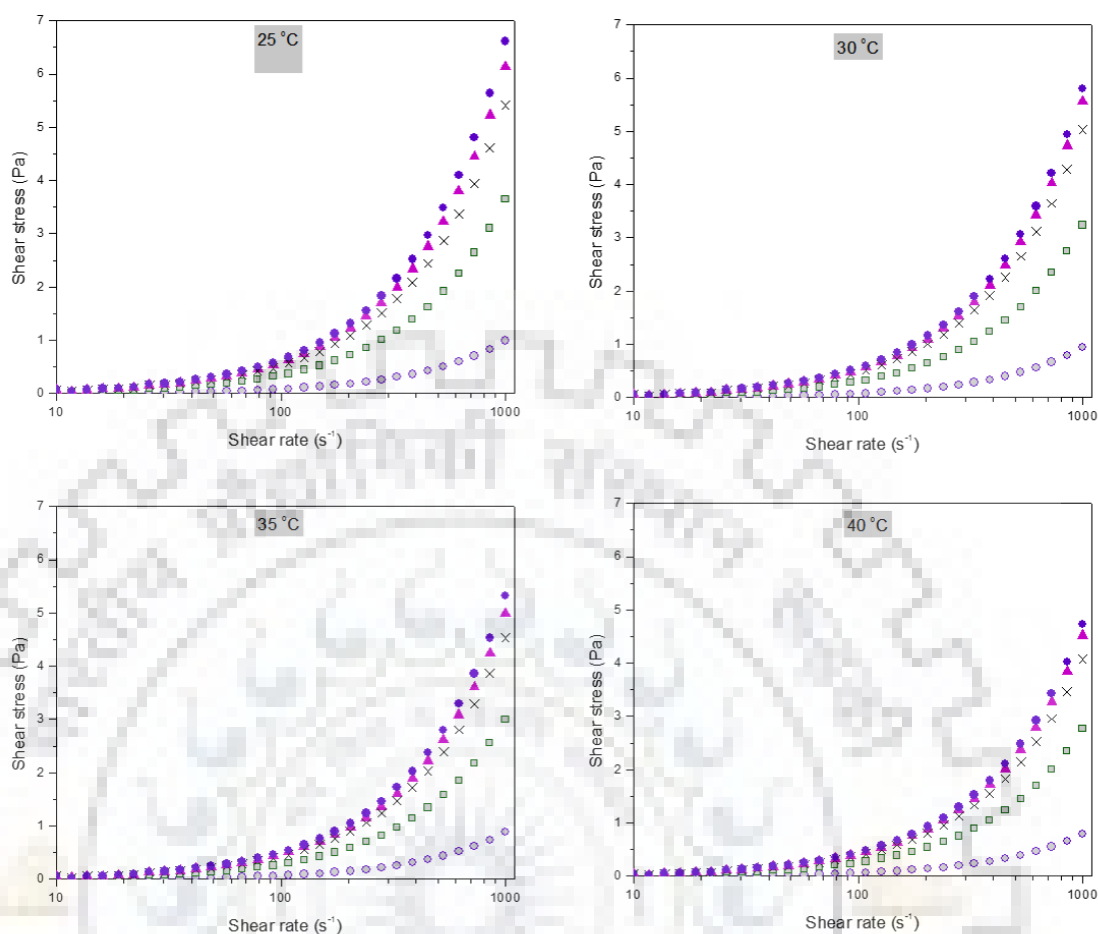
Fig. 4.8: Rheograms of different sets of w/o nano-emulsions, water and diesel at constant temperatures ranging from 25 ºC to 40 ºC. Sample 1 [▲]; Sample 2 [✕]; Sample 3 [●]; Diesel [□]; Water [○].

Furthermore, an increase in temperature, from 25 ºC to 40 ºC, resulted in to a decrease in shear stress at a particular shear rate. Reason behind this phenomenon lies in the fact that amount of dispersion suspended in the samples increased its viscosity whereas increase in temperature decreased its viscosity, as shown in Fig 4.9. Viscosity vs. shear rate plots (Fig 4.9) further supported the Newtonian behavior of Samples 1, 2 and 3, being constant at all values of shear rates (10 to 1000 s^{-1}) and at all temperatures ranging from 25 to 40 ºC.

4.1.5.2 Modeling of w/o NEs flow behavior

A two parameter Ostwald-de-Waele power law model was used to describe the flow behavior of tested nano-emulsion samples.

$$\tau = k\gamma^n \qquad\qquad (4.6)$$

In this equation, τ represents the shear stress (Pa) and γ represents shear rate (s^{-1}) whereas parameters k and n represent flow consistency (Pa.s^n) and flow behavior index, respectively.
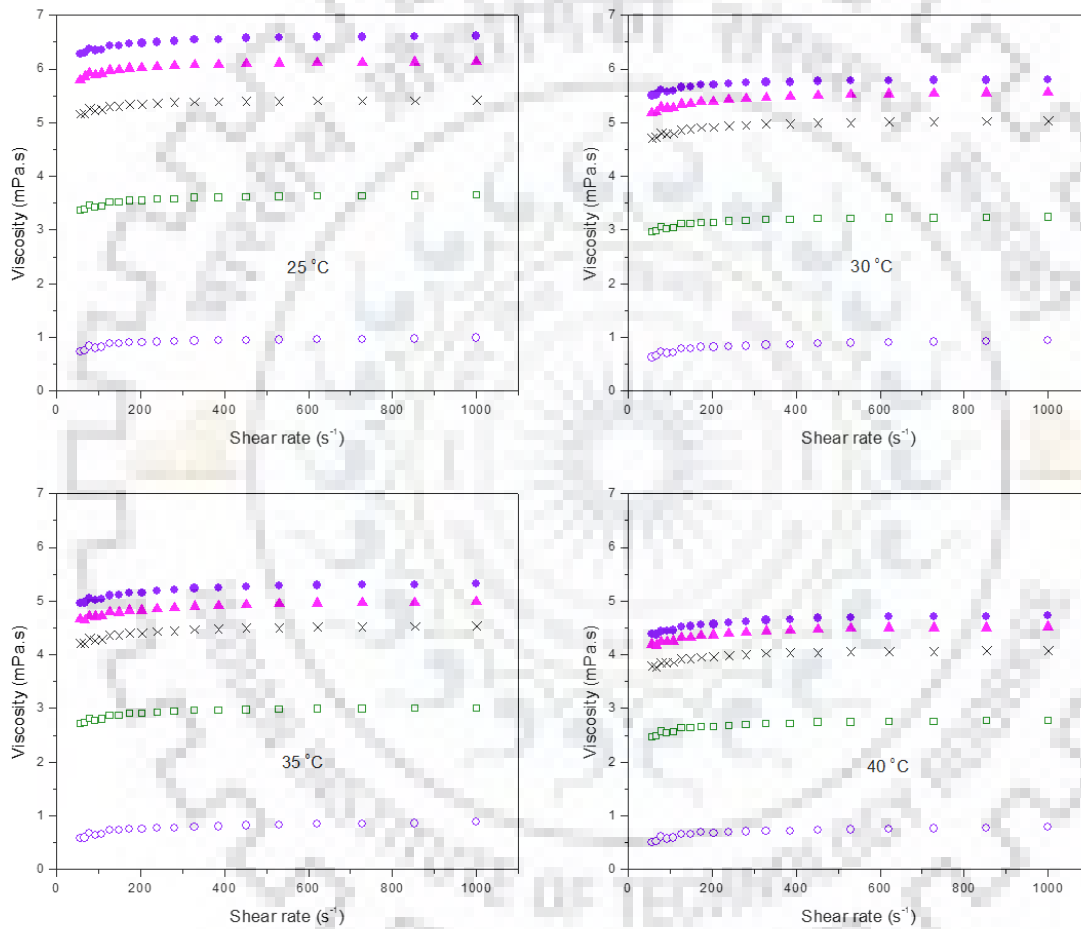
Fig. 4.9: The variation of viscosity vs. shear rate for different sets of nano-emulsions, water and diesel at constant temperature ranging from of 25 ºC to 40 ºC (Sample 1 [▲]; Sample 2 [✕]; Sample 3 [●]; Diesel [□]; Water [○]).

The power law model fitting parameters for all tested nano-emulsion samples by using Eqn. 4.6 are summarized in Table 4.3. All three samples viz. Sample 1 (8% S8+T6; 5:2 W/S), Sample 2 (8% S8+T6; 2:1 W/S) and Sample 3 (10% S8+T6; 2:1 W/S) fitted well with high correlation coefficient (R^2 ranging from 0.9862 to 0.9954) and smaller value of standard error of

regression (S ranging from 0.1003 to 0.1798) at all tested temperatures (Table 4.3). The value of flow behavior index n ranged in $1.0371 \leq n \leq 1.0826$ showed very close range to Newtonian behavior for all samples.

Table 4.3: Power law fitting parameters for w/o NEs at different temperatures.

Temperature (ºC) / Nano-emulsions	k (Pa.s^n).10^3	n	R^2	R-Square [Adj.]	Standard Error of Regression (S)
25 ºC					
Sample 1	4.9	1.0389	0.9945	0.9943	0.1103
Sample 2	4.1	1.0477	0.9922	0.9920	0.1318
Sample 3	5.3	1.0371	0.9954	0.9952	0.1003
30 ºC					
Sample 1	4.1	1.0520	0.9921	0.9918	0.1333
Sample 2	3.6	1.0577	0.9902	0.9898	0.1500
Sample 3	4.4	1.0448	0.9934	0.9931	0.1214
35 ºC					
Sample 1	3.5	1.0610	0.9925	0.9923	0.1309
Sample 2	3	1.0690	0.9862	0.9857	0.1798
Sample 3	3.8	1.0554	0.9919	0.9916	01356
40 ºC					
Sample 1	2.9	1.0723	0.9928	0.9926	0.1296
Sample 2	2.5	1.0826	0.9893	0.9889	0.1600
Sample 3	3.1	1.0712	0.9936	0.9934	0.1220

4.1.5.3 Effect of temperature on emulsion rheology

There was a slight increase in the value of n with an increase in temperature (25-40ºC) tested for three different sets of w/o nano-emulsions (Fig. 4.10). However at a particular temperature all three samples showed almost slight change in n values. A decrease in the value of flow consistency index (k) for all three samples with an increase in temperature from 25 to 40 ºC was observed, as shown in Fig. 4.11.
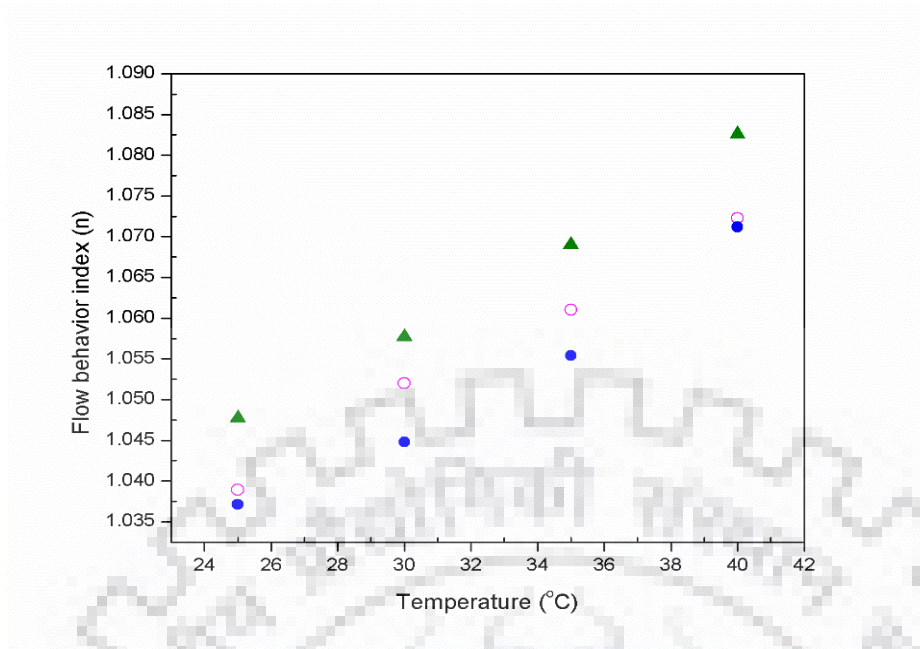
Fig. 4.10: Effect of temperature on flow behavior index (n) for different samples of w/o NEs (Sample 1 (○), Sample 2 (▲) and Sample 3 (●)) tested at temperatures ranging from 25-40°C.
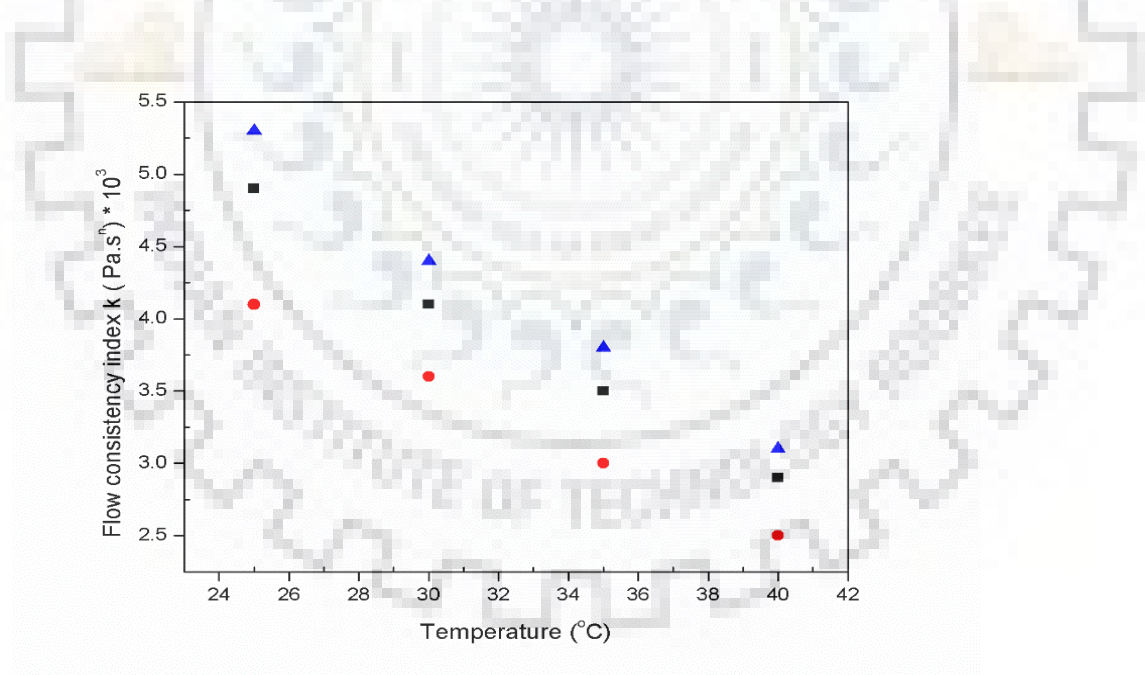
Fig 4.11: Effect of temperature on flow behavior index (n) for different samples of w/o NEs (Sample 1 (■), Sample 2 (●) and Sample 3 (▲)) shown according to the increment in temperate.

84

4.2 COMBINED ENERGY METHOD (CEMSNE)

4.2.1 Optimization of surfactant system

In case of high energy method, HLB value that corresponds to the least possible droplet size in a given set of process conditions was assessed based on the plot between droplets sizes (nm) obtained at respective HLB values. Fig. 4.12 illustrates the change in droplet size, $D_{z\text{-avg.}}$ (nm) and polydispersity index (PDI) as a function of HLB value at constant values of Φ_s (0.075) and Φ_w (0.05). Change in droplet size with respect to HLB value for both methods A and B is depicted in Fig. 4.12. In both methods, an increase in HLB value from 5 to 7 decreased the droplet size up to HLB 7, thereafter, droplet size starts increasing up to HLB 8. In method A, increase in HLB value from 5 to 7 reduced droplet size from 212 nm to 27 nm and thereafter increased up to 253 nm for HLB value of 8. On the contrary, application of method B additionally brought down droplet diameter as compared to method A (Fig. 4.12). $D_{z\text{-avg.}}$ reduced in method B from 78 nm to 25 nm as HLB values increased from 5 to 7, thereafter droplet diameter increased to 135 nm for HLB value of 8. Droplet size obtained in method A was further reduced by application of method B since Laplace pressure (p) of a spherical droplet is inversely proportional to the droplet radius (r) ($p=2\gamma/r$) (Tadros et al., 2004). Consequently application of high shear (p) brings more reduction in droplet size (r) at a particular interfacial tension for the emulsion system.

It can be seen from Eqn. $p=2\gamma/r$ that to break up a drop into smaller droplets, it must be strongly deformed, which further increases p. Therefore, the stress needed to deform the drop is higher for a smaller drop and justifies the application of high energy. Polydispersity in case of method A followed the $D_{z\text{-avg.}}$ vs. HLB curve and showed lower value (0.276) at lower droplet size (25 nm). Whereas in case of method B it was averaged near 0.233 and at lowest droplet size of 25 nm the value reported was 0.216. Since minimum droplet size attained in both methods was at a HLB value of 7, further study of nano-emulsions formation was performed keeping the same value.
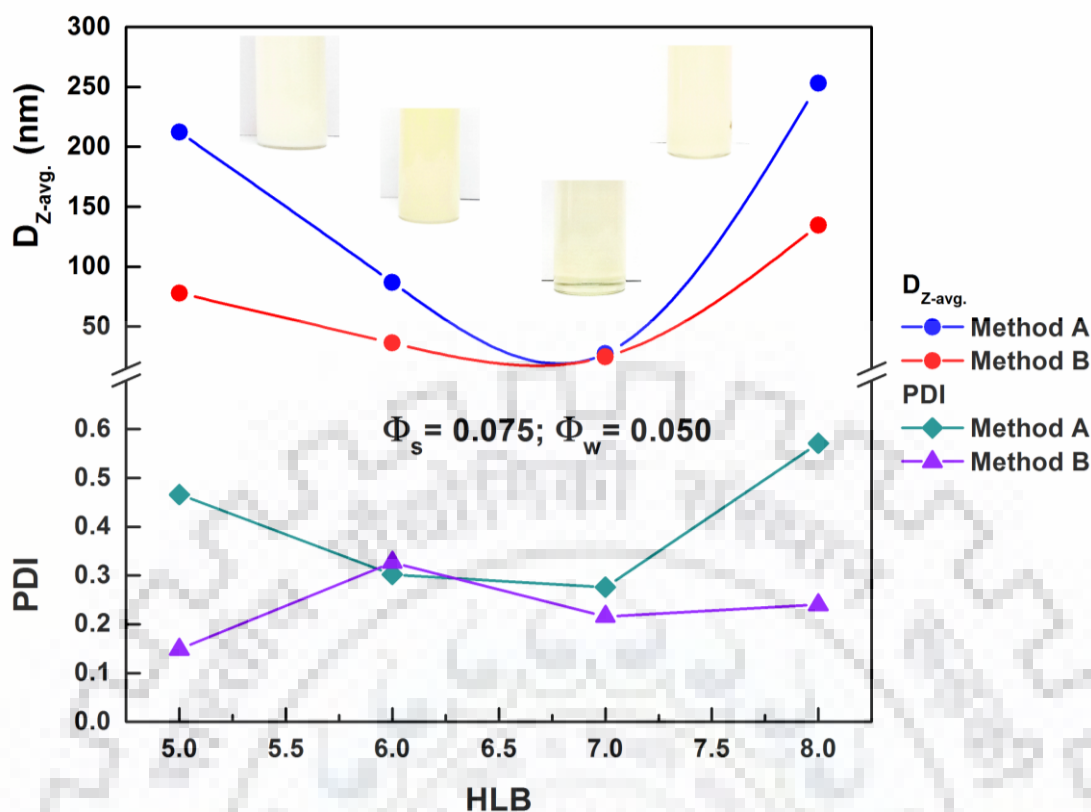
Fig. 4.12: Optimization of HLB value at constant Φ_s (0.075) and Φ_w (0.05) with change in $D_{z-avg.}$ (nm) and polydispersity index (PDI).

4.2.2 Optimization of ultrasonication parameters

Pre-emulsions formed after treatment given in method A were subsequently treated with method B. Application of high energy method in addition to low energy method was aimed to produce an additional reduction in average droplet size at optimized ultrasonication parameters of percent amplitude, pulse control mode (cycle) and sonication time (Table A3 in Appendix).

4.2.2.1 Effect of ultrasonication amplitude on droplet size

Pre-emulsion at constant Φ_s (0.02), Φ_w (0.01) and pulse mode factor (0.6) was ultrasonicated at four amplitude percentages of 25, 35, 45 and 55 and was optimized to achieve minimum droplet size. Ultrasonication time of 2 minutes was fixed for optimization of ultrasonication parameters. Variation in average droplet size, D_{z-avg}, with respect to percent amplitude depicted almost negligible increment in the values from 95.4 nm to 100.7 nm. For example at 25% amplitude, error margin based on replicate experiment was ≈4% (Fig. 4.13). Moreover, the marginal increment in droplet size with an increase in amplitude may be attributed to the start of the violent bubble collapse with further increase in the percent amplitude

(Adewuyi, 2001; Chen, 2012; Wu et al., 2013). Therefore in view of negligible increment or no effect of pressure amplitude on droplet size, 25 % amplitude was fixed for further study based on previous work reported in literature (Henglein and Gutiérrez, 1993, Leong et al., 2009).
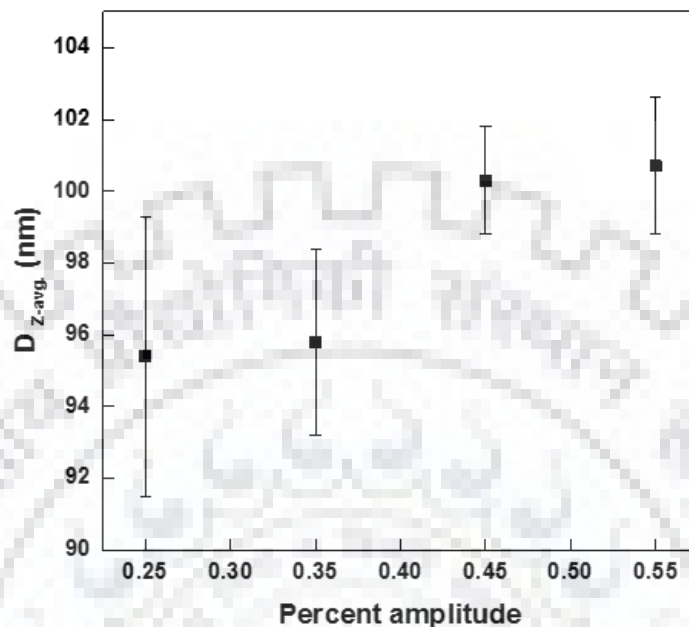
Fig. 4.13: Optimization of ultrasonication parameters at constant Φ_s (0.02) and Φ_w (0.01) as a change in $D_{z\text{-avg.}}$ with percent amplitude.

4.2.2.2 Effect of pulse control mode (cycle) on emulsification

Pulse control mode (cycle) regulates pulse mode factor that switches time on or off in seconds. Set value of 0.8 indicates acoustic irradiation power to be switched on for 0.8 sec and paused for 0.2 sec. Pulse mode control for the emulsion prepared at Φ_s (0.02) and Φ_w (0.01) was varied from 0.3 to 0.7 at an optimized value of amplitude (25%) for ultrasonication time of 2 minute (Fig. 4.14). Value of $D_{z\text{-avg.}}$ (nm) reduced from 146 nm to 94 nm as pulse mode factor was increased from 0.3 to 0.5 subsequently, average droplet size increased from 98 nm to 120 nm. At optimum pulse sonication value of 0.5 the relaxation interval produced suitable vibrational energy input inducing the shear forces necessary to disrupt the larger droplets (Carpenter and Saharan, 2017; Martinez-Guerra and Gude, 2015). Therefore, an optimum value of 0.5 pulse mode control was fixed for present study.
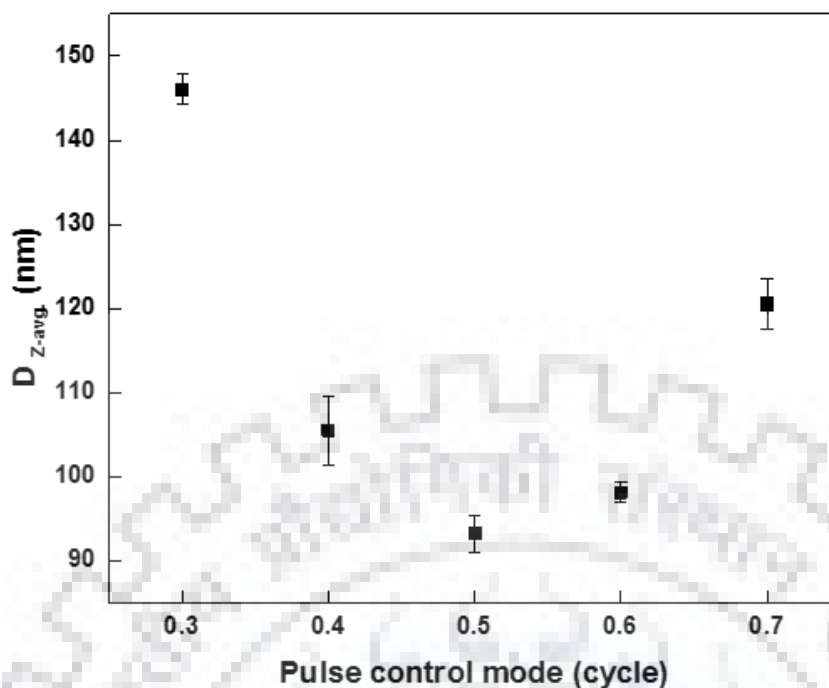
Fig. 4.14: Optimization of ultrasonication parameters at constant Φ_s (0.02) and Φ_w (0.01) as a change in $D_{z\text{-avg.}}$ with (c) percent amplitude (d) pulse control mode (cycle).

4.2.2.3 Effect of ultrasonication time

Optimized ultrasonicated parameters like percent amplitude (25) and pulse mode factor (0.5) were applied to the pre-emulsions formed at constant values of Φ_s (0.075) and Φ_w (0.05) at four HLB (5, 6, 7 and 8) values to study the effect of sonication time on the droplet size (Fig. 4.15). At all HLB values, increase in sonication time first reduced the droplet size afterwards, a constant value was obtained. Optimization time at which minimum droplet size obtained found to be different at different HLB values. At low HLB value of 5 the time required to reduce the droplet size from 212 nm to 78 nm was 28.5 minutes, afterwards no significant change in droplet size was obtained (Fig. 4.15). Likewise for HLB value at 6, it took 10.5 minutes to reduce size from 87 nm to 36 nm. For the optimized value of HLB (=7), 8.5 minute was required to reduce the size from 27 nm to 25 nm, whereas for HLB value of 8, only 1 minute was required to reduce the size from 253 nm to 131 nm. This phenomenon may be attributable to the dissimilar capability of surfactant layer at different hydrophilic lipophilic ratio to withstand shear stresses produced by cavitation effect. High HLB values decreased percentage of Span 80 available on the interface layer of micelle, hence weak packing of lipophilic molecules was achieved owing to less time required for breaking droplet (Carpenter and Saharan, 2017). Sonication time of 8.5 minutes was selected for subsequent study of emulsions at HLB value of 7.
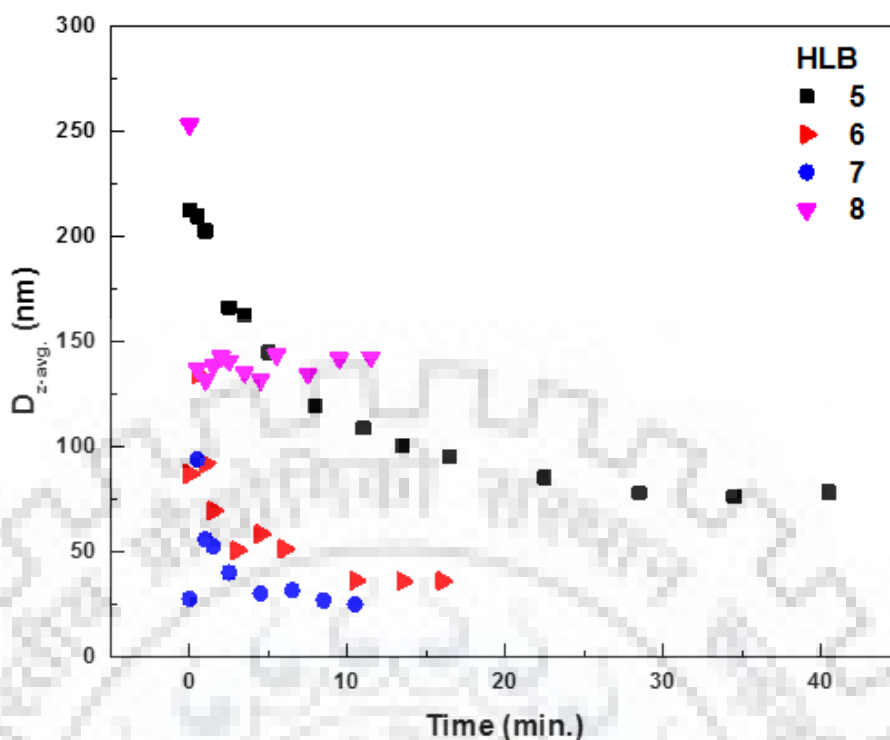
Fig. 4.15: Optimization of HLB value at constant Φ_s (0.075) and Φ_w (0.05) with variation in $D_{z\text{-}avg.}$ and time (minutes) at different HLB values.

4.2.3 Ternary diagram

To determine the composition at which formation of stable and transparent nano-emulsion formation takes place, a ternary diagram study was performed by varying weight fraction of water (Φ_w) and mixed surfactant (Φ_s) from 0.02 to 0.11 and 0.05 to 0.20, respectively. Ternary diagram was developed by application of methods A and B at constant temperature (37 ^{o}C) and HLB value (7). The coordinate points studied in the ternary diagram gave different droplet size and appearance of nano-emulsions. Both methods resulted in different $D_{z\text{-}avg.}$ values due to the difference in the energy input (Fig. 4.16 a, b). Transparent emulsions shown in the Figure 4.16 as open circle found in the droplet size range of $18 < D_{z\text{-}avg.} < 72$ nm, whereas translucent emulsions are shown as open triangle in the $D_{z\text{-}avg.}$ range of $72 < D_{z\text{-}avg.} < 111$ nm and opaque emulsions (color filled circle) in the range of $111 < D_{z\text{-}avg.} < 350$ nm.
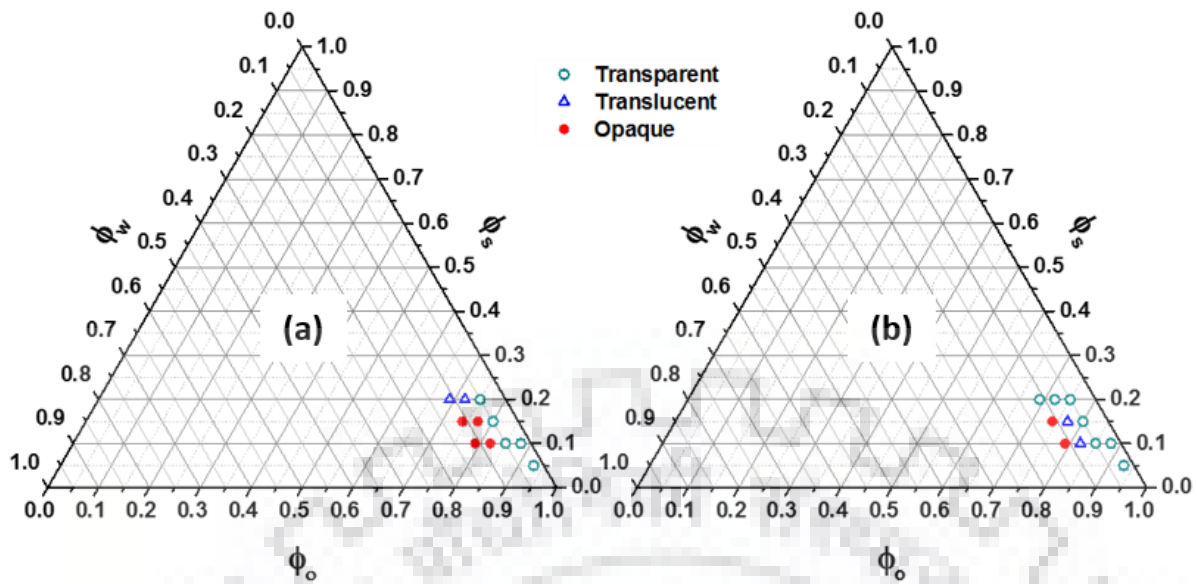
Fig. 4.16: Ternary diagrams for the system water/mixed surfactant/diesel illustrates the zones of [O] transparent, [△] translucent, and [●] opaque emulsions at constant temperature (= 37°C) and HLB (=7) by application of (a) method A (b) method B.
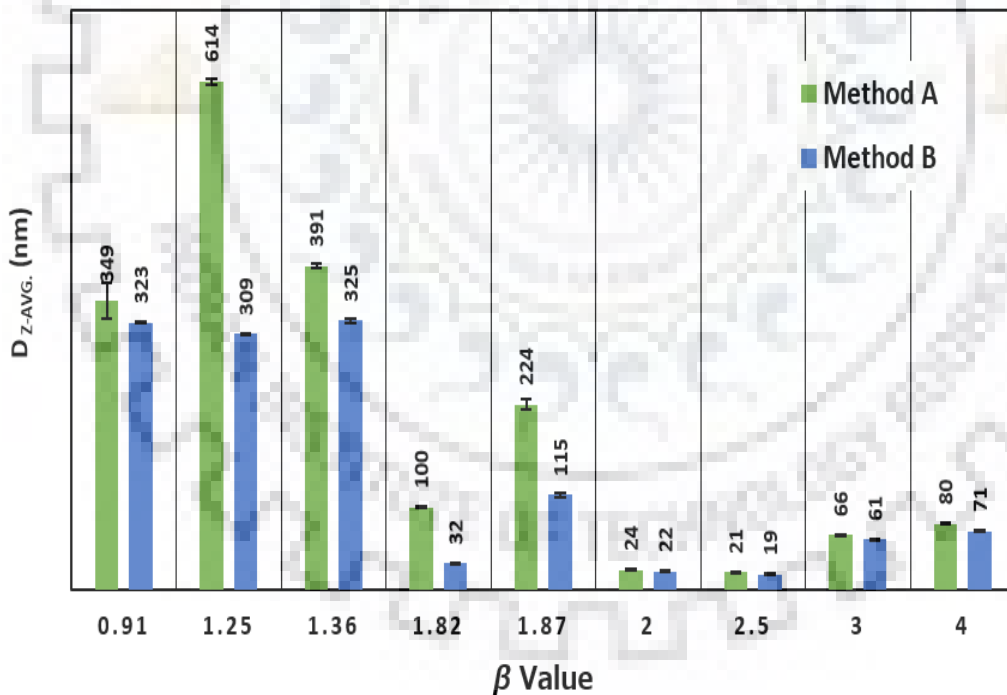
Fig. 4.17: Droplet size distribution as a function of surfactant to water ratio (β).

It can be observed from the ternary diagram that method B resulted in more transparent regions compared to method A. This study also helps in finding the surfactant water ratio (β) accountable for the formation of nano-emulsions (Table A2 in Appendix). Fig. 4.17 depicts the

surfactant to water ratio, β (w/w) as a function of $D_{z\text{-avg}}$ wherein the reduction in average droplet size (nm) at increased values of β (0.91-4.0) was observed. In both methods more pronounced reduction was observed for $\beta \leq 2$, i.e. 614 to 24 nm in case of method A (Table A2 in Appendix). Thereafter, minimum value of droplet sizes, i.e. $22 \leq D_{z\text{-avg.}} \leq 66$ nm for $2 \leq \beta \leq 3$ was observed in method A (Fig. 4.17). However $\beta \geq 3$ incorporated excess concentration of surfactant compared to the optimized value altering the physical properties of the system. Similar trends were observed for method B, as shown in Fig. 4.17 c and Table A2 in Appendix.

4.2.4 Effect of surfactant and water concentration

Formation of emulsions is inherently a non-spontaneous process hence introduction of surface active agent at the interphase of two immiscible phases is requisite so as to avoid separation of different polarity phases. Accordingly, surfactant plays a vital role in the formation and stability of droplets by micelle formation and avoiding coalescence phenomenon (Mason et al., 2006; Tadros et al., 2004). Mixing non-interacting surfactants of different functional groups modulates the emulsion properties like thickness, charge and rheology compared to used alone (McClements and Jafari, 2018). Change in CMC value of the mixed surfactant compared to single one is the reason of changing the behavior of the mixed surfactant (Khan and Marques, 2000; McClements and Jafari, 2018). To assess the effect of increase in mixed surfactant fraction in emulsion on average droplet size, three different samples (pre-emulsions from method A) consisting of Φ_s values as 0.10, 0.15 and 0.20 at a constant Φ_w (=0.08) and energy density (108 $J.ml^{-1}$) were sonicated. A fixed sonication time of 8.5 minute was applied and resultant CEMSNE was assessed for change in average droplet size by DLS technique (Fig. 4.18 (a)).

Application of method A at constant Φ_w (0.08) decreased the $D_{z\text{-avg}}$ from 615-71 nm however, method B decreased droplet size from 309-25 nm with an increment in Φ_s from 0.10-0.20. In both methods reduction in droplet size is more pronounced up to $\Phi_s=0.15$ thereafter it declines up to $\Phi_s=0.20$ (Fig. 4.18 (a)). Introduction of surfactant basically reduces the interfacial tension γ and that in turn reduces the droplet size ($p=2\gamma/r$). Amount of surfactant required to produce smallest drop depends on the activity (a) in emulsion and related to the Gibbs adsorption equation (Eqn. 4.7).
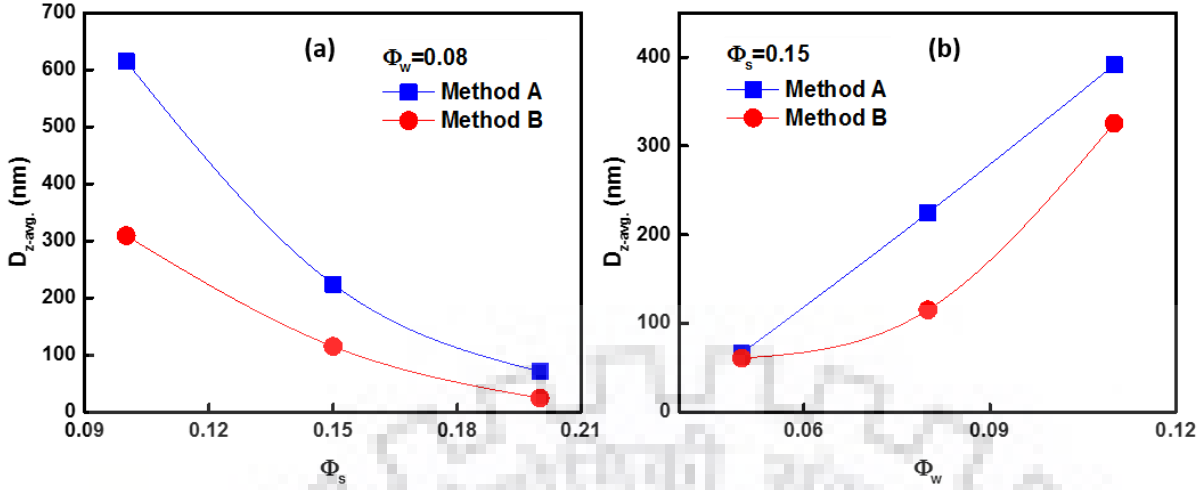
Fig. 4.18: (a) Effect of increase of surfactant fraction (Φ_s=0.10-0.20) on droplet size at a constant Φ_w (0.08) (b) Change in droplet size as function of increase of water fraction Φ_w (0.05-0.11) at a constant Φ_s (0.15).

$$-d\gamma = RT\Gamma d\ln a \tag{4.7}$$

This equation determines the value of γ (Tadros et al., 2004) where R, T and Γ are gas constant, absolute temperature and surface excess (moles adsorbed per unit area of interphase), respectively. The moles adsorbed per unit area of the interface (Γ) increased with an increase in surfactant concentration and in due course it reached a plateau value due to saturation. Hence in both methods reduction in droplet size was more pronounced up to Φ_s=0.15 thereafter it declined up to Φ_s=0.20 (Fig. 4.18 (a)).

To assess variation in droplet size corresponding to the change in water fraction Φ_w (0.05-0.11), emulsion samples were prepared at constant Φ_s (0.15) and HLB value (=7) by both methods (A and B). $D_{z\text{-avg.}}$ increased as water fraction increased in both methods (Fig. 4.18 (b)). A linear increase in droplet size was obtained from 66-391 nm at the prevailing emulsification conditions in case of method A. However, method B reduced the droplet size from 61-325 nm. The factor responsible for the nano-scale size of droplets was found to be β (2-3) in the present study.

4.2.5 Effect of energy density on droplet size

To assess the effect of energy density ($J.ml^{-1}$) on the average droplet size (nm) of the CEMSNE, a pre-emulsion was prepared at Φ_s (0.075) and Φ_w (0.05) at HLB value of 7. Inverse relationship between energy density and $D_{z\text{-avg.}}$ was observed during pulse sonication (Abismaïl et al., 1999; Canselier et al., 2002; Ramisetty et al., 2015) of this sample at 25% amplitude and

0.5 pulse mode factor at a maximum acoustic power density of 85 W.cm^{-2}. A prominent reduction in droplet size was observed up to 40 J.ml^{-1} energy density thereafter, $D_{z\text{-avg.}}$ decelerated up to 160 J. ml^{-1} (Fig. 4.19).

The general trend showed decrease in droplet size as energy density is increased. Moreover, it is important to notice that no further reduction in size was achieved past the energy density of 159.5 J/ml. Power law correlation (O'Sullivan et al., 2015) fitted well with the $D_{z\text{-avg.}}$ and energy density, representing the model shown in Eqn. (4.8):
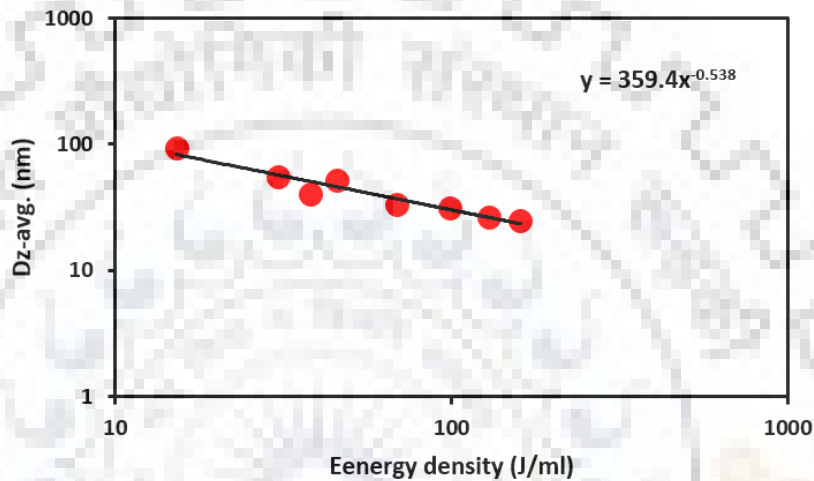
Fig. 4.19: Effect of energy density (J.ml^{-1}) on average droplet size (nm) of the w/o NEs (CEMSNE) at pre-emulsion conditions of Φ_s (0.075) and Φ_w (0.05) and constant ultrasonication parameters, i.e. amplitude (25%) and pulse sonication (pulse mode factor = 0.5).

$$D_{z-avg.} = \frac{a}{\varepsilon_v^{\ b}} \tag{4.8}$$

A product of power density per unit volume of emulsion P_V (W.ml^{-1}) and residence time t_R (s) within the shear field was used to calculate energy density (ε_v) (Canselier et al., 2002; Leong et al., 2009)

$$\varepsilon_v = P_V t_R \tag{4.9}$$

In Eqn. (4.9) ε_v (J.ml^{-1}) refers the energy density applied to the tested sample at different sonication times (seconds). Constant parameters a and b were found to be 359.4 and 0.538, respectively (Leong et al., 2009; Walstra, 1993). Results illustrating the change in energy density with respect to sonication time and droplet size are tabulated in Table A1 in Appendix. This relation may play a vital role in scaling up the samples prepared under similar set of conditions

and depicts the requirement of increased amount of energy to process higher sample volumes capable of tuning the $D_{z\text{-avg.}}$ (nm) (Gogate et al., 2003; O'Sullivan et al., 2015).

4.2.6 Stability analysis

4.2.6.1 Kinetic stability

Kinetic stability of nano-emulsions provides short term stability as well as predict long term stability of samples. Stability of nano-emulsions may alter by application of centrifugal force since speed up in the Brownian motion of the nano-emulsion particles takes place (McClements, 2015; Morais Diane and Burgess, 2014; Silva et al., 2015). As a result, coalescence or separation of dispersed phase with increase in droplet size may take place during the test. In the present study, stability of four CEMSNE samples were tested for evaluating the kinetic stability wherein, samples were kept for one week at room temperature before analysis. No observance of phase separation or coalescence in the tested samples was detected during centrifugation test performed at 5000 rpm for 15 minutes. No increase in droplet size of tested CEMSNE samples for β=2 (22 nm), β=2.5 (25 nm), β=3 (61 nm) and β=4 (71 nm) was observed during the test at a constant temperature of 25°C, which indicated the kinetic stability of the CEMSNE samples.

4.2.6.2 Long term stability

Variation in average droplet size of transparent w/o NEs samples was tested for duration of 45 days by keeping samples at room temperature for the observance of their reduction in $D_{z\text{-avg.}}$ (nm) value as a function of time (days) (Fig. 4.20 (b)). As the value of β increased from 2 to 4, change in $D_{z\text{-avg.}}$ increased accordingly. For β=2 ($\Phi_s = 0.10$; $\Phi_w = 0.05$) , no phase separation or coalescence was observed, no significant change in droplet size was obtained hence, this sample proved to be stable up to a time under study (Fig. 4.20 (b)). Polydispersity of β=2 sample was also observed constant in the range of 0.17 that essentially tend towards the mono-dispersion property of the tested nano-emulsion samples. However for β=2.5 (Φ_s=0.20; Φ_w=0.08), droplet size changed from 25±1 nm to 30±1 nm for first 6 days thereafter, almost constant values were obtained till 32±1 nm up to a time period of 40 days. The polydispersity in case of β=2.5 sample increased up to 0.456 and was under the accepted limit (PDI<0.7). In case of β=3.0 ($\Phi_s = 0.15$; $\Phi_w = 0.05$), droplet size was changed from 61±1 nm to 72±1 nm for the first 10 days thereafter, values stays almost constant and after duration of 43 days. Droplet size in case of β=4.0 ($\Phi_s = 0.20$; $\Phi_w = 0.05$) changed from 71±1 nm to 81±1 nm for the first 7 days thereafter, almost no change in the size was observed. Values of polydispersity of β=4.0 changed in the range of 0.26-

0.32, as shown in Fig. 4.20 (a). Consequently, w/o NEs with β=2.0 showed better stability compared to the β=2.5-4.0.
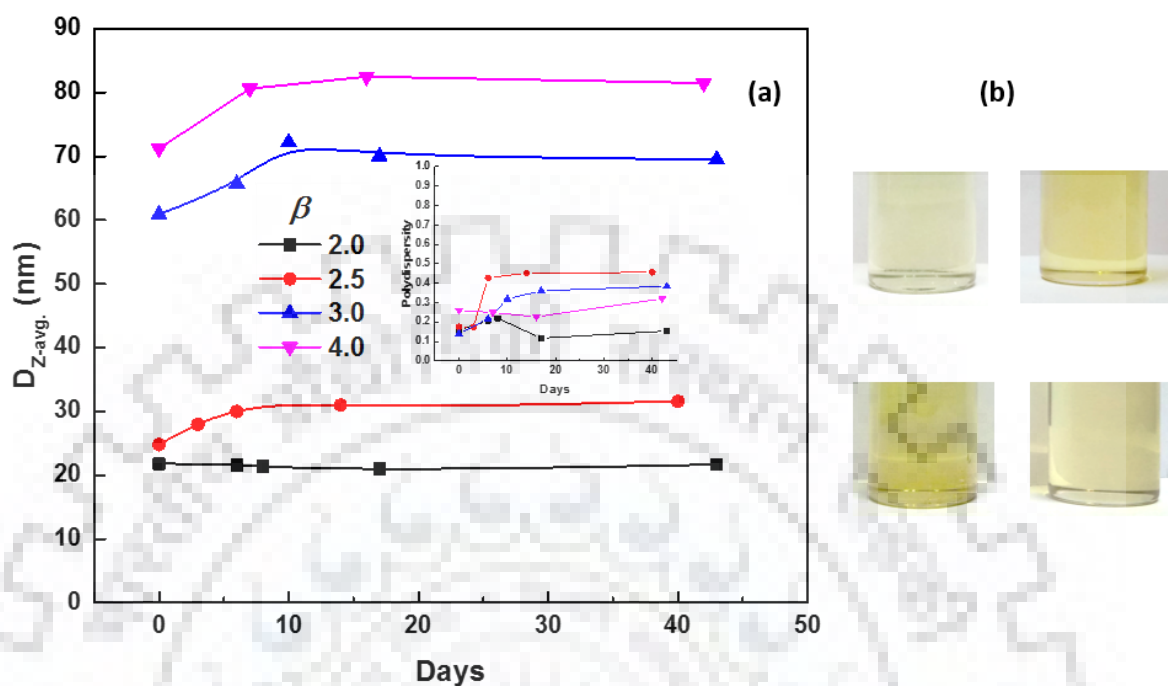
Fig. 4.20: (a) Stability of w/o NEs (CEMSNE) prepared at different β (2.0-4.0) values as a change in $D_{z\text{-avg.}}$ (nm) as a function of time for a 45 days study. (b) Photographs of transparent CEMSNE at different β values for the system W/S/Diesel.

Significant mechanisms responsible for the change in the droplet size with respect to time may be creaming, flocculation, coalescence and Ostwald ripening. In case of nano-emulsions effect of gravitation force diminishes due to excessively low size of droplets whereas, Brownian motion dominates. Therefore, phenomenon of creaming and flocculation were negated. Coalescence and Ostwald ripening mechanisms, therefore are most probable for explaining the instability mechanism of nano-emulsions.

Figure 4.20 (a) depicts the sample formulated with β=2.0 as free from coalescence and Ostwald ripening mechanisms throughout the 45 days period whereas, samples prepared with β=2.5, 3.0 and 4.0 showed an increase in $D_{z\text{-avg.}}$ with respect to time. All the three samples therefore tested with Ostwald ripening rate (m³. s⁻¹) model. Ostwald ripening is driven by the difference in solubility of the difference size droplets. According to the Laplace equation for spherical droplets, smaller droplet have higher Laplace pressure compared with the larger droplet consisting of lower Laplace pressure. Eqns. 4.2, 4.3 and 4.4 were used to model the Ostwald ripening rate ω_3, (m³.s⁻¹) with the experimental data, as shown in Fig. 4.21.
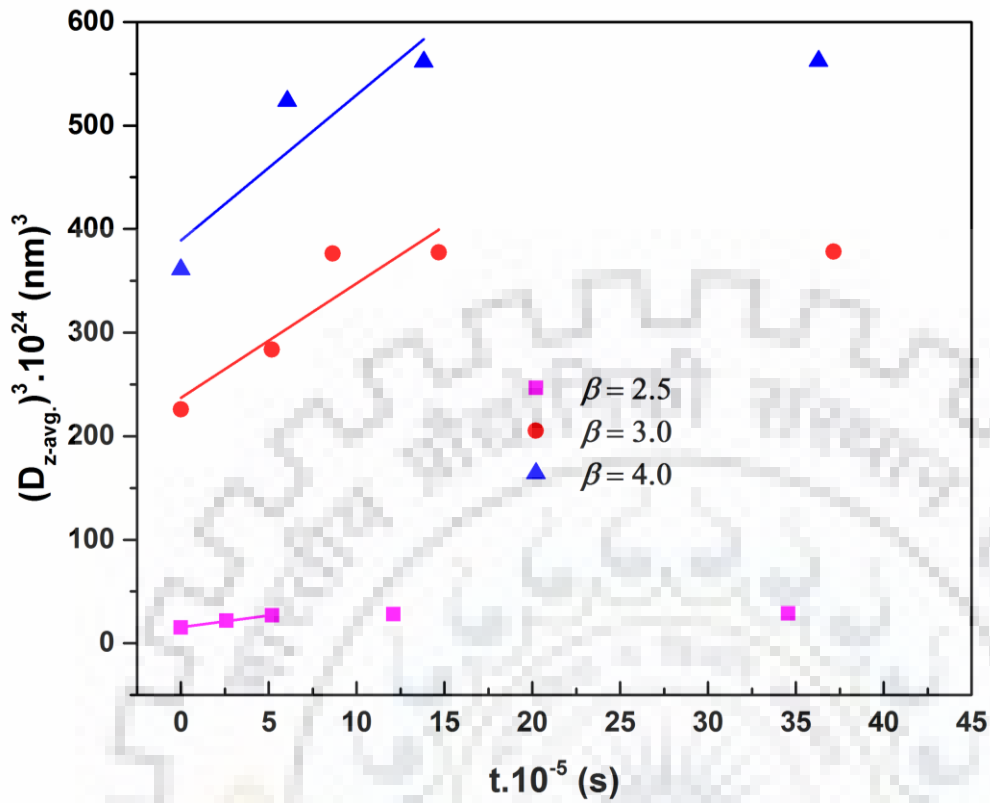
Fig. 4.21: Change in average diameter of the droplet size of three samples with different β values by cube of $D_{z\text{-avg.}}$ as a function of time for w/o NEs at 25°C.

Table 4.4: Ostwald ripening rate of transparent W/O (CEMSNE) prepared at different values of β

β (w/w)	Φ_w	Φ_s	$D_{z\text{-avg.}}$ (nm)	PDI	Ostwald Ripening		
					ω_3 (m³. s⁻¹) $\times 10^{29}$	R^2	Adj.R^2
2.5	0.08	0.20	25±1	0.175±0.015	2.3±0.2	0.993	0.987
3.0	0.05	0.15	61±1	0.140±0.040	11.1±3.4	0.840	0.760
4.0	0.05	0.20	71±0	0.260±0.030	14.1±6.2	0.836	0.672

Table 4.5: Comparative study of stability analysis for the system w/o NEs using high energy methods (Al-Sabagh et al., 2012b; Bidita et al., 2016)

Φ_w	Φ_s	Surfactant	$D_{z\text{-avg.}}$ (nm)	High energy method	Ostwald's ripening rate, ω_3 (m³/s)	[a]Stability (Days)	Ref.
0.05	0.10	SM80-EST85	30	High shear homogenizer	7.28 x 10⁻²²	14	(Al-Sabagh et al., 2012b)
		TX-100-Span 80	**22**	**Ultrasonication**	**NS**	**43**	**b**
0.08	0.10	SM80-EST85	21	High shear homogenizer	4.62 x 10⁻²²	14	(Al-Sabagh et al., 2012b)
		TX-100-Span 80	**25**	**Ultrasonication**	**2.27 x 10⁻²⁹**	**40**	**b**
0.005-0.009 (v/v)	0.0025-0.004 (v/v)	TX-100	17-325	Ultrasonication	5.10 x 10⁻²⁷ to 5.90 x 10⁻³⁷	16	(Bidita et al., 2016)

Note: [a]Stability without phase separation; [b]Present work. **NS:** No Significant increment in droplet size observed during stipulated period.

Ostwald ripening rate was modeled for three samples (β=2.5, 3.0 and 4.0) of CEMSNE system at 25ºC and results are tabulated in Table 4.4. Among the three samples most stable sample was found as $\omega_3 = 2.27 \times 10^{-29}$ ($m^3.s^{-1}$) with $R^2 = 0.993$. Smaller size droplets (with β=2.5) showed least values of Ostwald ripening rate compared to the larger one and resulted into more stable samples. Hence, stability of the samples in the present study was maximum at β=2.0 due to their smaller size and stability decreases with an increase in droplet size (Fig. 4.18 (a)). The sequence of stability from higher to lower is then β: 2.0 >2.5 >3.0 >4.0.

A comparative study regarding stability of the w/o NEs using high energy methods is summarized in the Table 4.5. An extensive literature was carried out considering the similar systems (water-in-diesel oil) prepared with high shear mixer and ultrasonication. It was observed that very less information pertaining to droplet size and stability using high energy methods is available considering the similar systems. Table 4.5 clearly shows better Ostwald's ripening rate and stability of the w/o nano-emulsions for the present work specifically at Φ_w=0.05 and Φ_s=0.10.

4.2.7 Rheological behavior of nano-emulsions prepared using Span 80/Triton X-100

4.2.7.1 Steady state shear rate behavior

In this study three samples of CEMSNE were prepared at different compositions of water (Φ_w) viz. 0.05, 0.08 and 0.11 keeping constant value of surfactant-to-water fraction (β=2) ratio. A new combination of non-ionic surfactants viz. SPAN 80/Triton x-100 was used in the mixed proportions for preparing the NEs. Prepared samples followed combined energy method wherein, pre-emulsions were formed using low energy method (isothermal dilution method) at 39 ºC ± 1 ºC. Thereafter, application of high energy (ultrasonic cavitation) method produced nano-emulsion at the process parameters of 0.5 cycle ratio, 25 % amplitude, and 4 minute of sonication time. To understand the flow behavior of prepared samples, rheometric tests were performed, wherein variation in shear rate and temperature in the range of 1-100 s^{-1} and 25 to 50 ºC, was applied on the CEMSNE samples. Each sample was tested twice and the average of two measurements were reported.

Fig. 4.22 depicts the effect of variation of water and surfactant percent on the flow behavior of formed w/o NEs at four different temperatures (25 ºC, 30 ºC, 40 ºC, and 50 ºC). In the rotational tests, three CEMSNE samples with varied water fraction of 0.05, 0.08, and 0.11 were tested at low to high shear rates ranging from 10 to 100 s^{-1}, shown in Fig. 4.22 (a), (b) and

(c). All three tested samples showed Newtonian behavior at all tested temperature ranging from 25 °C to 50 °C.
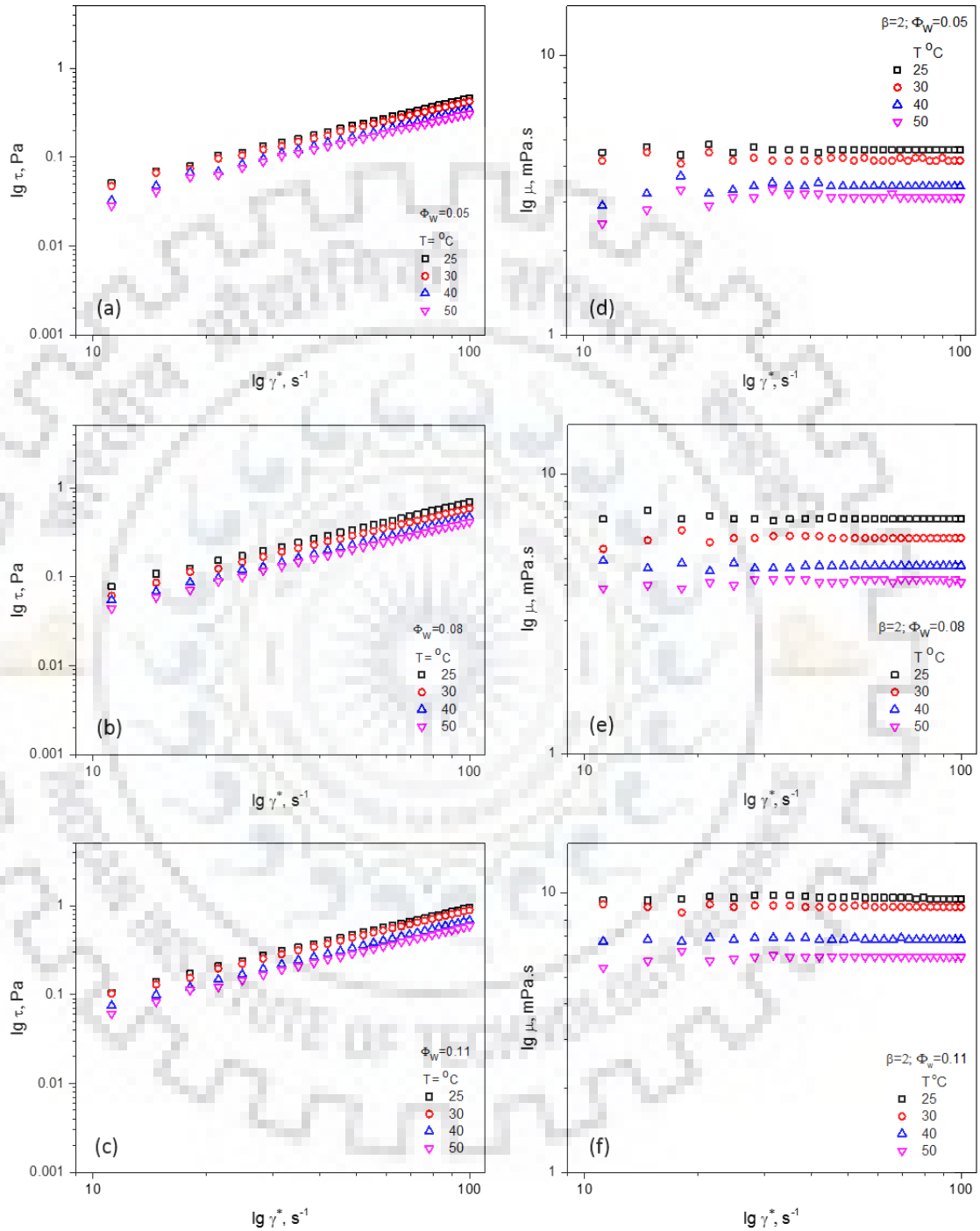
Fig. 4.22: Variation in shear stress (Pa) at varied shear rate (10-100 s^{-1}) is shown for three samples with water fraction (Φ_w) (a) 0.05 (b) 0.08 and (c) 0.11 at the temperature range of 25-50 °C and β =2. Viscosity (mPa. s) variations at different shear rates (10-100 s^{-1}) is shown for CEMSNE samples prepared at different water fractions (Φ_w) (d) 0.05 (e) 0.08 and (f) 0.11.

Sample 1 (Φ_w=0.05; Φ_s=0.10) showed lowest shear stress compared to the Sample 2 (Φ_w=0.08; Φ_s=0.16) and Sample 3 (Φ_w=0.11; Φ_s=0.22), however, all samples sheared at the same shear rate (10 to 100 s^{-1}). An understandable reason behind this behavior is the increase of dispersion in the formed emulsion increased viscosity of the samples as shown in Fig. 4.22 (d)-(f). However, Newtonian behavior for all three samples sustained starting from room temperature (25 ^{o}C) up to higher temperature measuring 50 ^{o}C. Therefore, based on shear stress and shear rate behavior, it can be inferred that CEMNSE samples formed can be transported with ease from low to high shear rate and wide temperature range under study.

4.2.7.2 Modeling of flow behavior for CEMSNE

Ostwald-de-Waele relationship power law model was fitted to identify flow properties of the flow behavior of CEMSNE samples. A two parametric mathematical expression for the model is shown in Eqn. (4.6). Power law model fit of the tested samples was performed at four different temperatures, viz. 25 ^{o}C, 30 ^{o}C, 40 ^{o}C, and 50 ^{o}C. Parametric expressions such as flow consistency index, k, (Pa.s^n) and flow behavior index, n, for all three tested samples (Φ_w: 0.05, 0.08 and 0.11) is summarized in the Table 4.6.

All three CEMSNE samples with different water (Φ_w) and surfactant (Φ_s) fractions showed excellent fit with the model with coefficient of performance, R^2 ranging from 0.9927 to 0.9998. A negligible difference between R^2 and Adj. R^2 for all samples modeled at temperature range of 25-50 ^{o}C, assured an excellent fit of model parameters. However, low values of residual sum of square represented tight fit of the model, as shown in Table 4.6. Values of flow behavior index ranging 0.9766$\leq$ n$\leq$ 1.0034 depicted strongly Newtonian behavior (n$\approx$1) of all tested samples.

The rheological properties shown in the Table 4.6 depicts the different values of flow consistency index (k, Pa. s^n). However, values of flow behavior index (n) are $\approx$1. So in this case flow consistency index resembles the viscosity of the tested sample (k, Pa.s). It is observed from the Table 4.6 that as the water fraction increases from the 0.05 to 0.11, values of k increases from 4.9 to 10.5 (Pa. s) tested at constant temperature of 25 ^{o}C. Likewise, same trend followed for temperature range of 30, 40 and 50 ^{o}C. Moreover, as the testing temperature increases at constant water fraction, value of k decreases accordingly as shown in Table 4.6 and Fig. 4.25. The flow behavior index (n) shown in Table 4.6, reports values near to one at all tested temperature (25-50 ^{o}C) when sheared in the range of 10-100 s^{-1} rate. Therefore all three tested samples with β=2, sustained their internal structure and shown ideal fluid or Newtonian behavior.

Table 4.6: Fitting parameters for the Power law modeled equation for CEMSNE samples.

Temperature (ºC)/ NEs	k $(Pa.s^n) \times 10^3$	n	R^2	Adj. R^2	*RSS
25 ºC					
$\Phi_w = 0.05$	4.9	0.9849	0.9985	0.9985	0.0184
0.08	6.8	1.0034	0.9991	0.9991	0.0112
0.11	10.5	0.9766	0.9982	0.9981	0.0228
30 ºC					
$\Phi_w = 0.05$	4.4	0.9920	0.9992	0.9992	0.0098
0.08	5.9	0.9979	0.9989	0.9988	0.0146
0.11	9.4	0.9869	0.9992	0.9992	0.0101
40 ºC					
$\Phi_w = 0.05$	3.4	1.0024	0.9954	0.9952	0.0594
0.08	3.9	1.0441	0.9927	0.9925	0.1024
0.11	6.9	0.9982	0.9998	0.9998	0.0029
50 ºC					
$\Phi_w = 0.05$	3.2	0.9909	0.9889	0.9885	0.1413
0.08	4.1	1.0024	0.9986	0.9985	0.0187
0.11	6.0	0.9971	0.9981	0.9980	0.0250

Note: *RSS denotes residual sum of square.

4.2.7.3 Effect of temperature on nano-emulsion rheology

Effect of temperature variations on the viscosity (mPs. s) of the CEMSNE samples from low (15 ºC) to high (50 ºC) temperature is shown in Fig. 4.23, measured at the constant shear rate of 100 s^{-1}. At lower temperature (15 ºC), CEMSNE samples showed higher viscosities, for $\Phi_w = 0.05$, 0.08 and 0.11 absolute viscosities were obtained as 13.65, 9.50 and 6.00 mPa. s, respectively. However, at high temperature (50 ºC) all three samples showed lower absolute viscosity, viz. 5.44, 4.00, 2.70 mPa. s, at water fractions (Φ_w) of 0.05, 0.08 and 0.11, respectively. At room temperature (25 ºC), absolute viscosities of samples reported as 10.45, 7.39 and 4.8 mPa. s at Φ_w 0.05, 0.08 and 0.11 respectively. At storage temperature of 25 ºC, however, Sample 1 (Φ_w 0.05; $\beta=2$) showed viscosity as 4.8 mPa. s, that may be favorable for transportation and flow properties of w/o NEs.

As flow behavior index, n, signifies the flow behavior of tested sample as n<1 and n>1 indicates the dilatant flow and pseudoplastic flow behavior. Therefore, flow behavior index, n,

of formed nano-emulsions (Φ_w: 0.05-0.11) was predicted at different temperature range starting from 25 to 50 °C, as shown in Fig. 4.24. It can be inferred from the Fig. 4.24 that no significant change in the flow behavior at all tested samples was observed. All samples maintained the Newtonian behavior keeping n$\approx$1. Flow consistency index, k, Pa, s^n dropped down for all three samples sharply for a temperature range of 25-40 °C, thereafter, became almost constant up to 50 °C, as shown in Fig. 4.25. For example, Sample 1 (Φ_w: 0.05), k changed sharply from 4.9 to 3.4 for temperature ranging from 25-40 °C, thereafter, 3.2 at 50 °C.
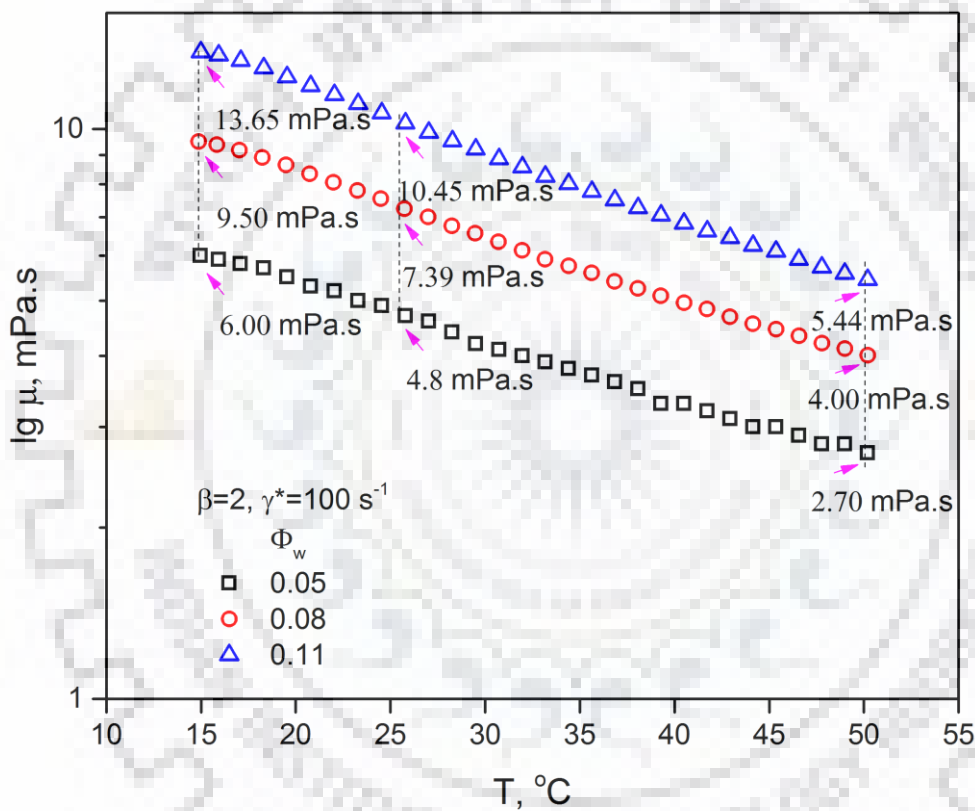
Fig. 4.23: Variation of viscosity (Pa. s) with temperature (T=15-50°C) is shown for three samples of CEMSNE formed at different water fraction, Φw (a) 0.05, (b) 0.08, and (c) 0.11 and constant β=2.
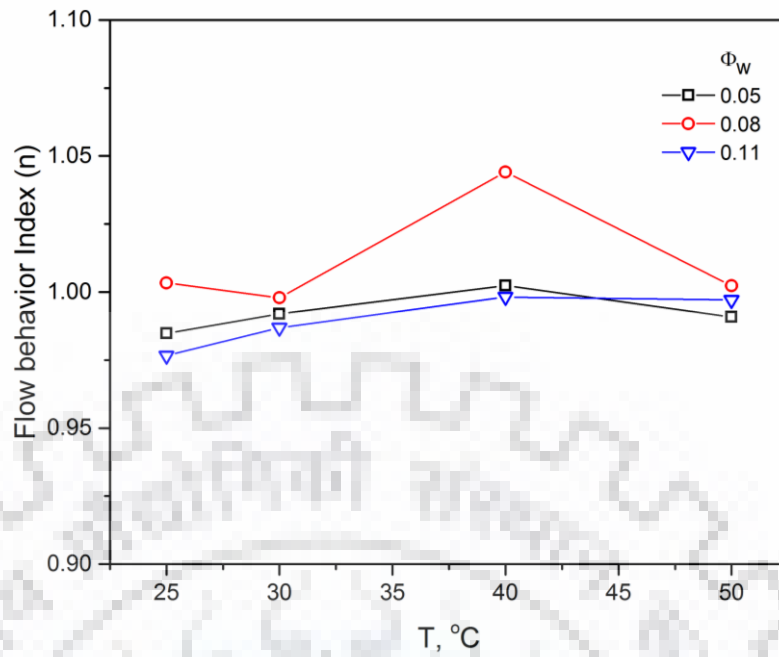
Fig. 4.24: Influence of temperature change (25-50 $^{\circ}$C) on flow behavior index (n) shown for three nano-emulsion (CEMSNE) samples at different water fractions (Φ_w) ranging from 0.05 to 0.11.
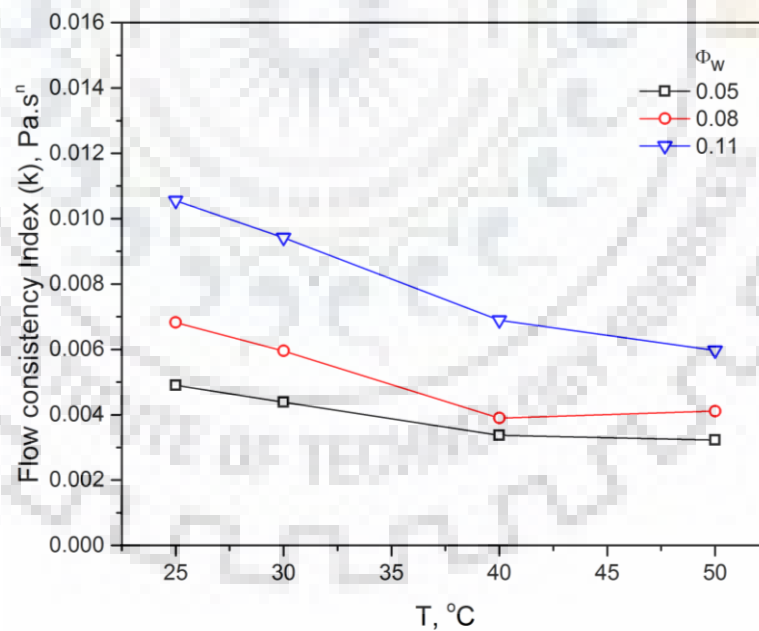
Fig. 4.25: Variations in flow consistency index (k), Pa.s^n for three CEMNSE samples prepared at different water compositions, Φ_w (0.05-0.11) and a β value of 2, tested at temperature range of 25-50 $^{\circ}$C.

All tested samples (CEMSNE) showed Newtonian behavior at all temperature range (25-50 °C) and shear rate (10-100 s^{-1}) range considered in the present work. Even at higher temperature of 50 °C all three tested samples with water fraction (Φ_w: 0.05-0.11) and surfactant fraction (Φ_s =0.10-0.22) maintained Newtonian behavior by maintaining linear profile in shear stress vs. shear strain diagram. Flow behavior index (n) for all tested samples was found in the range of 0.9766≤ n≤ 1.0034. Effect of increase in dispersed phase composition, however, increased the w/o NEs viscosity nevertheless keeping nano-emulsion behavior unchanged. Effect of change of temperature on CEMSNE viscosity was tested from 15-50 °C at constant shear rate of 100 s^{-1}. Results depicted the maximum increase in the viscosity of Sample 3 (Φ_w=0.11; β=2) at very low temperature of 15 °C, however, Sample 1 (Φ_w: 0.05; β=2) showed moderate viscosity (4.8 mPa.S) at 25 °C. A shear stress variations with shear rate change in the range of 10-100 s-1, inferred that the newly formed w/o NEs can be easily transported at the temperature ranging from of 25 to 50 °C.

CHAPTER 5

STATISTICAL MODELING OF W/O NANO-EMULSION FORMATION

In this chapter formation of w/o nano-emulsions (NEs) was intended to optimize process parameters like water and surfactant fractions, power density and ultrasonication time using back propagation artificial neural network (BPANN)-genetic algorithm (GA) coupled with rotatable central composite design-response surface methodology (RCCD-RSM) modeling scheme. Formation of w/o NE was achieved by application of low (isothermal dilution method) and high energy methods (ultrasonic cavitation) using mixed non-ionic surfactants. In this work, optimization was focused on imparting designer properties to the emulsified diesel fuel like lower droplet size and kinematic viscosity, simultaneously, that not only reduces pollution but also improves flow properties of resulting w/o NEs. Optimization techniques and results are discussed in sections 5.1 and 5.2, respectively.

5.1 STATISTICAL MODELING OF NANO-EMULSION FORMATION AND OPTIMIZATION OF PROCESS PARAMETERS

Optimization of process parameters for the formation of emulsions plays a vital role in efficient selection of variables. In recent years, response surface methodology (RSM) for efficient optimization of independent variables has been extensively tested and reported in literature specifically in emulsion formations (Alzorqi et al., 2016; Katsouli et al., 2018; Mehmood et al., 2018; Raviadaran et al., 2018; Saravanan et al., 2017). However, in optimization of nano-emulsions formation, experimental designs have been extensively used to find out significant variables by implementing low and high energy methods (Alzorqi et al., 2016; Gutiérrez et al., 2008; Mehmood et al., 2018; Pey et al., 2006).

Artificial neural network (ANN) has been effectively used as a tool for determining the factors controlling the particle size (Amani et al., 2008), predicting phase behavior (Alany et al., 1999), stability (Agatonovic-Kustrin et al., 2003) and rheological behavior of emulsions (Monazzami et al., 2018). Recently, central composite design (CCD) combined with ANN has been reported in the literature pertaining to food, landfill leachate treatment and other different fields (Fasuan and Akanbi, 2018; Sabour and Amiri, 2017) such as loading of nanoparticles on nanotubes for dispersion and removal of organic dye (Moghaddari et al., 2018). Whereas, ANN with genetic algorithm (GA) has also been used for identifying the phases behavior of colloids (Agatonovic-kustrin and Alany, 2001).

The most recurrent aim for optimization is to exploit the benefits of nano-emulsions compared with the conventional macro-emulsions with respect to their smaller size and low polydispersity index (PDI). Parameters of heuristic and metaheuristic algorithms have been tuned by using different approaches by several researchers (Ghanavati Nasab et al., 2018; Jacob and Banerjee, 2016; Kundu et al., 2015). In a metaheuristic approach, researchers have evaluated guidelines to select parameters for particle swamp optimization and validated them by using experimental design (Shi and Eberhart, 1998). Whereas in other studies parameters of Tabu search algorithm were tuned by factorial design (Taillard, 1991). Several studies have used experimental design (RSM) for getting the optimized combination of parameters that would help in fine tuning the ANN. Furthermore, many studies involved the use of different optimization techniques like Taguchi method, Evolutionary Algorithms, etc., for improvements in performance of ANN (Ding et al., 2013; Khaw et al., 1995; Peterson et al., 1995). The lack of knowledge and information of these tools in analyzing the results poses the difficulty in working in this area (Bashiri and Farshbaf Geranmayeh, 2011). Present work therefore uses the heuristic approach wherein, algorithm includes first the parametric optimization through RSM, thereafter ANN is applied on the RSM generated design points. Further, genetic algorithm (GA) finally tuned the results by making use of hybrid GA technique wherein, RSM generated fitness function and ANN generated data points were used to initialize the algorithm. Therefore this work applies both models viz. RCCD-RSM and ANN-GA for finding the optimized conditions for the formation of water-in-diesel oil nano-emulsions (w/o NEs) that comprise of minimum droplet with lower kinematic viscosity simultaneously.

5.1.1 RCCD-RSM modeling

A three-level-four factor RCCD generated statistical model term was tested by performing the analysis of variance (ANOVA) to identify the significant variables and predicting the suitable model equation. Collaborative and individual effect of variation of process factors viz. water θ_w (A), and surfactant fractions θ_s (B), power density (C) and ultrasonication time (D), on average droplet size of dispersed phase Y_{Dia} (nm) and kinematic viscosity Y_{KV} (mm^2.s^{-1}) are depicted in Table 5.1. The acceptability of the models for predicting two responses was determined by using analysis of models, lack-of fit test and coefficient of determination (R^2) analysis.

Table 5.1. Design arrangement, prediction and experimental results for the formation of w/o nano-emulsion by application of ultrasonic cavitation

| Run | Independent Variables | | | | Response Variables | | | |
| | A (θ_w) | B (θ_s) | C (PD) | D (UT) | Y_{Dia}: Droplet size (nm) | | Y_{KV}: KV (mm^2.s^{-1}) | |
					Exp.	Pred.	Exp.	Pred.
1	1	-1	1	-1	176.3	175.6	2.02	2.05
2	1	1	1	-1	57.6	51.0	5.66	5.20
3	-1	1	1	-1	56.7	56.2	4.37	4.48
4	1	1	-1	-1	57.4	73.2	5.11	5.13
5	0	0	0	0	61.5	64.5	2.55	2.80
6	1	1	-1	1	56.6	56.5	5.72	5.75
7	1	-1	1	1	194.5	199.0	2.15	2.05
8	-1	-1	-1	1	52.4	62.6	1.21	1.40
9	-1	-1	1	-1	64.3	68.0	2.70	2.42
10	2	0	0	0	170.7	168.8	3.77	4.05
11	0	-2	0	0	181.5	183.3	1.57	1.63
12	-1	1	-1	1	80.3	76.9	3.77	3.56
13	0	0	-2	0	57.0	46.9	2.63	2.58
14	0	0	0	0	60.4	64.4	3.50	2.80
15	0	0	2	0	53.6	64.2	2.65	3.15
16	0	0	0	0	63.8	64.4	2.96	2.80
17	0	0	0	-2	64.2	57.7	2.76	2.86
18	1	-1	-1	-1	156.0	156.0	2.00	2.03
19	0	0	0	2	68.1	75.2	2.63	2.97
20	0	0	0	0	63.8	64.5	2.63	2.80
21	1	1	1	1	64.6	58.6	5.58	5.34
22	-1	-1	-1	-1	50.9	52.7	1.38	1.44
23	-1	-1	1	1	122.1	102.1	2.09	1.90
24	-1	1	1	1	70.9	74.6	4.41	4.11
25	-2	0	0	0	79.0	81.5	2.06	2.23
26	0	0	0	0	60.7	64.5	2.25	2.80
27	-1	1	-1	-1	83.7	82.8	3.62	3.45
28	1	-1	-1	1	158.8	155.1	2.80	2.51
29	0	2	0	0	74.2	72.95	6.54	6.93
30	0	0	0	0	76.7	64.48	2.89	2.80

To evaluate the adequacy of the models, F and p-values were analyzed through ANOVA test. F-values of models for evaluating the Y_{Dia} and Y_{KV} responses were found as 44.41 and 25.69, respectively, inferring that models were significant and there was only a 0.01% chance that model F-values this large could happen due to noise. Values (p > F) <0.05, in Table 5.1, indicate

that the model terms are significant. Table 5.2 (a) and (b) depicts that in predicting response Y_{Dia}, model terms like A, B, AB, A^2 and B^2 are highly significant (<0.0001) whereas, C, D, BC and CD are significant (0.0001 <p-value <0.05). However, in predicting the response Y_{KV}, model terms like A and B, are highly significant (<0.0001) whereas, AB, AC and B^2 are significant (0.0001<p-value <0.05).

Lack of fit can be tested with the F-distribution using the ratio of media of square of lack of fit (MS_{LOF}) and of pure error (MS_{PE}), as shown in Eqn. (5.1) (Bezerra et al., 2008):

$$\frac{MS_{LOF}}{MS_{PE}} = F_{LOF,PE} \tag{5.1}$$

$$MS_{LOF} = \frac{SS_{LOF}}{DOF_{LOF}} \tag{5.2}$$

$$MS_{PE} = \frac{SS_{PE}}{DOF_{PE}} \tag{5.3}$$

Value of MS_{LOF} can be computed from Eqn. (5.2) as the ratio of sum of the square of lack of fit (SS_{LOF}) and of degree of freedom of lack of fit (DOF_{LOF}). If the ratio $F_{LOF,PF}$ associated with lack of fit (LOF) and pure error (PE), as shown in Eqn. (5.1), is higher than the F-value corresponding to lack of fit (Table 5.2 (a) and (b)), there is a need for improvement in the model. Whereas, if the value is lower than the tabulated value, model is considered satisfactory (Bezerra et al., 2008). Considering model for Y_{Dia} response, values correspond to MS_{LOF} (Eqn. 5.2) and MS_{PE} (Eqn. 5.3) are 123.184 (=1231.84/10) and 38.014 (= 190.07/5), respectively (Table 5.2 (a) and (b)). $F_{LOF,PF}$ value generated (3.24) therefore is less than F-value (44.41) signifying the model fitness as satisfactory. Likewise, Y_{KV} model showed $F_{LOF,PF}$ value as 0.74 that is clearly less than the tabulated value of 25.69 representing the model to be satisfactory.

Table 5.2 (a): ANOVA for the RSM-CCD model illustrating model parameters for droplet size, $D_{z\text{-avg.}}$ (nm)

Source	Sum of Squares	df	Mean Square	F-value	p-value	Remark
Model	58932.50	14	4209.46	44.41	< 0.0001	Highly significant
A-Water frac.	11432.81	1	11432.81	120.61	< 0.0001	Highly significant
B-Surfactant frac.	18261.27	1	18261.27	192.64	< 0.0001	Highly significant
C-Power density	451.19	1	451.19	4.76	0.0455	Significant
D-Ultrasonic time	460.78	1	460.78	4.86	0.0435	Significant
AB	12733.99	1	12733.99	134.33	< 0.0001	Highly significant
AC	19.23	1	19.23	0.2028	0.6589	Not significant
AD	115.35	1	115.35	1.22	0.2874	Not significant
BC	1750.17	1	1750.17	18.46	0.0006	Significant
BD	249.96	1	249.96	2.64	0.1252	Not significant
CD	589.03	1	589.03	6.21	0.0249	Significant
A²	6303.96	1	6303.96	66.50	< 0.0001	Highly significant
B²	6943.12	1	6943.12	73.24	< 0.0001	Highly significant
C²	136.07	1	136.07	1.44	0.2495	Not significant
D²	6.46	1	6.46	0.0681	0.7976	Not significant
Residual	1421.91	15	94.79			
Lack of Fit	1231.84	10	123.18	3.24	0.1032	Not significant
Pure Error	190.07	5	38.01			
Cor Total	60354.41	29				

Table 5.2 (b): ANOVA for the RSM-CCD scheme depicting model parameters for kinematic viscosity ($mm^2.s^{-1}$)

Source	Sum of Squares	df	Mean Square	F-value	p-value	Remarks
Model	54.12	14	3.87	25.69	< 0.0001	Highly significant
A-Water frac.	4.97	1	4.97	33.04	< 0.0001	Highly significant
B-Surfactant frac.	42.21	1	42.21	280.47	< 0.0001	Highly significant
C-Power density	0.4793	1	0.4793	3.19	0.0945	Not significant
D-Ultrasonic time	0.0153	1	0.0153	0.1019	0.7540	Not significant
AB	1.17	1	1.17	7.76	0.0138	Significant
AC	0.9152	1	0.9152	6.08	0.0262	Significant
AD	0.2661	1	0.2661	1.77	0.2035	Not significant
BC	0.0029	1	0.0029	0.0195	0.8908	Not significant
BD	0.0201	1	0.0201	0.1334	0.7201	Not significant
CD	0.2312	1	0.2312	1.54	0.2342	Not significant
A²	0.1987	1	0.1987	1.32	0.2685	Not significant
B²	3.76	1	3.76	24.97	0.0002	Significant
C²	0.0082	1	0.0082	0.0546	0.8184	Not significant
D²	0.0249	1	0.0249	0.1654	0.6900	Not significant
Residual	2.26	15	0.1505			
Lack of Fit	1.35	10	0.1347	0.7397	0.6805	Not significant
Pure Error	0.9104	5	0.1821			
Cor Total	56.38	29				

For Y_{Dia} response model, value of coefficient of performance R^2 (0.9764) confirmed the excellent fit of the model predicted and experimental values of the present work. Moreover, the difference of 0.0766 in adjusted R^2 (0.9545) and predicted R^2 (0.8779) was in reasonable agreement between adj-R^2 and pred-R^2 (difference should be <0.2). Likewise, R^2 value (0.96) for Y_{KV} response model showed good fit of predicted and experimental values with reasonable difference between adj. R^2 and pred. R^2, as shown in Table 5.3. Adequate precision (signal/noise

ratio) in case of predicting response models Y_{Dia} and Y_{KV} were ~22 & ~20, respectively. Since desirable value should be greater than 4, response models indicated very good signal/noise ratio. Consequently, these models can be used to navigate the design space. Fig. 5.1 (a) and (b) shows the competence between the predicted verses experimental responses like Y_{Dia} and Y_{KV} and indicates that models are suitable for predicting minimum droplet size (nm) and kinematic viscosity (mm^2.s^{-1}) by application of RCCD-RSM model.

Table 5.3. Fit statistics of RSM-CCD model.

Fit Statistics	R²	Adjusted R²	Predicted R²	Adeq. Precision	Std. Dev.	Mean	C.V. %
Droplet Size	0.9764	0.9545	0.8779	22.0985	9.73	87.946	11.071
Kinematic Viscosity	0.9600	0.9226	0.8391	20.1489	0.3879	3.20	12.12

Model adequacy for predicting the minimum droplet size of dispersed phase and minimum kinematic viscosity of w/o NEs can be arbitrated by analyzing the Fisher's F-test, p-value (<0.05) and coefficient of performance (R^2). Linear, 2FI and quadratic terms were analyzed by using terms shown in Table 5.2 (a) and (b). On the basis of fit summary (Table A4 to A7 in Appendix A) for both the responses, higher order model was selected. Based on multiple regression analysis, second order polynomial eqns. for assessing effect of process variables (in coded terms) on mean diameter (Y_{Dia}) and kinematic viscosity (Y_{KV}) are written in Eqns. (5.4 and 5.5) within confidence interval of CI>95%:

$$Y_{Dia}(nm) = 64.48 + 21.83A - 27.58B + 4.34C + 4.38D - 28.21AB - 10.46BC + 6.07CD + 15.16A^2 + 15.91B^2$$

$$(5.4)$$

$$Y_{KV}(mm^2.s^{-1}) = 2.8 + 0.4551A + 1.33B + 0.2702AB - 0.2392AC + 0.3701B^2 \qquad (5.5)$$
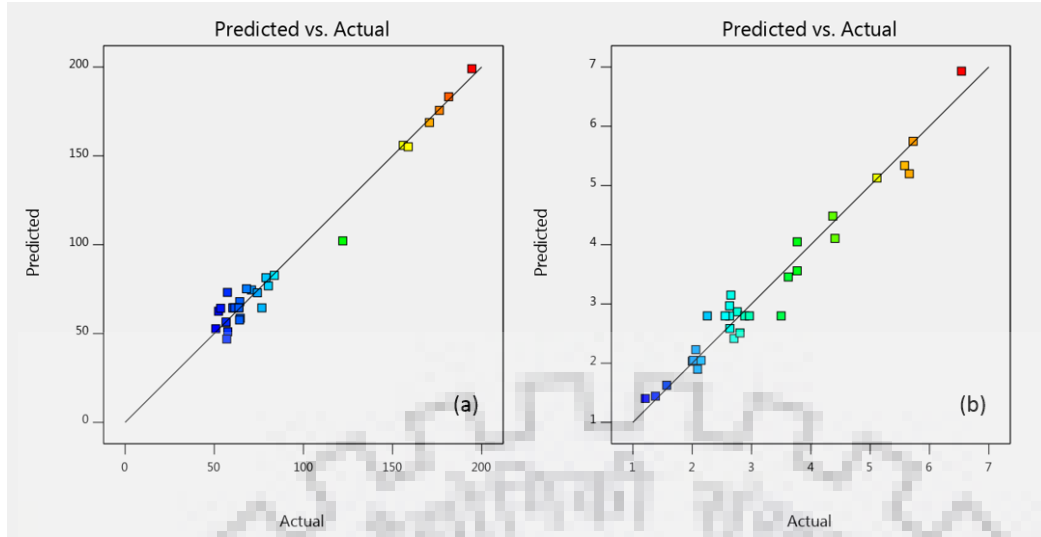
Fig. 5.1. Predicted verses actual response for (a) droplet size (nm) and (b) kinematic viscosity (mm^2.s^{-1}) by application of RCCD-RSM model.

5.1.2 Back propagation-ANN modeling

Fig. 3.6 (a) shows the structure of ANN applied for modeling. Experimental data designed in the RCCD-RSM were fed to the FFBP-ANN structure. ANN inputs were allocated randomly in training, validation and test groups for both responses in the ratio of 20:10:10 feed forward three layer structures. Eqns. (5.6) and (5.7) were used for converting responses, Y_{Dia} and Y_{KV} in coded terms (-1 to 1) for FFBP-ANN input in finding the hidden layer neurons.

$$y_{D,nor} = \frac{2(Y_{Dia} - 50.9)}{(194.5 - 50.9)} - 1 \tag{5.6}$$

$$y_{KV,nor} = \frac{2(Y_{KV} - 1.21)}{(6.54 - 1.21)} - 1 \tag{5.7}$$

Detailed steps involved in network training for function approximation are described in section 3.2 (training parameters are depicted in Table A8 in Appendix A). Number of hidden neurons were decided by lower values of MSE (mean square error) and higher values of coefficient of performance (R^2), simultaneously to avoid over fitting of results. In developing a suitable network structure total 15 neurons were tested and results are tabulated in Table 5.4. For the response average diameter (Y_{Dia}), optimal configuration was found at 9th neuron on the basis of overall and training MSE and R^2 data, respectively. Moreover, eight hidden layer neurons were found in case of kinematic viscosity (Y_{KV}) response.

Variation of MSE and R^2 with number of hidden neurons is plotted in Fig. 5.2 for both responses. Performance of FFBP-ANN model is shown in Fig. 5.3 wherein MSE values 0.026137 and 0.0078924 are depicted for both responses at epoch 4 and 3, respectively. It can be inferred from Fig. 5.3 (a) and (b) that MSE values first decreased sharply up to 4 and 3 epochs respectively, thereafter, finally it reaches a saturation point in both cases. Validation error (MSE) in both responses also found minimum at epoch 4 and 3, as shown in Fig. 5.3 (a) and (b). Consequently, validation data set was made a stopping criteria for training process, moreover, it has been reported (Kundu et al., 2015) that early stopping provides better generalization. Fig. 5.4 depicts the fitting between output and target at optimized hidden neurons extracted from FFBP-ANN training, validation, test and overall for responses average diameter and kinematic viscosity.
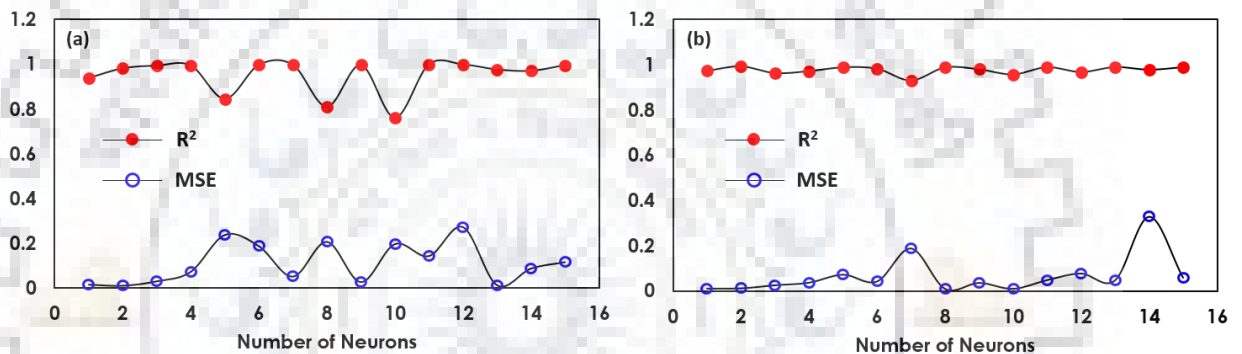
Fig. 5.2. Optimization of neurons with respect to mean square error (MSE) and regression coefficient (R^2) for responses (a) Y_{Dia} and (b) Y_{KV}.

Overall correlation coefficients (R^2) for Y_{Dia} and Y_{KV} were found in good fit with values 0.9681 and 0.9744, respectively. However, regression coefficient (R^2) associated with the training has shown a very good fit with values 0.9969 and 0.9881, respectively. The reason behind very good fit corresponds to the 66.6% data used in the training as compared to the validation (16.7%) and testing (16.7%).

Table 5.4: Optimization of number of neurons in a hidden layer for Y_{Dia} and Y_{KV}

| No. of neurons | Optimal RCCD-ANN Configuration | | | | | | | |
| | Y_{Dia} | | | | Y_{KV} | | | |
	MSE overall	R^2 overall	MSE training	R^2 training	MSE overall	R^2 overall	MSE training	R^2 training
1.	0.0398	0.9524	0.0148	0.9391	0.0217	0.9604	0.0091	0.9730
2.	0.1959	0.7389	0.0100	0.9822	0.0135	0.9759	0.0104	0.9930
3.	0.0286	0.9641	0.0296	0.9944	0.0195	0.9630	0.024	0.9627
4.	0.0575	0.9349	0.0722	0.9948	0.0399	0.9327	0.0354	0.9717
5.	0.1390	0.8642	0.2363	0.8454	0.0231	0.9567	0.071	0.9885
6.	0.0836	0.9121	0.1861	0.9977	0.0300	0.9503	0.0407	0.9823
7.	0.0254	0.9674	0.0507	0.9980	0.0771	0.8560	0.1872	0.9297
8.	0.1538	0.8222	0.2055	0.8099	**0.0147**	**0.9744**	**0.0079**	**0.9881**
9.	**0.0253**	**0.9681**	**0.0261**	**0.9970**	0.0411	0.9396	0.0343	0.9797
10.	0.2373	0.7251	0.1955	0.7610	0.0295	0.9545	0.0081	0.9568
11.	0.0297	0.9645	0.1420	0.9999	0.0188	0.9640	0.0468	0.9893
12.	0.1017	0.8903	0.2715	0.9998	0.0418	0.9180	0.0759	0.9675
13.	0.0367	0.9529	0.0125	0.9773	0.0423	0.9341	0.0459	0.9898
14.	0.0769	0.9181	0.0862	0.9711	0.0821	0.8775	0.3280	0.9779
15.	0.0659	0.9321	0.1151	0.9962	0.0505	0.9257	0.0574	0.9892
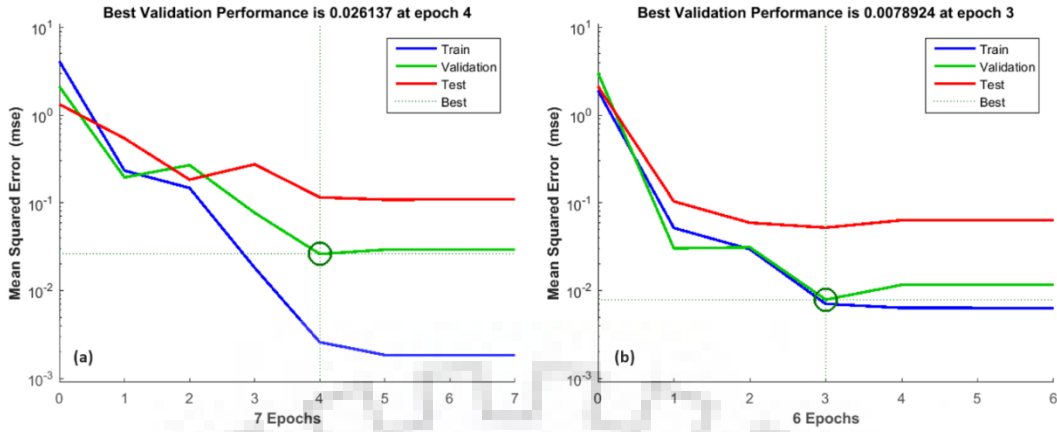
Fig. 5.3. Performance of FFBP-ANN model is shown for two responses with performance values (MSE) **(a)** 0.026137 (Y_{Dia}) and **(b)** 0.0078924 (Y_{KV}) at epoch 4 and 3 respectively.
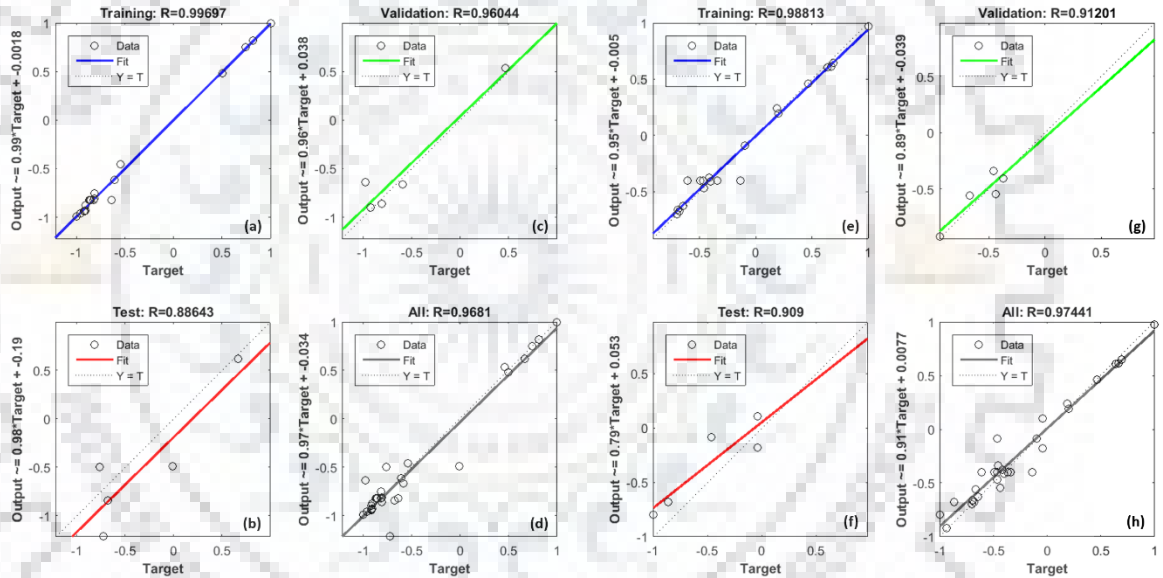
Fig. 5.4. Fitting for coded data sets at optimized hidden neurons rendered from FFBP-ANN training, validation test and overall for response Y_{Dia} (a-d) and Y_{KV} (f-h).

Weights and biases associated with the respective layers at the optimized number of neurons were used in combination with GA are reported in Tables 5.5 and 5.6. Flow chart for RCCD-RSM and FFBP-ANN combined approach for finding weights and biases is shown in Fig. 5.5. Parity plots of responses for droplet size and kinematic viscosity are shown in Fig. 5.6, where, scattered data in the Fig. 5.6 (a) and (b) suggests the non-linear relationship between parameters involved in the formation of w/o NEs. Moreover high values of correlation coefficients obtained in training (R^2=0.9969 and 0.9881) and overall (R^2=0.9681 and 0.9744) in both responses are indicative of good predictive capability of FFBP-ANN model.

Table 5.5: Weight and Bias for CCD-ANN model for Y_{Dia}

Neuron No.	Weights from input layer to hidden layers for response Y_{Dia}				Bias to hidden layer	Weights from hidden layer to output layer	Bias to output layer
1	-0.4990	0.7175	0.7977	2.0671	2.3417	-0.0931	-0.1298
2	1.5315	0.3409	-1.5138	-0.1706	-2.0398	-0.3148	
3	-0.2464	-1.816	0.8736	1.2683	-1.5024	0.1715	
4	2.649	-2.7323	0.7639	-0.7459	-1.5894	1.0546	
5	0.6364	-1.823	1.2347	-1.5855	-0.6051	-0.2890	
6	1.1945	-0.257	-1.812	-1.183	1.0414	-0.1588	
7	-1.2625	1.6914	-0.1524	1.0962	-1.2921	0.0787	
8	0.7181	-1.3838	-1.5458	-0.5455	2.2746	1.0312	
9	-0.8203	1.3766	-0.1440	-1.5945	-2.5871	0.7619	

Table 5.6: Weight and Bias for CCD-ANN model for Y_{KV}

Neuron No.	Weights from input layer to hidden layers for response Y_{KV}				Bias to hidden layer	Weights from hidden layer to output layer	Bias to output layer
1	-0.3847	1.8673	1.0918	-0.7735	-1.8442	0.3098	0.2849
2	0.9284	-1.4116	1.5733	0.5347	-1.7424	-0.1081	
3	0.8774	1.9509	-0.5243	0.2035	-0.6783	0.7593	
4	-0.2197	-1.4267	0.8571	1.8039	-0.0716	0.1679	
5	1.5135	-1.2547	1.0175	-1.9013	0.6370	-0.0928	
6	1.4453	0.5584	1.6694	-0.5685	1.1592	0.0613	
7	1.3778	-0.3904	1.8145	-0.8574	2.1094	0.4107	
8	0.2450	-0.4948	-1.4447	1.8048	2.3049	-0.4415	
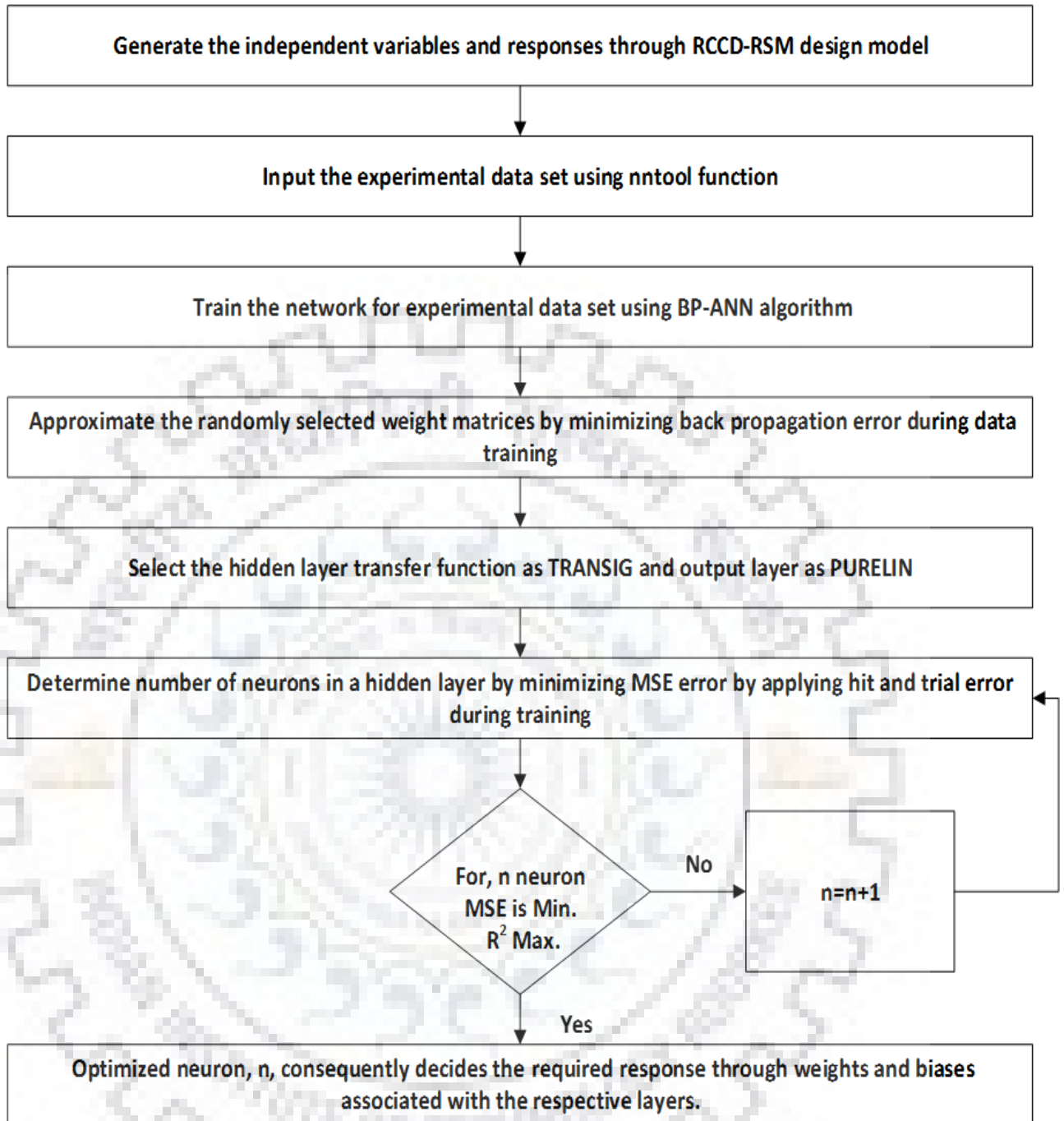
Fig. 5.5. Flow chart of RCCD-RSM and FFBP-ANN combined approach.
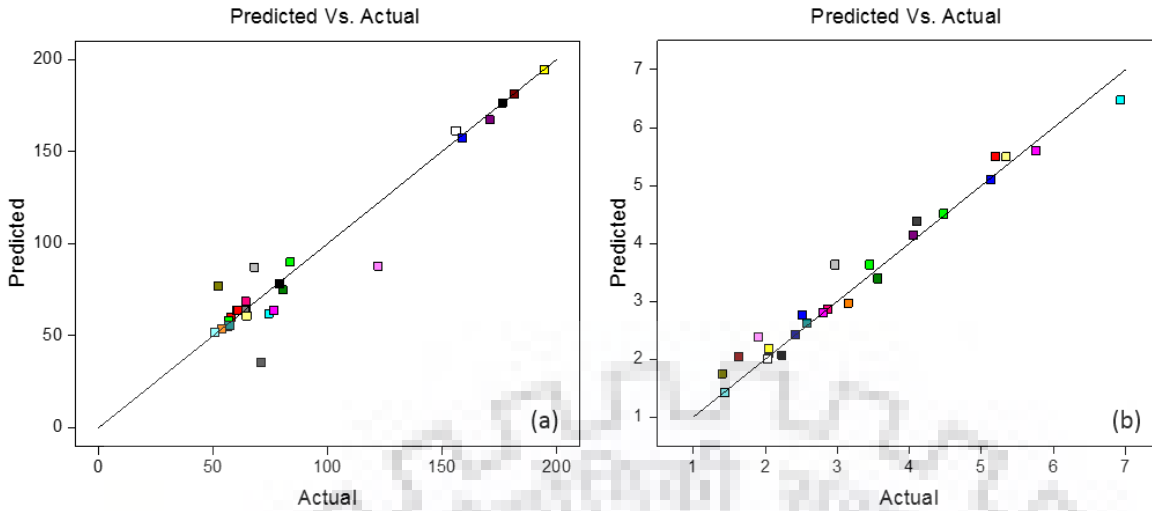
Fig. 5.6. Predicted verses actual response in case of FFBP-ANN scheme for **(a)** droplet size (Y_{Dia}) and **(b)** kinematic viscosity (Y_{KV}).

5.1.3 Multi-objective hybrid ANN-GA model for optimization

Optimization of process variables for attaining minimal values of droplet size and kinematic viscosity simultaneously for the formation of w/o NEs, a hybrid GA scheme was adopted. Steps implemented in hybrid GA, i.e. FFBP-ANN coupled with GA, for solving proposed problem are illustrated in Fig. 3.8. Minimum and maximum values used in optimizing four process parameters viz. θ_w, θ_s, PD and UT via statistical modeling were used as hybrid GA constraints, as shown in Eqn. (5.8).

$$\begin{bmatrix} 0.02 \leq A(\theta w) \leq 0.14 \\ 0.05 \leq B(\theta s) \leq 0.25 \\ 21.25 \leq C(PD) \leq 55.25 \\ 1 \leq D(UT) \leq 13 \end{bmatrix} \tag{5.8}$$

Genetic algorithm (GA) highly depends on the initial population and genetic operators like crossover, selection, mutation etc. Therefore, for obtaining the valid results GA parameters should be carefully selected. In this regard, weights obtained in the RCCD-RSM and FFBP-ANN were used as the initial population in the hybrid GA scheme. However, population size, crossover fraction, and migration fraction were selected based on trial and error method, as shown in Table 5.7. Stopping criteria causing the GA algorithm to terminate was based on weighted average value. If, the relative change in weighted average within the Pareto solutions spread over stall generations was less than function tolerance ($\sim 10^{-4}$), simultaneously, Pareto solutions spread was smaller than the avg. spread over the previous stall generations, then GA stopped. Generation of

100 refers to as hundred times number of variables considered in the optimization was based on the maximum number of iterations algorithm performs (as shown in Table 5.7).

Table 5.7: Criteria of GA-ANN hybrid optimization scheme considered for optimal solution.

Parameters	Values / Function type
Population size	50
Creation function	Feasible population
Selection function	Tournament
Crossover Fraction	0.8
Mutation Function	Adaptive feasible
Crossover Function	Heuristic
Migration Fraction	0.2
Generation	100
Pareto front population fraction	0.35

In case of multi-objective optimization problem (MOP), two or more objective functions has to be optimized, where a decision on optimality of process variables has to be taken by bringing a balance between the conflicting objectives. For MOP, no single optimized solution for objectives was generated; instead a set of optimal or Pareto optimal solutions were attained. A final choice was made depending on preference made on one of the objectives. A Mathematical equation describing MOP is as follows (Eqn. (5.9)) (Wang et al., 2019):

$$\min F(\pi) = [f_1(\pi), f_2(\pi), ..., f_n(\pi)]$$
$$s.t. \pi \in \Pi \tag{5.9}$$

where, π denotes the decision vector containing parameters to be optimized, n is the number of objectives (n $\geq$2), Π is the set of optimized solution depending upon constraint functions. A Pareto front denoting the conflict between the average diameters, $D_{Z\text{-avg.}}$ and kinematic viscosity, KV (mm^2.s^{-1}) is shown in the Fig. 5.9. Optimal solutions shown in Pareto front may be considered by opting three sets, A_1, A_2 and A_3 depending on the preference given to the individual function (Fig. 5.9). Optimal point A_1 [35.77 4.579] gives more importance to the average droplet diameter (nm) compared to the kinematic viscosity. Nearly equal importance to the conflicting functions has been given to the optimal point A_2 [48.62 2.881]. Optimal point A_3 [59.57 1.406] imparts more importance to the kinematic viscosity (mm^2.s^{-1}) compared to the $D_{Z\text{-avg.}}$ (nm). Opting A_1 and A_3 certainly does not solve the purpose, whereas optimal point A_2 conflicts with the co-

ordinate point (48.77, 1.719) to be very near to the $D_{z-avg.}$ and very far away in kinematic viscosity as shown in Fig. 5.9. A co-ordinate point (53.54, 1.459) was considered for hybrid GA, so that the performance of MOP could be compared with the RCCD-FFBP model generated results (58.86, 1.473) at nearly same process parameters as shown in Table 5.8 and Appendix A9 and A10.

In this work 30 numbers of statistically designed data sets in coded form were used in the RCCD-RSM and FFBP-ANN combined model. Subsequently, parameters generated from the model were used as initial population in GA. Model predicted results from RCCD-RSM and hybrid GA were validated by performing confirmatory experiment at the prevailing conditions (Table 5.8). Optimal values corresponding to the simultaneously minimum in $D_{z-avg.}$ and kinematic viscosity as 53.54 nm and 1.459 $mm^2.s^{-1}$, respectively, were selected leading to the process parameter values of θ_w, θ_s, power density and ultrasonication time as 0.052, 0.105, 29.94 $W.cm^{-2}$ and 9.7 min, respectively as shown in Table 5.8.

From the hybrid GA results, an observance has been made in the fact that the minimum droplet value found at the $\beta=2.02$ (0.052/0.105), however, that corresponds to the better stability at $\beta=2$ as described in the chapter 4, section 4.2.6. The probable reason be the saturation of the surfactant layer on the water droplets found enough to hold the hydrophilic and lipophilic groups intact. Moreover, the sample corresponding to that ratio ($\beta=2$) found free from coalescence and Ostwald's ripening effect for a longer duration of time (45 days) as described in section 4.2.6.

Table 5.8: Comparative table of model generated results with confirmatory experiments.

Parameters	Models								
	CCD-RSM						Hybrid GA		
	Criteria-I			Criteria-II			Exp. value	Opt. value	Error (%)
	Exp. value	Opt. value	Error (%)	Exp. value	Opt. value	Error (%)			
Water fraction, θ_w	0.049	0.050		0.050	0.050		0.049	0.052	
Surfactant fraction, θ_s	0.102	0.106		0.100	0.101		0.102	0.105	
Energy density (W.cm^{-2})	29.75	29.75		29.75	29.76		29.75	29.94	
Ultrasonication time (minutes)	10.0	10.0		4.0	4.0		10.0	9.7	
Droplet diameter, $D_{z\text{-avg.}}$ (nm)	52.40	58.86	12.32	50.90	52.50	3.14	52.40	53.54	2.17
Kinematic viscosity (mm^2.s^{-1})	1.454	1.473	1.31	1.38	1.45	5.07	1.454	1.459	0.34

5.1.4 Interaction of process parameters

ANOVA analysis results shown in Table 5.2 (a) and (b) illustrates that the model parameters like water (θ_W) and surfactant (θ_S) fractions effected most significantly ($p<0.0001$) as compared to power density and ultrasonication time ($p<0.05$) in predicting the average droplet size (nm). However, mutual interaction of parameters like θ_W-θ_S effected more profoundly ($p<0.0001$) as compared to θ_S-power density and power density-ultrasonication time ($p<0.05$) in producing smaller droplet size w/o NEs. Likewise in predicting the kinematic viscosity of w/o NEs, most significant parameters (<0.0001) were water (θ_W) and surfactant (θ_S) fractions as compared to power density and ultrasonication time ($p<0.05$). Whereas, mutual interaction parameters like θ_W-θ_S and θ_W-power density effected significantly ($p<0.05$) in predicting Y_{KV} response.

Effect of single parameter on the average droplet size and kinematic viscosity of w/o NEs are shown in Fig. 5.7. Increase in water fraction (Fig. 5.7 (a)) from 0.02 to 0.06 first decreased the droplet size from ~80 nm to ~55 nm showing very less change ($\Delta25$nm), thereafter, increased for long range of water fraction ($0.06<\theta_W<0.12$) up to ~170 nm. This behavior of increase of droplet size with water fraction has been reported in the literature. However, increase of water fraction changed the kinematic viscosity by a factor of $\Delta2$ $mm^2.s^{-1}$.
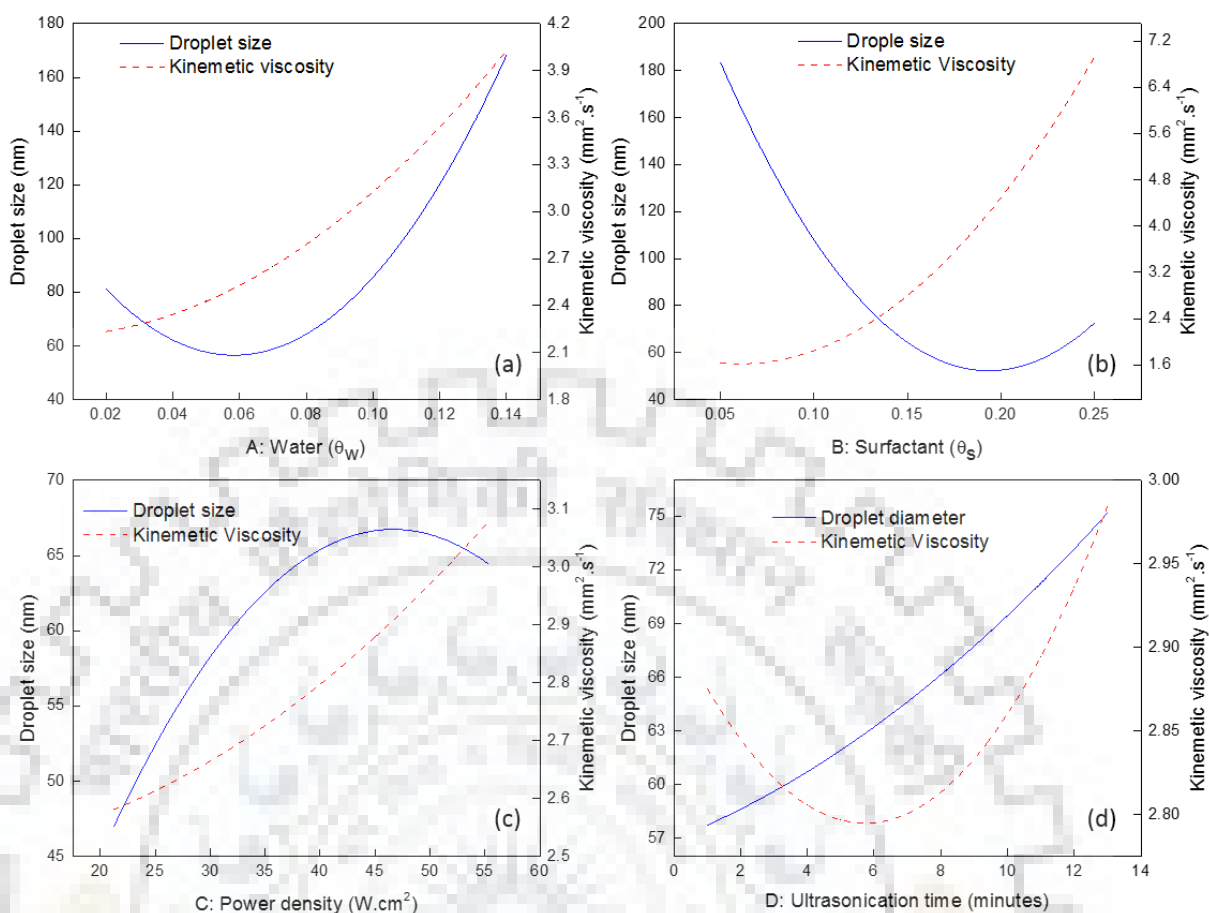
Fig. 5.7. Variation in droplet size (nm) with respect to single variables for design parameters as (a) water (wt. fraction) (b) surfactant (wt. fraction) (c) power density (W.cm^{-2}), and (d) ultrasonication time (minute).

Fig. 5.7 (b) shows the variation of single parameter surfactant fraction (θ_s) with respect to avg. droplet size (nm). A decrease in avg. droplet size was observed with an increase in surfactant fraction from ~183 to ~52 nm as surfactant fraction was increased from $0.05<\theta_s<0.2$. Further, increase in surfactant in the range $0.2<\theta_s<0.25$ showed merely Δ20 nm change in droplet size. Observed result might be the consequence of increase in the ratio of surface film thickness to the avg. droplet size that avoids collision between droplets (Liu et al., 2006). In contrast, kinematic viscosity kept on increasing almost linearly from ~1.63 to ~6.92 mm^2.s^{-1} when surfactant fraction was increased in the range of $0.05<\theta_s<0.25$. Obvious reason behind increase of kinematic viscosity of w/o NEs with surfactants was due to its high viscosity. An increment in power density from 21.25 to 46.25 W.cm^{-2} increased droplet size from 47 to 67 nm, thereafter, it showed no significant effect up to 55.25 W.cm^{-2} (Fig. 5.7 (c)). The minimal increase in droplet size with power density may be credited to the violent bubble collapse (Adewuyi, 2001; Chen, 2012). Hence, lower power density of 21.25 W.cm^{-2} may be suitable for the formation of w/o

NEs under constrained process variables. However, no significant variation in the kinematic viscosity of the w/o NEs was observed. Fig. 5.7 (d) illustrates the effect of increase of ultrasonication time (minute), where, optimized time of 6 minutes produced avg. droplet size of 63 nm. However, no significant change in kinematic viscosity of nano-emulsion diesel was observed.

Mutual parametric interaction of variables on the change in average droplet size and kinematic viscosity of w/o NEs is shown in Fig. 5.8. Two parameter interaction for water, A (θ_w) and surfactant, B (θ_s) found to be highly significant (p<0.0001) in case of response Y_{Dia} (Table 5.2 (a) and (b)). 3D and 2D surface plots shown in Fig. 5.8 (a) and (b) illustrate that $D_{z\text{-avg.}}$<100 nm is achievable only if the ratio of θ_s/θ_w is ≥ 2 is maintained. An optimum value of $\theta_w = 0.08$ and $\theta_s = 0.15$ was obtained by the surface plots at a constant power density of 38.25 W.cm^{-2} and 7 minutes of ultrasonication time. Interaction of two parameters, viz. surfactant fraction, B (θ_s) vs. power density, C (W.cm^{-2}) found significant (p<0.05), as shown in Table 5.2. Interaction of parameters θ_s and power density, as shown in Fig. 5.8 (c) and (d), suggests that $D_{z\text{-avg.}}$<50 nm is possible at θ_s≥0.12 at prevailing constant parameters.

An optimized value of θ_s=0.15 with power density of 38.25 (W.cm^{-2}) was obtained when studied at a constant θ_w (= 0.08) and ultrasonication time (7 minute). Effect of interaction parameters A (θ_w) and surfactant B (θ_s) on kinematic viscosity (mm^2.s^{-1}) of w/o NEs was found significant (p<0.05), as shown in ANOVA results (Table 5.2 (a) and (b)). Fig. 5.8 (e-f) depicts that the lower values of surfactant fraction within the range 0.07<θ_s<0.13 can lead to a kinematic viscosity ≤ 2 mm^2.s^{-1} at water ranges 0.03<θ_w<0.14. However, increase of surfactant θ_s>0.13 at water fraction range of 0.03<θ_w<0.14 simultaneously lead to kinematic viscosity >2 mm^2.s^{-1}.
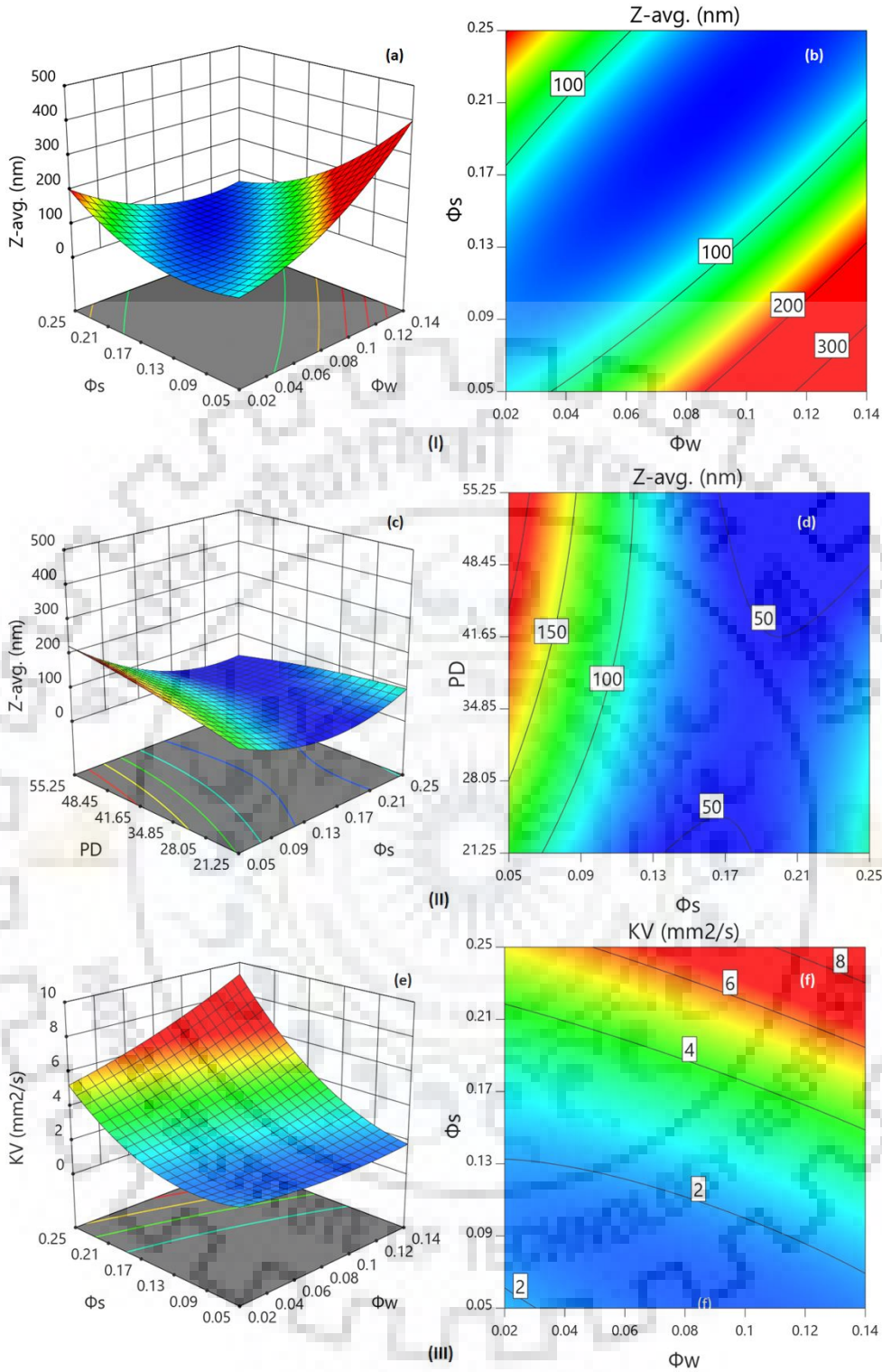
Fig. 5.8. (i) Variation in droplet size, d$_{z\text{-avg.}}$ (nm) with two parameters interactions viz. mixed surfactant (θ_s) and water (θ_w), **(ii)** interaction of power density, PD (W.cm^{-2}) vs. MS (θ_s) for depicting change in d$_{z\text{-avg.}}$ (nm), and **(iii)** change in kinematic viscosity (mm^2.s^{-1}) with mutual interaction of MS (θ_s) and W (θ_w) [(a) 3D-surface and (b) contour plot]

125

5.2 VALIDATION OF RSM-ANN AND HYBRID GA MODEL

Optimum parameters generated by the two proposed models like RSM-ANN (RCCD-RSM and FFBP-ANN) and hybrid GA targeted for achieving the minima in avg. droplet size of dispersed phase, $D_{z-avg.}$ and kinematic viscosity of the w/o NEs simultaneously were validated by performing the confirmatory experiment, as shown in Table 5.8 (details in supplementary Tables A9 and A10 in Appendix A). Percent deviation in the experimental results and simulated results was found in the percentage error range of $\sim\pm 5\%$. This indicated the prediction capability of models were satisfactory. Henceforth, adequacy of RSM-ANN and hybrid GA models on predicting the droplet size and kinematic viscosity of water emulsified nano-emulsion diesel was confirmed.
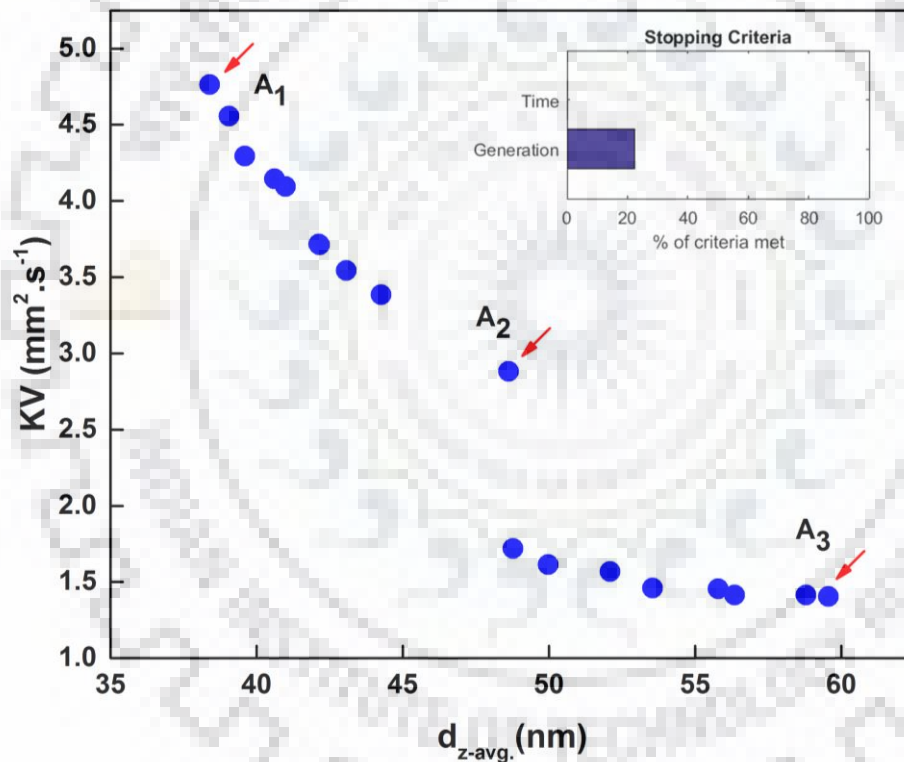

Fig. 5.9. Pareto-front of multi-objective hybrid genetic algorithm.

CHAPTER 6

CONCLUSIONS AND RECOMMENDATIONS

6.1 CONCLUSIONS

Based on the work carried out in this thesis for the preparation and characterization of water-in-oil nano-emulsions (w/o NEs) via two routes, i.e. low (isothermal dilution method) and high energy methods, in terms of stability, rheology and statistical modeling approach, following inferences can be made:

6.1.1 Nano-emulsion formation

In the present work formation of w/o nano-emulsions (NEs) was achieved via two different routes based on energy input to the process. In the first approach, w/o NEs formation was based on the low energy input wherein, isothermal dilution method (IDM) was implemented at a constant temperature of ± 37 °C. However, in the second approach, combination of low and high energy (ultrasonic cavitation) method was implemented at the optimized process parameters viz. water and surfactant fraction, power density, and sonication time. The later method was named combined energy mixed surfactant nano-emulsion (CEMSNE) method, wherein, NE formation was achieved by implementing optimized process parameters. Formation of NEs was achieved by implementing two sets of non-ionic surfactants in mixed proportions viz. Span 80/Tween 60 (S80/T60) and Span 80/Triton X-100 (S80/TX-100), however, combination of individual surfactants helped in producing a synergistic effect.

Formation of w/o NEs based on first approach (IDM) with non-ionic surfactants combination viz. sorbitan esters surfactants, sorbitan monooleate (S80) and PEG20-sorbitan monostearate (T60) was characterized in detail first time for their stability for longer duration and flow properties (rheology). Some of the findings of this work for the system water/S80:T60/diesel can be summarized as follows:

- Best ratio of S80/T60 responsible for the formation of nanometer ($\approx$44.87 nm) sized droplets of w/o NEs was found as 65:35 (w/w) by changing the water and surfactant composition at an HLB value of 8.01.

- A ternary diagram study was conducted at a constant temperature of ± 37°C by varying water and surfactant compositions in the bounded range of 4-20% and 2-10%, respectively, to predict the zones of transparent and translucent nano-emulsions. Droplet

127

sizes of formed NEs were found as 44 nm<droplet size<700nm in the co-ordinates of ternary diagram within the bounded range.

- Effect of increase of oil to surfactant ratio on droplet size at a constant concentration of water (12 wt. %) at 37°C concluded that at lower O/S ratio, a lower droplet size was obtained and with an increase in the O/S ratio, the droplet size increased almost linearly.

Formation of transparent combined energy mixed surfactant w/o nano-emulsion was achieved by application of ultrasonic cavitation in combination with isothermal low energy (IDM) for water/mixed surfactant (TX-100:S80)/diesel. from this work following inferences were made:

- A mixture of two functional groups (ether and ester) non-ionic surfactants was optimized at a ratio of 0.71/0.29 (Span 80/TX-100; w/w) imparting nano-sized droplets in the formed w/o NEs.
- A ternary diagram study was performed to recognize the compositions accountable for the formation of transparent, translucent and opaque emulsions in the bounded range of water ($0.02 < \Phi_w < 0.11$) and surfactant fraction ($0.10 < \Phi_s < 0.20$).
- Optimization of ultrasonication parameters and ternary diagram study helped in finding out the zones of formation of transparent nano-emulsions.
- Average droplet size down to $\approx 25 \pm 1$ nm was achieved by adopting.
- Optimization of ultrasonicated parameters resulted in 25% amplitude, 0.5 pulse mode factor and 8.5 minutes of sonication time.
- It was demonstrated that the formation of transparent nano-emulsions can be achieved by maintaining the composition of individual constituents within the range of surfactant-to-water ratio (β) as $2 \leq \beta \leq 3$.
- Influence of increase of mixed surfactant composition in the nano-emulsion decreased droplet diameter ($D_{z\text{-avg.}}$) value, whereas, an inverse relationship was found in case of increase of water percent.
- An increase in energy density ($J.ml^{-1}$) applied to the pre-emulsions at the prevailing conditions predicted power law reduction of $D_{z\text{-avg.}}$ value and found helpful in scaling up and tuning of the droplet size ($D_{z\text{-avg.}}$).
- Prediction of average droplet size modeled with energy density fitted well and could be used for scaling up and tuning the nano-droplet size. An empirical correlation was proposed for scale up of w/o NE production process:

$$D_{z-avg.} = \frac{359.4}{\varepsilon_v^{0.538}}$$

- Reduction in droplet size was prominently found in the range of energy density from 15.23 J.ml^{-1} to 40 J.ml^{-1}, thereafter, it decelerated up to 160 J.ml^{-1}.

6.1.2 Stability of nano-emulsions

Stability of tested w/o NE samples prepared by using mixed surfactants i.e. S80/T60 by adopting isothermal dilution method can be summarized as follows:

- Stability of nano-emulsions was tested for 30 days for finding out the instability mechanism of formed NEs.
- Mechanism responsible for instability of NEs, was explained by Ostwald ripening. Samples with lower nano-drop sizes depicted lower values of Ostwald ripening rate, ω_3 (m^3.s^{-1}), indicative of higher stability.
- In case of w/o nano-emulsion of droplet size 64.28 nm the Oswald ripening rate was found as 0.0874x10^{-27} m^3.s^{-1}. Comparison of Ostwald ripening rate with other set of surfactants obtained by different authors showed the lowest rate among them indicative of enhanced stability.
- Highly stable and transparent emulsion sample found at 10% surfactant composition (S80/T60) and 2:1 water-to-surfactant ratio with 64.28 nm droplet size.
- Comparison of Ostwald ripening rate for droplet sizes of 70±7 nm reported in the literature for different set of mixed surfactants showed lowest value, endorsing better stability of formed w/o nano-emulsion.

Long term and kinetic stability of the NE samples formed by implementing the combined energy mixed surfactant nano-emulsion (CEMSNE) method prepared with mixed surfactants S80/TX-100 can be summarized as follows:

- A kinetic stability test performed on four samples (surfactant-to-water ratio, β=2.0, 2.5, 3.0 and 4.0) reveled no change in droplet size and phase under centrifugation at 5000 RPM for 15 minutes (Span 80/TX-100).
- Whereas long term stability (45 days) assessed using Ostwald ripening model showed stability in the order of β=2.0>β=2.5>β=3.0>β=4.

6.1.3 Rheological behavior of w/o nano-emulsions

The inferences depicting changes in composition of water, surfactant, and effect of change of temperature on the rheological behavior of the w/o NEs formed by adopting IDM can be summarized as follows:

- Rheological study of formed w/o nano-emulsions was performed in the temperature range of 25 to 40 °C and shear rate range of 10 to 1000 s^{-1}.
- Rheological behavior of w/o nano-emulsions samples, i.e. Sample 1 (20% water; 8% surfactant), Sample 2 (16 % water; 8% surfactant), and Sample 3 (20% water; 10% surfactant), water and diesel at different constant temperatures was tested.
- Sample 3 (20% water; 10% surfactant) and Sample 1 (20% water; 8% surfactant) showed higher shear stress at any value of shear rate between 10 to 1000 s^{-1} as compared to Sample 2 (16 % water; 8% surfactant) with the diesel and water at the bottom (i.e. at 25 °C and 108 s^{-1} shear rate, shear stress for Sample 3, Sample 1, Sample 2, diesel and water as 0.689, 0.640, 0.566, 0.372 and 0.088 Pa, respectively).
- An increase in temperature, from 25 °C to 40 °C, resulted in to a decrease in shear stress at a constant shear rate.
- A two parameter Ostwald-de-waele power law model was used to describe the flow behavior of tested w/o nano-emulsion samples.
- The tested set of w/o nano-emulsion samples depicted Newtonian behavior ($1.0371 \leq n \leq 1.0826$) over a wider range of shear rate (10 - 1000 s^{-1}) at different temperatures (25 - 40 °C).

Water-in-oil nano-emulsions formed by application of combination of mixed surfactants (S80/TX-100) were tested for rheological analysis at varied temperatures and shear rates, and following inferences were made:

- Three samples with varied water fraction, Φ_w (0.05, 0.08. 0.11) and constant β (=2) value were tested for rheological analysis at four temperature ranges viz. 25 °C, 30 °C, 40 °C, and 50 °C.
- All three samples showed a Newtonian behavior at shear rate range of 10-100 s^{-1}.
- Power law model fitting resulted the flow behavior index (n) in the range of $0.9766 \leq n \leq 1.0034$.
- Effect of increase in dispersed phase composition, however, increased the w/o NEs viscosity nevertheless keeping NEs flow behavior unchanged.

- Effect of change of temperature on CEMSNE viscosity was tested from 15-50 $^{\circ}$C at a constant shear rate of 100 s^{-1}. Results depicted the maximum increase in the viscosity of Sample 3 (Φ_w=0.11; β=2) at a very low temperature of 15 $^{\circ}$C, however, Sample 1 (Φ_w: 0.05; β=2) showed moderate viscosity (4.8 mPa.S) at 25 $^{\circ}$C.

- A shear stress variations with shear rate change in the range of 10-100 s^{-1}, inferred that the newly formed w/o NEs can be easily transported at the temperature ranging from of 25 to 50 $^{\circ}$C.

6.1.4 Statistical optimization of process parameters

Optimization techniques such as RSM, ANN, and GA were used for developing model techniques for the w/o NEs system. Capability of statistical model and optimization tools in predicting the minimum droplet size of w/o NEs by retaining minimum kinematic viscosity, simultaneously, was tested and following conclusions were made.

- A rotatable central composite design (RCCD) was implemented to design 30 numbers of experimental data. Model equations therefore obtained provided the parametric interactions of process variables on the response variables ($Y_{Dia.}$ and Y_{KV}).

- Surface plots suggested that process parameters like water and surfactant fraction (θ_w and θ_s) influenced most effectively on droplet size ($Y_{Dia.}$) and kinematic viscosity (Y_{KV}). However, power density and ultrasonication time acted significantly on avg. droplet size of nano-emulsion.

- 3D surface plots suggested that if the ratio of surfactant and water fractions maintained as $\theta_s/\theta_w \geq 2$, droplet size of $D_{z\text{-avg.}} \leq 100$ nm was achievable for the present system under study.

- RCCD-RSM and multi objective hybrid GA (BPANN-GA) schemes predicted response variables (droplet size $D_{z\text{-avg.}}$ and kinematic viscosity) were validated by performing confirmatory experiments.

- Optimized process parameters in case of RCCD-RSM model predicted response variables Y_{Dia} and Y_{KV} as 58.86 nm and 1.473 mm^2.s^{-1}, respectively, however, optimized processes variables predicted water fraction as 0.050 (θ_w), surfactant fraction as 0.106 (θ_s), power density as 29.75 W.cm^{-2}, and ultrasonication time as 10 minutes with desirability of 0.95.

- In case of multi objective GA optimization, an optimized response variables viz. Y_{Dia} and Y_{KV} were found as 53.54 nm and 1.459 mm^2.s^{-1}, respectively with optimized values for

water fraction (θ_w), surfactant fraction (θ_s), power density as 0.052, 0.105, 29.94 W.cm^{-2}, and 9.7 minutes, respectively.

- Percentage error between the experimental and predicted results was approximately in the range of ~±5% showing precedence of hybrid genetic algorithm over RCCD-RSM model.

- Method proposed in this work can be helpful in the formation of w/o nano-emulsion diesel with tuning in the droplet size and kinematic viscosity with reduced water and surfactant fraction, number of experiments, power requirement and therefore substantiated as a cost effective method.

6.2 RECOMMENDATIONS

1. An alternative fuel similar to water-in-diesel can be developed using oxygenated compounds like alcohols, ethers, etc. that can improve its combustion properties. Therefore, blending of these fuels with diesel may further increase combustion properties and emission standards.

2. Blending of bio-fuels with diesel is also to be explored targeted towards improving fuel properties with alternative sources of energy.

3. New non-ionic surfactants can be designed showing compatibility with water/diesel nano-emulsion systems. The largest category of commercially available nonionic surfactants is the ethylene oxide adducts of the fatty alcohol and alkyl phenol. Therefore it is proposed to synthesize the non-ionic surfactants by changing the stoichiometric ratios for the preparation of nano-emulsions.

4. Formation of water-in-diesel oil nano-emulsions can be formed by exploring the capability of bio-surfactants as a surface active agents. This may increase the eco-friendly choice, however cost associated may be a constraint to be considered for study.

5. A detailed analysis regarding scale up study is recommended for further study in the formation of w/o nano-emulsions including cost estimation.

REFERENCES

Abismaïl, B., Canselier, J.P., Wilhelm, A.M., Delmas, H., Gourdon, C., 1999. Emulsification by ultrasound: Drop size distribution and stability. Ultrasonics Sonochemistry 6, 75–83.

Abu-Zaid, M., 2004. Performance of single cylinder, direct injection Diesel engine using water fuel emulsions. Energy Conversion and Management 45, 697–705.

Adewuyi, Y.G., 2001. Sonochemistry: Environmental Science and Engineering Applications. Industrial & Engineering Chemistry Research 40, 4681–4715.

Agatonovic-kustrin, S., Alany, R.G., 2001. Role of Genetic Algorithms and Artificial Neural Networks in Predicting the Phase Behavior of Colloidal Delivery Systems 18, 1049–1055.

Agatonovic-Kustrin, S., Glass, B.D., Wisch, M.H., Alany, R.G., 2003. Prediction of a Stable Microemulsion Formulation for the Oral Delivery of a Combination of Antitubercular Drugs Using ANN Methodology. Pharmaceutical Research 20, 1760–1765.

Alahmer, A., Yamin, J., Sakhrieh, A., Hamdan, M.A., 2010. Engine performance using emulsified diesel fuel. Energy Conversion and Management 51, 1708–1713.

Alany, R.G., Agatonovic-Kustrin, S., Rades, T., Tucker, I.G., 1999. Use of artificial neural networks to predict quaternery phase systems from limited experimental data. Journal of Pharmaceutical and Biomedical Analysis 19, 443–452.

Al-Sabagh, A.M., Emara, M.M., Noor El-Din, M.R., Aly, W.R., 2011. Formation of water-in-diesel oil nano-emulsions using high energy method and studying some of their surface active properties. Egyptian Journal of Petroleum 20, 17–23.

Al-Sabagh, A.M., Emara, M.M., Noor El-Din, M.R., Aly, W.R., 2012a. Preparation of Water-in-Diesel Fuel Nanoemulsions Using High-Energy Emulsification Method and a Study of Some of Their Surface Active Properties. Journal of Dispersion Science and Technology 33, 970–976.

Al-Sabagh, A.M., Emara, M.M., Noor El-Din, M.R., Aly, W.R., 2012b. Water-in-diesel fuel nanoemulsions prepared by high energy: Emulsion drop size and stability, and emission characteristics. Journal of Surfactants and Detergents 15, 139–145.

Alzorqi, I., Ketabchi, M.R., Sudheer, S., Manickam, S., 2016. Optimization of ultrasound induced emulsification on the formulation of palm-olein based nanoemulsions for the incorporation of antioxidant β-D-glucan polysaccharides. Ultrasonics Sonochemistry 31, 71–84.

Amani, A., York, P., Chrystyn, H., Clark, B.J., Do, D.Q., 2008. Determination of factors controlling the particle size in nanoemulsions using Artificial Neural Networks. European Journal of Pharmaceutical Sciences 35, 42–51.

Anderson, R., Buscall, R., Eldridge, R., Mulvaney, P., Scales, P.J., 2014. Ostwald ripening of comb polymer stabilised Ag salt nanoparticles. Colloids and Surfaces A: Physicochemical and Engineering Aspects 459, 58–64.

Angkuratipakorn, T., Sriprai, A., Tantrawong, S., Chaiyasit, W., Singkhonrat, J., 2017. Fabrication and characterization of rice bran oil-in-water Pickering emulsion stabilized by cellulose nanocrystals. Colloids and Surfaces A: Physicochemical and Engineering Aspects 522, 310–319.

Anton, N., Vandamme, T.F., 2011. Nano-emulsions and micro-emulsions: Clarifications of the critical differences. Pharmaceutical Research 28, 978–985.

Armas, O., Ballesteros, R., Martos, F.J., Agudelo, J.R., 2005. Characterization of light duty Diesel engine pollutant emissions using water-emulsified fuel. Fuel 84, 1011–1018.

Barradas, T.N., de Campos, V.E.B., Senna, J.P., Coutinho, C. dos S.C., Tebaldi, B.S., Silva, K.G. de H. e, Mansur, C.R.E., 2015. Development and characterization of promising o/w nanoemulsions containing sweet fennel essential oil and non-ionic sufactants. Colloids and Surfaces A: Physicochemical and Engineering Aspects 480, 214–221.

Basha, J.S., Anand, R.B., 2011. An experimental study in a CI engine using nanoadditive blended water-diesel emulsion fuel. International Journal of Green Energy 8, 332–348.

Bashiri, M., Farshbaf Geranmayeh, A., 2011. Tuning the parameters of an artificial neural network using central composite design and genetic algorithm. Scientia Iranica 18, 1600–1608.

Baskar, P., Kumar, S.A., 2017. Experimental investigation on performance characteristics of a diesel engine using diesel-water emulsion with oxygen enriched air. Alexandria Engineering Journal 56, 137–146.

Bazylin´ska, U., Kulbacka, J., Wilk, K.A., 2014. Dicephalic ionic surfactants in fabrication of biocompatible nanoemulsions: Factors influencing droplet size and stability. Colloids and Surfaces A: Physicochemical and Engineering Aspects 460, 312–320.

Bezerra, M.A., Santelli, R.E., Oliveira, E.P., Villar, L.S., Escaleira, L.A., 2008. Response surface methodology (RSM) as a tool for optimization in analytical chemistry. Talanta 76, 965–977.

Bidita, B.S., Suraya, A.R., Shazed, M.A., Salleh, M.A.M, Idris, A., 2014. Influence of fuel additive in the formulation and combustion characteristics of water-in-diesel nanoemulsion fuel. Energy and Fuels 28, 4149–4161.

Bidita, B.S., Suraya, A.R., Shazed, M.A., Salleh, M.A.M., Idris, A., 2016. Preparation, characterization and engine performance of water in diesel nanoemulsions. Journal of the Energy Institute 89, 354–365.

Boxall, J., Koh, C., Sloan, E.D., Sum, A.K., Wu, D.T., 2012. Droplet size scaling of water-in-oil emulsions under turbulent flow. Langmuir 28, 104–10.

Canselier, J.P., Delmas, H., Wilhelm, A.M., Abismaïl, B., 2002. Ultrasound Emulsification-an overview. Journal of Dispersion Science and Technology 23, 333–349.

Carpenter, J., Saharan, V.K., 2017. Ultrasonic assisted formation and stability of mustard oil in water nanoemulsion: Effect of process parameters and their optimization. Ultrasonics Sonochemistry 35, 422–430.

Chen, D., 2012. Applications ultrasound in water and wastewater treatment, Handbook on Applications of Ultrasound: Sonochemistry for Sustainability. CRC Press, Taylor and Francis Group.

Chen, G., Tao, D., 2005. An experimental study of stability of oil-water emulsion. Fuel Processing Technology 86, 499–508.

Chiaramonti, D., Bonini, M., Fratini, E., Tondi, G., Gartner, K., Bridgwater, A. V., Grimm, H.P., Soldaini, I., Webster, A., Baglioni, P., 2003. Development of emulsions from biomass pyrolysis liquid and diesel and their use in engines - Part 1: Emulsion production. Biomass and Bioenergy 25, 85–99.

Ding, S., Li, H., Su, C., Yu, J., Jin, F., 2013. Evolutionary artificial neural networks: A review. Artificial Intelligence Review 39, 251–260.

Du, Z., Wang, C., Tai, X., Wang, G., Liu, X., 2016. Optimization and Characterization of Biocompatible Oil-in-Water Nanoemulsion for Pesticide Delivery. ACS Sustainable Chemistry and Engineering 4, 983–991.

Dwivedi, G., Jain, S., Sharma, M.P., 2011. Impact analysis of biodiesel on engine performance - A review. Renewable and Sustainable Energy Reviews 15, 4633–4641.

Ee, S.L., Duan, X., Liew, J., Nguyen, Q.D., 2008. Droplet size and stability of nano-emulsions produced by the temperature phase inversion method. Chemical Engineering Journal 140, 626–631.

Fahd, M.E.A., Wenming, Y., Lee, P.S., Chou, S.K., Yap, C.R., 2013. Experimental investigation of the performance and emission characteristics of direct injection diesel engine by water emulsion diesel under varying engine load condition. Applied Energy 102, 1042–1049.

Farfaletti, A., Astorga, C., Martini, G., Manfredi, U., Mueller, A., Rey, M., De Santi, G., Krasenbrink, A., Larsen, B.R., 2005. Effect of water/fuel emulsions and a cerium-based combustion improver additive on HD and LD diesel exhaust emissions. Environmental Science and Technology 39, 6792–6799.

Fasuan, T.O., Akanbi, C.T., 2018. Application of osmotic pressure in modification of Amaranthus viridis starch. Lwt 96, 182–192.

Feng, J., Shi, Y., Yu, Q., Sun, C., Yang, G., 2016. Effect of emulsifying process on stability of pesticide nanoemulsions. Colloids and Surfaces A: Physicochemical and Engineering Aspects 497, 286–292.

Ghanavati Nasab, S., Semnani, A., Teimouri, A., Kahkesh, H., Momeni Isfahani, T., Habibollahi, S., 2018. Removal of congo red from aqueous solution by hydroxyapatite nanoparticles loaded on zein as an efficient and green adsorbent: Response Surface Methodology and Artificial Neural Network-Genetic Algorithm. Journal of Polymers and the Environment 26, 3677–3697.

Ghannam, M.T., Selim, M.Y.E., 2014. Rheological properties of water-in-diesel fuel emulsions. International Journal of Ambient Energy 37, 24–28.

Ghojel, J., Honnery, D., Al-Khaleefi, K., 2006. Performance, emissions and heat release characteristics of direct injection diesel engine operating on diesel oil emulsion. Applied Thermal Engineering 26, 2132–2141.

Gogate, P.R., Wilhelm, A.M., Pandit, A.B., 2003. Some aspects of the design of sonochemical reactors. Ultrasonics Sonochemistry 10, 325–330.

Gupta, A., Narsimhan, V., Hatton, T.A., Doyle, P.S., 2016. Kinetics of the Change in Droplet Size during Nanoemulsion Formation. Langmuir 32, 11551–11559.

Gutiérrez, J.M., González, C., Maestro, A., Solè, I., Pey, C.M., Nolla, J., 2008. Nano-emulsions: New applications and optimization of their preparation. Current Opinion in Colloid and Interface Science 13, 245–251.

Hasannuddin, A.K., Wira, J.Y., Srithar, R., Sarah, S., Ahmad, M.I., Aizam, S.A., Aiman, M.A.B., Zahari, M., Watanabe, S., Azrin, M.A., Mohd, S.S., 2016. Effect of emulsion fuel on engine emissions-A review. Clean Technologies and Environmental Policy 18, 17–32.

He, B.Q., Shuai, S.J., Wang, J.X., He, H., 2003. The effect of ethanol blended diesel fuels on emissions from a diesel engine. Atmospheric Environment 37, 4965–4971.

Helgeson, M.E., 2016. Colloidal behavior of nanoemulsions: Interactions, structure, and rheology. Current Opinion in Colloid and Interface Science 25, 39–50.

Henglein, A., Gutiérrez, M., 1993. Sonochemistry and sonoluminescence: Effects of external pressure. Journal of Physical Chemistry 97, 158–162.

Hinze, J.O., 1955. Fundamentals of the hydrodynamics mechanisms of splitting in dispersion process. AIChE Journal 1, 289–295.

Homayoonfal, M., Khodaiyan, F., Mousavi, S.M., 2014. Walnut Oil Nanoemulsion: Optimization of the Emulsion Capacity, Cloudiness, Density, and Surface Tension. Journal of Dispersion Science and Technology 35, 725–733.

Ishiguro, S., Naito, T., 2010. Method for production of emulsion fuel and apparatus for production of the fuel. US 2010/0186288 A1.

Ithnin, A.M., Noge, H., Kadir, H.A., Jazair, W., 2014. An overview of utilizing water-in-diesel emulsion fuel in diesel engine and its potential research study. Journal of the Energy Institute 87, 273–288.

Izquierdo, P., Esquena, J., Tadros, T.F., Dederen, C., Garcia, M.J., Azemar, N., Solans, C., 2002. Formation and stability of nano-emulsions prepared using the phase inversion temperature method. Langmuir 18, 26–30.

Jacob, S., Banerjee, R., 2016. Modeling and optimization of anaerobic codigestion of potato waste and aquatic weed by response surface methodology and artificial neural network coupled genetic algorithm. Bioresource Technology 214, 386–395.

Jaworska, M., Sikora, E., Ogonowski, J., 2015. Rheological Properties of Nanoemulsions Stabilized by Polysorbate 80. Chemical Engineering & Technology 38, 1469–1476.

Karbstein, H., Schubert, H., 1995. Developments in the continuous mechanical production of oil-in-water macro-emulsions. Chemical Engineering and Processing: Process Intensification 34, 205–211.

Karimi, H., Yousefi, F., 2012. Fluid Phase Equilibria Application of artificial neural network – genetic algorithm (ANN – GA) to correlation of density in nanofluids. Fluid Phase Equilibria 336, 79–83.

Katsouli, M., Polychniatou, V., Tzia, C., 2018. Optimization of water in olive oil nano-emulsions composition with bioactive compounds by response surface methodology. LWT - Food Science and Technology 89, 740–748.

Khalife, E., Tabatabaei, M., Demirbas, A., Aghbashlo, M., 2017. Impacts of additives on performance and emission characteristics of diesel engines during steady state operation. Progress in Energy and Combustion Science 59, 32–78.

Khan, A., Marques, E.F., 2000. Synergism and polymorphism in mixed surfactant systems. Current Opinion in Colloid and Interface Science 4, 402–410.

Khaw, J.F.C., Lim, B.S., Lim, L.E.N., 1995. Optimal design of neural networks using the Taguchi method. Neurocomputing 7, 225–245. Khaw, J.F.C., Lim, B.S., Lim, L.E.N., 1995. Optimal design of neural networks using the Taguchi method. Neurocomputing 7, 225–245.

Kothekar, S.C., Ware, A.M., Waghmare, J.T., Momin, S.A., 2007. Comparative analysis of the properties of Tween-20, Tween-60, Tween-80, Arlacel-60, and Arlacel-80. Journal of Dispersion Science and Technology 28, 477–484.

Kumar, M., Misra, A., Babbar, A.K., Mishra, A.K., Mishra, P., Pathak, K., 2008. Intranasal nanoemulsion based brain targeting drug delivery system of risperidone. International Journal of Pharmaceutics 358, 285–291.

Kumar, N., Mandal, A., 2018. Thermodynamic and physicochemical properties evaluation for formation and characterization of oil-in-water nanoemulsion. Journal of Molecular Liquids 266, 147–159.

Kundu, P., Agrawal, A., Mateen, H., Mishra, I.M., 2013. Stability of oil-in-water macro-emulsion with anionic surfactant: Effect of electrolytes and temperature. Chemical Engineering Science 102, 176–185.

Kundu, P., Paul, V., Kumar, V., Mishra, I.M., 2015. Formulation development, modeling and optimization of emulsification process using evolving RSM coupled hybrid ANN-GA framework. Chemical Engineering Research and Design 104, 773–790.

Kundu, P., Paul, V., Kumar, V., Mishra, I.M., 2016. An adaptive modeling of petroleum emulsion formation and stability by a heuristic multiobjective artificial neural network-genetic algorithm. Petroleum Science and Technology 34, 350–358.

Kwanchareon, P., Luengnaruemitchai, A., Jai-In, S., 2007. Solubility of a diesel-biodiesel-ethanol blend, its fuel properties, and its emission characteristics from diesel engine. Fuel 86, 1053–1061.

Leal-Calderon, F., Bibette, J., Schmitt, V., 2007. Emulsion science: Basic principles, second ed. ed, Emulsion Science: Basic Principles. Springer Verlag.

Leong, T.S.H., Wooster, T.J., Kentish, S.E., Ashokkumar, M., 2009. Minimising oil droplet size using ultrasonic emulsification. Ultrasonics Sonochemistry 16, 721–727.

Li, P.H., Chiang, B.H., 2012. Process optimization and stability of D-limonene-in-water nanoemulsions prepared by ultrasonic emulsification using response surface methodology. Ultrasonics Sonochemistry 19, 192–197.

Liang, Y., Shu, G., Wei, H., Zhang, W., 2013. Effect of oxygen enriched combustion and water-diesel emulsion on the performance and emissions of turbocharged diesel engine. Energy Conversion and Management 73, 69–77.

Lif, A., Holmberg, K., 2006. Water-in-diesel emulsions and related systems. Advances in Colloid and Interface Science 123–126, 231–239.

Lin, C., Wang, K., 2004a. Effects of an oxygenated additive on the emulsification characteristics of two- and three-phase diesel emulsions. Fuel 83, 507–515.

Lin, C., Wang, K., 2004b. Effects of a combustion improver on diesel engine performance and emission characteristics when using three-phase emulsions as an alternative fuel. Energy & Fuels 18, 477–484.

Lin, C., Chen, L.W., 2006. Emulsification characteristics of three- and two-phase emulsions prepared by the ultrasonic emulsification method. Fuel Processing Technology 87, 309–317.

Liu, W., Sun, D., Li, C., Liu, Q., Xu, J., 2006. Formation and stability of paraffin oil-in-water nano-emulsions prepared by the emulsion inversion point method. Journal of Colloid and Interface Science 303, 557–563.

Liu, Y., Wei, F., Wang, Y., Zhu, G., 2011. Studies on the formation of bifenthrin oil-in-water nano-emulsions prepared with mixed surfactants. Colloids and Surfaces A: Physicochemical and Engineering Aspects 389, 90–96.

Lovelyn, C., Attama, A.A., 2011. Current State of Nanoemulsions in Drug Delivery. Journal of Biomaterials and Nanobiotechnology 02, 626–639.

Maali, A., Mosavian, M.T.H., 2013. Preparation and Application of Nanoemulsions in the Last Decade (2000–2010). Journal of Dispersion Science and Technology 34, 92–105.

Martinez-Guerra, E., Gude, V.G., 2015. Continuous and pulse sonication effects on transesterification of used vegetable oil. Energy Conversion and Management 96, 268–276.

Mason, T.G., Wilking, J.N., Meleson, K., Chang, C.B., Graves, S.M., 2006. Nanoemulsions: formation, structure, and physical properties. Journal of Physics: Condensed Matter 18, R635--R666.

Matalanis, A., Jones, O.G., McClements, D.J., 2011. Structured biopolymer-based delivery systems for encapsulation, protection, and release of lipophilic compounds. Food Hydrocolloids 25, 1865–1880.

Mccall, J., 2005. Genetic algorithms for modelling and optimisation. Journal of computational and applied mathematics 184, 205–222.

McClements, D.J., 2015. Food Emulsions: Principles, practices and techniques, 3rd ed. CRC Press.

McClements, D.J., Jafari, S.M., 2018. Improving emulsion formation, stability and performance using mixed emulsifiers: A review. Advances in Colloid and Interface Science 251, 55–79.

Mehmood, T., Ahmed, A., Ahmad, A., Ahmad, M.S., Sandhu, M.A., 2018. Optimization of mixed surfactants-based β-carotene nanoemulsions using response surface methodology: An ultrasonic homogenization approach. Food Chemistry 253, 179–184.

Mehta, R.N., More, U., Malek, N., Chakraborty, M., Parikh, P.A., 2015. Study of stability and thermodynamic properties of water-in-diesel nanoemulsion fuels with nano-Al additive. Applied Nanoscience 5, 891–900.

Moghaddari, M., Yousefi, F., Ghaedi, M., Dashtian, K., 2018. A simple approach for the sonochemical loading of Au, Ag and Pd nanoparticle on functionalized MWCNT and subsequent dispersion studies for removal of organic dyes: Artificial neural network and response surface methodology studies. Ultrasonics Sonochemistry 42, 422–433.

Monazzami, A., Vahabzadeh, F., Aroujalian, A., Mogharei, A., 2018. An artificial neural network approach to determine the rheological behavior of pickering-type diesel-in-water emulsion prepared with the use of β-cyclodextrin. Korean Journal of Chemical Engineering 35, 847–852.

Montgomery, D.C., 2001. Design and analysis of experiments, fifth. ed, Quality and Reliability Engineering International. John Wiley & Sons, Inc.

Morais Diane, J.M., Burgess, J., 2014. Vitamin e nanoemulsions characterization and analysis. International Journal of Pharmaceutics 465, 455–463.

Myers, R.H., Montgomery, D.C., Anderson-Cook, C.M., 2016. Response surface methodology: process and product optimization using designed experiments, Fourth. ed. John Wiley & Sons.

Nadeem, M., Rangkuti, C., Anuar, K., Haq, M.R.U., Tan, I.B., Shah, S.S., 2006. Diesel engine performance and emission evaluation using emulsified fuels stabilized by conventional and gemini surfactants. Fuel 85, 2111–2119.

Nash, J.J., Erk, K.A., 2017. Stability and interfacial viscoelasticity of oil-water nanoemulsions stabilized by soy lecithin and Tween 20 for the encapsulation of bioactive carvacrol. Colloids and Surfaces A: Physicochemical and Engineering Aspects 517, 1–11.

Nejadmansouri, M., Hosseini, S.M.H., Niakosari, M., Yousefi, G.H., Golmakani, M.T., 2016. Physicochemical properties and oxidative stability of fish oil nanoemulsions as affected by hydrophilic lipophilic balance, surfactant to oil ratio and storage temperature. Colloids and Surfaces A: Physicochemical and Engineering Aspects 506, 821–832.

Nesterenko, A., Drelich, A., Lu, H., Clausse, D., Pezron, I., 2014. Influence of a mixed particle/surfactant emulsifier system on water-in-oil emulsion stability. Colloids and Surfaces A: Physicochemical and Engineering Aspects 457, 49–57.

Noor El-Din, M.R., El-Gamal, I.M., El-Hamouly, S.H., Mohamed, H.M., Mishrif, M.R., Ragab, A.M., 2013. Rheological behavior of water-in-diesel fuel nanoemulsions stabilized by mixed surfactants. Colloids and Surfaces A: Physicochemical and Engineering Aspects 436, 381–334.

Noor El-Din, M.R., El-Hamouly, S.H., Mohamed, H.M., Mishrif, M.R., Ragab, A.M., 2013a. Water-in-diesel fuel nanoemulsions: Preparation, stability and physical properties. Egyptian Journal of Petroleum 22, 517–530.

Noor El-Din, M.R., El-Hamouly, S.H., Mohamed, H.M., Mishrif, M.R., Ragab, A.M., 2013b. Formation and Stability of Water-in-Diesel Fuel Nanoemulsions Prepared by High-Energy Method. Journal of Dispersion Science and Technology 34, 575–581.

Noor El-Din, M.R., El-Hamouly, S.H., Mohamed, H.M., Mishrif, M.R., Ragab, A.M., 2014. Investigating factors affecting water-in-diesel fuel nanoemulsions. Journal of Surfactants and Detergents 17, 819–831.

Noor El-Din, M.R., Mishrif, M.R., Morsi, R.E., El-Sharaky, E.A., Haseeb, M.E., Ghanem, R.T.M., 2017. A new modified low-energy emulsification method for preparation of water-in-diesel fuel nanoemulsion as alternative fuel. Journal of Dispersion Science and Technology 38, 248–255.

Noor El-Din, M.R., Osman, D.I., Rashad, A.M., Mishrif, M.R., El-Sharaky, E.A., 2017. Physicochemical and rheological characterization of diesel fuel nanoemulsions at different water and surfactant contents. Journal of Molecular Liquids 231, 440–450.

O'Sullivan, J., Murray, B., Flynn, C., Norton, I., 2015. Comparison of batch and continuous ultrasonic emulsification processes. Journal of Food Engineering 167, 114–121.

Oldfield, A.S., Thompson, L., 2010. Diesel fuel emulsion. US 7,731,768 B2.

Pajouhandeh, A., Kavousi, A., Schaffie, M., Ranjbar, M., 2017. Experimental measurement and modeling of nanoparticle-stabilized emulsion rheological behavior. Colloids and Surfaces A: Physicochemical and Engineering Aspects 520, 597–611.

Pareek, V., Brungs, M.., Adesina, A., Sharma, R., 2002. Artificial neural network modeling of a multiphase photodegradation system. Journal of Photochemistry and Photobiology A: Chemistry 149, 139–146.

Patil, H., Gadhave, A., Mane, S., Waghmare, J., 2015. Analyzing the Stability of the Water-in-Diesel Fuel Emulsion. Journal of Dispersion Science and Technology 36, 1221–1227.

Patist, A., Bhagwat, S.S., Penfield, K.W., Aikens, P., Shah, D.O., 2000. On measurement of Critical Micelle Concentrations of Pure and Technical-Grade Non-ionic Surfactants. Journal of surfactants and detergents 3, 53–58.

Peng, L.C., Liu, C.H., Kwan, C.C., Huang, K.F., 2010. Optimization of water-in-oil nanoemulsions by mixed surfactants. Colloids and Surfaces A: Physicochemical and Engineering Aspects 370, 136–142.

Peshkovsky, A.S., Peshkovsky, S.L., Bystryak, S., 2013. Scalable high-power ultrasonic technology for the production of translucent nanoemulsions. Chemical Engineering and Processing: Process Intensification 69, 77–82.

Peterson, G.E., Bond, W.E., Clair, D.C., Aylward, S.R.S., 1995. Using Taguchi's Method of Experimental Design to Control Errors in Layered Perceptrons. IEEE Transactions on Neural Networks 6, 949–961.

Pey, C.M., Maestro, A., Solé, I., González, C., Solans, C., Gutiérrez, J.M., 2006. Optimization of nano-emulsions prepared by low-energy emulsification methods at constant temperature using a factorial design study. Colloids and Surfaces A: Physicochemical and Engineering Aspects 288, 144–150.

Porras, M., Solans, C., González, C., Martínez, A., Guinart, A., Gutiérrez, J.M., 2004. Studies of formation of W/O nano-emulsions. Colloids and Surfaces A: Physicochemical and Engineering Aspects 249, 115–118.

Porras, M., Solans, C., González, C., Gutiérrez, J.M., 2008. Properties of water-in-oil (W/O) nano-emulsions prepared by a low-energy emulsification method. Colloids and Surfaces A: Physicochemical and Engineering Aspects 324, 181–188.

Ramisetty, K.A., Pandit, A.B., Gogate, P.R., 2015. Ultrasound assisted preparation of emulsion of coconut oil in water: Understanding the effect of operating parameters and comparison of reactor designs. Chemical Engineering and Processing: Process Intensification 88, 70–77.

Raviadaran, R., Chandran, D., Shin, L.H., Manickam, S., 2018. Optimization of palm oil in water nano-emulsion with curcumin using microfluidizer and response surface methodology. Lwt 96, 58–65.

Rebolleda, S., Sanz, M.T., Benito, J.M., Beltrán, S., Escudero, I., González San-José, M.L., 2015. Formulation and characterisation of wheat bran oil-in-water nanoemulsions. Food Chemistry 167, 16–23.

Ribier, A., Simonnet, J.-T., 1980. Transparent nanoemulsion less than 100 nm based on fluid non-ionic amphiphilic lipids and use in cosmetic or in dermopharmaceuticals. US005485919A.

Sabour, M.R., Amiri, A., 2017. Comparative study of ANN and RSM for simultaneous optimization of multiple targets in Fenton treatment of landfill leachate. Waste Management 65, 54–62.

Sahin, Z., Tuti, M., Durgun, O., 2014. Experimental investigation of the effects of water adding to the intake air on the engine performance and exhaust emissions in a di automotive diesel engine. Fuel 115, 884–895.

Saravanan, S., Rajesh Kumar, B., Varadharajan, A., Rana, D., Sethuramasamyraja, B., Lakshmi Narayana rao, G., 2017. Optimization of DI diesel engine parameters fueled with iso-butanol/diesel blends – Response surface methodology approach. Fuel 203, 658–670.

Satgé De Caro, P., Mouloungui, Z., Vaitilingom, G., Berge, J.C., 2001. Interest of combining an additive with diesel-ethanol blends for use in diesel engines. Fuel 80, 565–574.

Schramm, L.L., 2005. Emulsions, foams and suspensions. Wiley Weinheim.

Seifi, M.R., Hassan-Beygi, S.R., Ghobadian, B., Desideri, U., Antonelli, M., 2016. Experimental investigation of a diesel engine power, torque and noise emission using water-diesel emulsions. Fuel 166, 392–399.

Selim, M.Y.E., Ghannam, M.T., 2010. Combustion study of stabilized water-in-diesel fuel emulsion. Energy Sources, Part A: Recovery, Utilization and Environmental Effects 32, 256–274.

Shakeel, F., Baboota, S., Ahuja, A., Ali, J., Aqil, M., Shafiq, S., 2007. Nanoemulsions as Vehicles For Transdermal Delivery Ofaceclofenac. AAPS Pharm Sci Tech 8, 104.

Shi, Y., Eberhart, R.C., 1998. Parameter selection in particle swarm optimization. Evolutionary programming VII 591–600.

Shi, X., Pang, X., Mu, Y., He, H., Shuai, S., Wang, J., Chen, H., Li, R., 2006. Emission reduction potential of using ethanol-biodiesel-diesel fuel blend on a heavy-duty diesel engine. Atmospheric Environment 40, 2567–2574.

Silva, H.D., Cerqueira, M.A., Vicente, A.A., 2015. Influence of surfactant and processing conditions in the stability of oil-in-water nanoemulsions. Journal of Food Engineering 167, 89–98.

Sivakumar, M., Tang, S.Y., Tan, K.W., 2014. Cavitation technology - A greener processing technique for the generation of pharmaceutical nanoemulsions. Ultrasonics Sonochemistry 21, 2069–2083.

Solans, C., Izquierdo, P., Nolla, J., Azemar, N., Garcia-Celma, M.J., 2005. Nano-emulsions. Current Opinion in Colloid & Interface Science 10, 102–110.

Solans, C., Solé, I., 2012. Nano-emulsions: Formation by low-energy methods. Current Opinion in Colloid and Interface Science 17, 246–254.

Solè, I., Maestro, A., Pey, C.M., González, C., Solans, C., Gutiérrez, J.M., 2006. Nano-emulsions preparation by low energy methods in an ionic surfactant system. Colloids and Surfaces A: Physicochemical and Engineering Aspects 288, 138–143.

Solè, I., Solans, C., Maestro, A., González, C., Gutiérrez, J.M., 2012. Study of nano-emulsion formation by dilution of microemulsions. Journal of Colloid and Interface Science 376, 133–139.

Soni, D.K., Gupta, R., 2017. Application of nano emulsion method in a methanol powered diesel engine. Energy 126, 638–648.

Stalidis, G., Avranas, A., Jannakoudakis, D., 1990. Interfacial Properties and Stability of Oil-in-Water Emulsions Stabilized With Binary-Mixtures of Surfactants. Journal of Colloid and Interface Science 135, 313–324.

Suryawanshi, B., Mohanty, B., 2018. Application of an artificial neural network model for the supercritical fluid extraction of seed oil from Argemone mexicana (L.) seeds. Industrial Crops and Products 123, 64–74.

Syu, J.Y., Chang, Y.Y., Tseng, C.H., Yan, Y.L., Chang, Y.M., Chen, C.C., Lin, W.Y., 2014. Effects of water-emulsified fuel on a diesel engine generator's thermal efficiency and exhaust. Journal of the Air and Waste Management Association 64, 970–978.

Tadros, T., Izquierdo, P., Esquena, J., Solans, C., 2004. Formation and stability of nano-emulsions. Advances in Colloid and Interface Science 108–109, 303–318.

Tadros, T.F., 2013. Emulsion Formation, Stability, and Rheology, in: Tadros, T.F. (Ed.), Emulsion Formation and Stability. WILEY-VCH Verlag Gmbh and Co. KGaA, Weinheim, Germany, p. 262.

Taillard, E., 1991. Robust tabu search for the quadratic assignment problem. Parallel computing 17, 443–455. Taillard, E., 1991. Robust tabu search for the quadratic assignment problem. Parallel computing 17, 443–455.

Usón, N., Garcia, M.J., Solans, C., 2004. Formation of water-in-oil (W/O) nano-emulsions in a water/mixed non-ionic surfactant/oil systems prepared by a low-energy emulsification method. Colloids and Surfaces A: Physicochemical and Engineering Aspects 250, 415–421.

Vellaiyan, S., Amirthagadeswaran, K.S., 2016a. Formulation of stable water-in-diesel emulsion fuel and investigation of its properties. Energy Sources, Part A: Recovery, Utilization, and Environmental Effects 38, 2575–2581.

Vellaiyan, S., Amirthagadeswaran, K.S., 2016b. The role of water-in-diesel emulsion and its additives on diesel engine performance and emission levels: A retrospective review. Alexandria Engineering Journal 55, 2463–2472.

Velev, O.D., 1997. Stability of emulsions under static and dynamic conditions. Journal of Dispersion Science and Technology 18, 625–645.

Walstra, P., 1993. Principles of emulsion formation. Chemical Engineering Science Science 48, 333–349.

Wang, L., Li, X., Zhang, G., Dong, J., Eastoe, J., 2007. Oil-in-water nanoemulsions for pesticide formulations. Journal of Colloid and Interface Science 314, 230–235.

Wang, P., Yan, X., Zhao, F., 2019. Multi-objective optimization of control parameters for a pressurized water reactor pressurizer using a genetic algorithm. Annals of Nuclear Energy 124, 9–20.

Watanabe, H., Suzuki, Y., Harada, T., Matsushita, Y., Aoki, H., Miura, T., 2010. An experimental investigation of the breakup characteristics of secondary atomization of emulsified fuel droplet. Energy 35, 806–813.

Wooster, T.J., Golding, M., Sanguansri, P., 2008. Impact of oil type on nanoemulsion formation and Ostwald ripening stability. Langmuir : the ACS journal of surfaces and colloids 24, 12758–12765.

Wu, T.Y., Guo, N., Teh, C.Y., Hay, J.X.W., 2013. Theory and Fundamentals of Ultrasound, in: Advances in Ultrasound Technology for Environmental Remediation. Springer Netherlands, pp. 5–12.

Xin, X., Zhang, H., Xu, G., Tan, Y., Zhang, J., Lv, X., 2013. Influence of CTAB and SDS on the properties of oil-in-water nano-emulsion with paraffin and span 20/Tween 20. Colloids and Surfaces A: Physicochemical and Engineering Aspects 418, 60–67.

Xing-Cai, L., Jian-Guang, Y., Wu-Gao, Z., Zhen, H., 2004. Effect of cetane number improver on heat release rate and emissions of high speed diesel engine fueled with ethanol-diesel blend fuel. Fuel 83, 2013–2020.

Yang, W.M., An, H., Chou, S.K., Vedharaji, S., Vallinagam, R., Balaji, M., Mohammad, F.E.A., Chua, K.J.E., 2013. Emulsion fuel with novel nano-organic additives for diesel engine application. Fuel 104, 726–731.

Yao, C., Cheung, C.S., Cheng, C., Wang, Y., Chan, T.L., Lee, S.C., 2008. Effect of Diesel/methanol compound combustion on Diesel engine combustion and emissions. Energy Conversion and Management 49, 1696–1704.

Yilmaz, N., 2012. Comparative analysis of biodiesel-ethanol-diesel and biodiesel-methanol-diesel blends in a diesel engine. Energy 40, 210–213.

Yukuyama, M.N., Ghisleni, D.D.M., Pinto, T.J.A., Bou-Chacra, N.A., 2016. Nanoemulsion: Process selection and application in cosmetics - A review. International Journal of Cosmetic Science 38, 13–24.

APPENDIX

Table A1: Energy density (J/ml) of the pre-emulsions at different sonication times formed at 25% amplitude and 0.5 pulse mode factor.

Sonication time (sec)	Energy density input to the sample (J/ml)	Droplet size, (nm)	PDI
30	15.2	94±1	0.533±0.026
60	30.5	56±1	0.354±0.038
90	45.7	52±1	0.396±0.051
75	38.0	40±1	0.389±0.043
135	68.5	33±3	0.298±0.056
195	99.0	32±6	0.263±0.081
255	129.4	27±2	0.284±0.067
315	159.9	25±0	0.216±0.060

Table A2: Comparative table for method A and method B.

β value	Surfactant fraction (w/w) ϕ_s	water fraction (w/w) ϕ_w	Method A	PDI	Method B	PDI	Δ (Method A –Method B) nm
0.91	10	11	349±21	0.471±0.047	323±1	0.415±0.010	26
1.25	10	8	614±4	0.467±0.091	309± 1	0.461±0.033	305
1.36	15	11	391±3	0.412±0.042	325±2	0.483±0.012	66
1.82	20	11	100±1	0.217±0.018	32±1	0.244± 0.012	68
1.87	15	8	224±6	0.439±0.053	115±3	0.400±0.095	109
*2.00	10	5	24±1	0.325±0.011	22±1	0.249± 0.090	2
2.50	5	2	21±1	0.427±0.019	19±1	0.303± 0.151	3
*2.50	20	8	71±7	0.248±0.023	25±1	0.175± 0.015	46
*3.00	15	5	66±1	0.208±0.031	61±1	0.138± 0.002	5
*4.00	20	5	80±1	0.258±0.001	71±1	0.236±0.031	9

Note: β value of 2.5 has encountered two times in the coordinates of ternary diagram. Moreover the values marked (*) are studied for stability analysis of nanoemulsions.

Table A3. Optimized Ultrasonicator parameters and conditions used in the study.

Parameters	values
Sample weight	0.050 gm
Sample density	0.837 gm/ml
Pulse mode factor	0.5
Percent amplitude	25
Useful acoustic power input at 25% amplitude	21.5 J/s per cm^2 of tip diameter

Table A4. Fit Summary for predicting droplet size (Y_{Dia})

Source	Sequential p-value	Lack of Fit p-value	Adjusted R²	Predicted R²	
Linear	0.0011	0.0004	0.4282	0.2583	
2FI	0.0183	0.0010	0.6386	0.5607	
Quadratic	**< 0.0001**	**0.1032**	**0.9545**	**0.8779**	**Suggested**
Cubic	0.0402	0.4965	0.9827	0.8489	Not recommended

Table A5. Fit summary for predicting kinematic viscosity (Y_{KV})

Source	Sequential p-value	Lack of Fit p-value	Adjusted R²	Predicted R²	
Linear	< 0.0001	0.2038	0.8209	0.7751	
2FI	0.2839	0.2222	0.8348	0.7607	
Quadratic	**0.0033**	**0.6805**	**0.9226**	**0.8391**	**Suggested**
Cubic	0.8730	0.2781	0.8884	-0.5779	Not recommended

Table A6. Sequential model Sum of Squares for droplet diameter (Y_{KV})

Source	Sum of Squares	df	Mean Square	F-value	p-value	
Mean vs Total	2.320E+05	1	2.320E+05			
Linear vs Mean	30606.04	4	7651.51	6.43	0.0011	
2FI vs Linear	15457.73	6	2576.29	3.43	0.0183	
Quadratic vs 2FI	**12868.73**	**4**	**3217.18**	**33.94**	**< 0.0001**	**Suggested**
Cubic vs Quadratic	1170.41	8	146.30	4.07	0.0402	Not recommended
Residual	251.50	7	35.93			
Total	2.924E+05	30	9746.31			

Table A7. Sequential model sum of squares for kinematic viscosity (Y_{KV})

Source	Sum of Squares	df	Mean Square	F-value	p-value	
Mean vs Total	307.29	1	307.29			
Linear vs Mean	47.67	4	11.92	34.22	< 0.0001	
2FI vs Linear	2.60	6	0.4339	1.35	0.2839	
Quadratic vs 2FI	**3.85**	**4**	**0.9614**	**6.39**	**0.0033**	**Suggested**
Cubic vs Quadratic	0.7382	8	0.0923	0.4252	0.8730	Not recommended
Residual	1.52	7	0.2170			
Total	363.67	30	12.12			

Table A8. Training parameters used in ANN

Parameters	Values
epoch	1000
time	Inf
goal	0
min_grad	1.00 e-07
max_fail	6
mu	0.001
mu_dec	0.1
mu_inc	10
mu_max	1e+10

Table A9. Optimized result generated from the RCCD-ANN model

No.	Water (θ_w)	Surfactant (θ_s)	Power density $(W.cm^{-2})$	Ultrasonic time (minutes)	Droplet size (nm)	Kinematic viscosity $(mm^2.s^{-1})$	Desirability
1	0.050	0.106	29.75	4.0	51.03	1.477	0.97
2	0.050	0.105	29.75	4.0	51.15	1.473	0.97
3	0.050	0.106	29.75	4.0	50.92	1.48	0.97
4	0.050	0.105	29.75	4.0	51.29	1.47	0.97
5	0.050	0.105	29.75	4.0	51.28	1.47	0.97
6	0.050	0.104	29.75	4.1	51.45	1.466	0.97
7	0.050	0.105	29.75	4.1	51.25	1.472	0.97
8	0.050	0.107	29.75	4.1	50.90	1.481	0.97
9	0.050	0.103	29.75	4.0	51.62	1.462	0.97
10	0.050	0.107	29.75	4.2	50.92	1.482	0.97
11	0.050	0.108	29.75	4.4	50.94	1.483	0.97
12	0.050	0.106	29.75	4.0	50.94	1.483	0.97
13	0.050	0.106	29.75	4.3	51.44	1.47	0.97
14	0.050	0.105	29.75	4.5	51.79	1.461	0.97
15	0.050	0.107	29.75	4.5	51.27	1.475	0.97
16	0.050	0.105	29.75	4.5	51.71	1.463	0.97

17	0.050	0.107	29.75	4.6	51.42	1.471	0.97
18	0.050	0.108	29.75	4.5	50.91	1.485	0.97
19	0.050	0.108	29.75	4.6	51.04	1.483	0.97
20	0.050	0.105	29.75	4.7	52.03	1.457	0.97
21	0.050	0.102	29.75	4.4	52.51	1.445	0.97
22	0.050	0.106	29.75	4.8	51.95	1.46	0.97
23	0.050	0.108	29.75	4.8	51.41	1.475	0.97
24	0.050	0.102	29.75	4.3	52.58	1.444	0.97
25	0.050	0.103	29.75	4.7	52.65	1.443	0.97
26	0.050	0.106	29.75	4.0	51.34	1.479	0.97
27	0.050	0.107	29.75	5.0	51.77	1.467	0.97
28	0.050	0.106	29.75	5.0	52.20	1.456	0.97
29	0.050	0.107	29.85	4.2	51.11	1.485	0.97
30	0.050	0.106	29.75	5.0	52.21	1.457	0.97
31	0.050	0.101	29.76	4.0	52.50	1.45	0.97
32	0.050	0.107	29.75	5.1	51.91	1.466	0.97
33	0.050	0.106	29.75	5.1	52.35	1.455	0.97
34	0.051	0.108	29.75	4.0	50.90	1.494	0.97
35	0.050	0.104	29.75	5.0	52.92	1.44	0.97
36	0.050	0.107	29.75	5.2	52.05	1.464	0.97
37	0.050	0.104	29.76	5.1	52.92	1.441	0.97
38	0.050	0.103	29.75	5.1	53.27	1.433	0.97
39	0.050	0.109	29.75	5.3	51.61	1.478	0.97
40	0.051	0.106	29.75	4.0	51.47	1.482	0.97
41	0.050	0.107	29.75	5.4	52.26	1.462	0.97
42	0.050	0.106	29.95	4.2	51.40	1.485	0.97
43	0.050	0.1	29.75	4.0	53.00	1.444	0.97
44	0.050	0.109	29.75	5.4	51.95	1.472	0.97
45	0.050	0.105	29.75	5.5	53.01	1.444	0.97
46	0.050	0.108	29.75	5.6	52.44	1.46	0.97
47	0.050	0.11	29.75	5.5	51.82	1.479	0.97
48	0.051	0.108	29.75	4.0	50.90	1.503	0.97
49	0.050	0.113	29.75	5.5	51.00	1.51	0.97
50	0.050	0.112	29.75	5.8	51.53	1.497	0.97

51	0.050	0.108	29.76	6.1	52.96	1.461	0.97
52	0.050	0.108	29.75	6.2	53.19	1.455	0.97
53	0.050	0.107	29.75	6.4	53.84	1.444	0.97
54	0.050	0.111	29.75	6.3	52.38	1.484	0.97
55	0.052	0.107	29.75	4.0	52.04	1.497	0.97
56	0.050	0.112	29.75	6.5	52.45	1.49	0.97
57	0.050	0.107	29.75	6.7	54.04	1.448	0.97
58	0.050	0.108	29.75	6.8	53.95	1.452	0.97
59	0.050	0.107	29.75	7.1	54.54	1.446	0.96
60	0.050	0.107	29.75	7.1	54.86	1.44	0.96
61	0.050	0.11	30.39	4.0	50.90	1.546	0.96
62	0.050	0.115	29.75	6.8	52.10	1.517	0.96
63	0.050	0.117	30.01	5.7	50.90	1.557	0.96
64	0.050	0.111	29.75	7.4	53.90	1.478	0.96
65	0.050	0.103	29.75	7.2	56.24	1.415	0.96
66	0.050	0.108	29.75	7.5	55.15	1.446	0.96
67	0.053	0.114	29.75	5.0	51.45	1.547	0.96
68	0.050	0.11	29.75	7.6	54.36	1.47	0.96
69	0.050	0.111	29.75	7.5	53.99	1.481	0.96
70	0.050	0.11	29.75	7.6	54.44	1.469	0.96
71	0.050	0.119	29.75	6.4	50.90	1.566	0.96
72	0.050	0.119	29.77	4.9	49.47	1.581	0.96
73	0.050	0.109	29.75	8.2	55.51	1.463	0.96
74	0.050	0.1	29.75	7.7	58.28	1.39	0.96
75	0.050	0.105	29.75	8.3	57.25	1.426	0.96
76	0.050	0.109	29.75	8.5	55.98	1.464	0.96
77	0.050	0.109	29.75	8.6	56.40	1.462	0.96
78	0.050	0.115	29.75	8.8	54.85	1.522	0.96
79	0.050	0.103	29.75	8.7	59.08	1.409	0.95
80	0.050	0.112	29.75	9.1	56.35	1.491	0.95
81	0.050	0.113	29.75	9.2	55.89	1.508	0.95
82	0.050	0.113	29.75	9.3	56.37	1.503	0.95
83	0.050	0.11	29.75	9.4	57.20	1.481	0.95
84	0.050	0.109	29.75	9.4	57.60	1.471	0.95

85	0.054	0.112	29.75	7.8	55.86	1.529	0.95
86	0.050	0.113	29.75	9.6	56.46	1.514	0.95
87	0.050	0.112	29.75	9.8	57.31	1.501	0.95
88	0.050	0.113	29.75	9.8	57.02	1.514	0.95
89	0.050	0.115	29.75	9.8	56.12	1.54	0.95
90	0.050	0.109	29.75	10.0	58.86	1.473	0.95
91	0.050	0.112	29.75	10.0	57.52	1.512	0.95
92	0.050	0.127	29.75	4.0	48.29	1.691	0.95
93	0.058	0.105	29.75	4.0	57.32	1.523	0.95
94	0.057	0.124	29.75	4.0	50.90	1.723	0.94
95	0.050	0.13	29.75	10.0	53.57	1.732	0.94
96	0.050	0.115	33.77	4.0	52.75	1.779	0.93
97	0.050	0.114	34.31	4.3	54.21	1.781	0.93
98	0.050	0.111	34.90	4.0	54.99	1.798	0.92
99	0.050	0.101	31.84	10.0	67.95	1.464	0.92
100	0.065	0.126	29.75	4.0	55.42	1.84	0.92

Table A10. Optimized result generated from the ANN-GA hybrid model

No.	Water (θ_w)	Surfactant (θ_s)	Power density (W.cm^{-2})	Ultrasonic time (minutes)	Droplet size (nm)	Kinematic viscosity (mm^2.s^{-1})
1	0.050	0.100	30.03	9.3	59.57	1.406
2	0.052	0.135	29.76	9.9	48.62	2.882
3	0.085	0.200	46.75	4.0	38.40	4.764
4	0.071	0.165	45.99	4.2	40.62	4.145
5	0.077	0.178	46.37	4.1	49.98	1.613
6	0.052	0.108	29.90	9.6	43.07	3.545
7	0.051	0.114	30.18	9.1	42.16	3.713
8	0.075	0.194	46.29	4.1	39.60	4.295
9	0.082	0.196	46.61	4.1	55.79	1.455
10	0.069	0.176	46.02	4.2	40.99	4.095
11	0.052	0.117	29.90	9.6	44.26	3.386
12	0.052	0.105	29.94	9.7	53.54	1.460
13	0.076	0.188	46.36	4.1	52.09	1.569
14	0.070	0.161	43.68	4.3	48.77	1.720
15	0.082	0.197	46.56	4.1	56.36	1.414
16	0.051	0.122	29.89	9.7	58.80	1.413
17	0.070	0.168	46.00	4.2	39.06	4.556
18	0.063	0.159	43.26	4.3	42.13	3.717

BIO-DATA

Name	:	**Hemant Kumar**
Date of Birth	:	15th July 1974
Nationality	:	Indian

Educational qualification:

- B.E. in Chemical Engineering, (1999), Sant Longowal Institute of Engineering and Technology, Longowal - 148106, Distt. Sangrur (Pb.), India.
- M.Tech. in Chemical Engineering, (2011), Indian Institute of Technology, Guwahati, Guwahati-781039, India.

PUBLICATIONS FROM THE THESIS

<u>Book Chapter</u>

[1] **Kumar H**, Shukla MK, Kumar V. Water-in-Diesel Nanoemulsion Fuels for Diesel Engine: Combustion Properties and Emission Characteristics. In: Singh Akhilendra P., Agarwal Rashmi Avinash, Agarwal Avinash Kumar., Dhar Atul SMK, editor. Prospects of Alternative Transportation Fuels Energy, Environment, and Sustainability, Springer, Singapore; 2018, p. 299–342.

<u>International Journals</u>

[1] **Hemant Kumar** and Vimal Kumar; Ultrasonication assisted formation and stability of water-in-oil nanoemulsions: Optimization and ternary diagram analysis. Ultrasonics Sonochemisty 2018, 49, 79–88.

[2] **Hemant Kumar** and Vimal Kumar; Preparation of water-in-diesel oil nano-emulsion using nonionic surfactants with enhanced stability and flow properties. Journal of Dispersion Science and Technology 2018, 39, 560-570.

[3] **Hemant Kumar** and Vimal Kumar; Formulation, modeling and optimization of water-in-diesel nanoemulsion using hybrid ANN-GA algorithm coupled with statistical modeling 2019. (Communicated)

International Conference

[1] **Hemant Kumar** and Vimal Kumar "W/O Nano-emulsion formation using mixed non-ionic surfactants" International Conference on Complex Fluids and Soft Matter, COMPFLU, Indian Institute of Technology Roorkee, December 6-9, 2018.

[2] **Hemant Kumar** and Vimal Kumar "Eco-friendly nanoemulsion fuel preparation by synergism in energy and surfactant". Applied Nanotechnology and Nanoscience International Conference – ANNIC 2018 Berlin, Germany. October 22-24, 2018.

[3] Ketan Mahawar, **Hemant Kumar**, Vimal Kumar "Study of optimum HLB of span80 and Triton X-100 and its stability in water-in-diesel nano-emulsion". CHEMCON 2017; Conference proceedings of 70th Annual session of Indian Institute of Chemical Engineers organized by IIChE & the Haldia Regional Centre (HRC) of the IIChE in association with the Department of Chemical Engineering, Haldia Institute of Technology, Haldia, West Bengal. December 27-30, 2017.

[4] Ritik Shah, Sanjana, **Hemant Kumar,** Vimal Kumar "Formation and stability of water-in-oil nano-emulsions of high viscous oils using high energy method". CHEMCON 2017; Conference proceedings of 70th Annual session of Indian Institute of Chemical Engineers organized by IIChE & the Haldia Regional Centre (HRC) of the IIChE in association with the Department of Chemical Engineering, Haldia Institute of Technology, Haldia, West Bengal. December 27-30, 2017.

Workshop

[1] Indo-US workshop on soft matter, IUWSM, IIT Roorkee, December 9-11, 2018.

[2] Workshop on "Modeling, Optimization and Simulation of Stochastic Systems" at Department of Mathematics, IIT Roorkee. November 26, 2016.